DESIGNING AERO-ACOUSTIC WALL OPENINGS FOR NATURAL VENTILATION

by

Sephir D. Hamilton

B.S., Mechanical Engineering (1999)

Clarkson University

Submitted to the Department of Mechanical Engineering in partial fulfillment of the requirements for the degree of

MASTER OF SCIENCE IN MECHANICAL ENGINEERING

at the

MASSACHUSETTS INSTITUTE OF TECHNOLOGY

June 2001

Signature of Author . . . . . .
Department of Mechanical Engineering
May 11, 2001

Certified by . . . . . .
Leon Glicksman
Professor of Mechanical Engineering
Thesis Supervisor

Approved by . . . . . .
Ain A. Sonin
Chairman, Department Committee on Graduate Students

DESIGNING AERO-ACOUSTIC WALL OPENINGS FOR NATURAL VENTILATION

by

SEPHIR D. HAMILTON

Submitted to the Department of Mechanical Engineering on May 11, 2001 in partial fulfillment of the requirements for the degree of Master of Science in Mechanical Engineering.

ABSTRACT

Building designers and owners continue to avoid natural ventilation despite the promise of significant annual energy savings. The fact is, natural ventilation is riddled with problems. Acoustic privacy, air quality, humidity, and fire safety are just four problems associated with natural ventilation that place it far short of meeting current living standards in many countries.

This thesis focuses on overcoming the problem of noise privacy by proposing new designs, dubbed "aero-acoustic wall openings," that permit natural ventilation without sacrificing acoustic privacy. Instead of opening doors and windows, people will open these aero-acoustic wall openings to let in air for natural ventilation.

Two aero-acoustic wall opening designs (a transfer duct and a U-shaped duct) are investigated and refined to meet design goals for noise transmission loss and pressure loss. Empirical and theoretical models predict the performance of the designs, and experiments verify the predictions.

The final U-shaped duct design has a sound transmission class (STC) rating of 25 (comparable to well-sealed doors and windows), and allows 10 air changes per hour (ACH) through three walls (in series) of a standard 120m^2 (1614ft^2) apartment under a total pressure gradient of 8Pa (produced by wind speeds of 3.7m/s – 8.3mph), while occupying only 20% of the available wall area. Profit margin estimates are promising (50% – 83%) and encourage bringing aero-acoustic wall openings to market.

Whether for an office building, a private home, or a large apartment complex, aero-acoustic wall openings are easily integrated with the architecture to produce an aesthetically pleasing and energy-efficient building. Hopefully, now with one less reason to avoid it, and every reason to use it, building designers and owners will freely adopt natural ventilation for buildings.

Thesis Supervisor: Leon Glicksman
Title: Professor of Mechanical Engineering

Table of Contents

Title Page 1

Abstract 2

Table of Contents 3

Acknowledgments 5

Chapter 1 – Introduction 7
1.1 Purpose
1.2 Background
1.3 Natural Ventilation Basics
1.4 Acoustics Basics
1.5 Existing Technology
1.6 Possibilities
1.7 Overview

Chapter 2 – Prototype Design 19
2.1 Reference Case
2.2 Design Goals
2.3 Existing Technology – Performance
2.4 Design Ideas
2.5 Acoustic Prediction
2.6 Airflow Prediction
2.7 Initial Prototypes

Chapter 3 – Experiments 37
3.1 Acoustic Experiments
3.1.1 Procedure
3.1.2 Results
3.1.3 Discussion
3.2 Airflow Computation (CFD)
3.2.1 Procedure
3.2.2 Results
3.2.3 Discussion

Chapter 4 – Refined Designs 57
4.1 Refined Prediction Methods
4.2 Refined Designs

Chapter 5 – Discussion 61
5.1 Integration into Architecture
5.2 Practicality of each design for each application

5.2.1 Cost
5.2.2 Performance
5.2.3 Life Cycle Analysis
5.3 Future Exploration

Chapter 6 – Conclusion 72
6.1 Summary
6.2 Vision of the Future

References 74

Appendix A. Experimental Data 76
A.1 Receiver Room Absorption Test Data
A.2 Transmission Loss Test Data for Straight Ducts
A.3 Transmission Loss Test Data for Prototypes
A.4 Output from CFD Computations

Appendix B. Supporting Material 91
B.1 Kammerud, et. al. (1984) Study on Ventilation Energy Savings

Acknowledgments

This thesis work was sponsored by the Kann-Rasmussen Foundation and the Alliance for Global Sustainability. Carl Rosenberg of Acentech Corporation helped get the work off the ground with advice and guidance on acoustics. John Doherty's generous assistance and expertise was instrumental in the success of the acoustic experiments, and BBN Technologies graciously provided the experimental facilities. Professor Leon Glicksman allowed me to explore the horizon, then skillfully guided me back to earth during the two years I was fortunate enough to have him as my thesis advisor and personal mentor.

Patricia Alikakos gave me comfort, support, and encouragement when I needed it most. I will be forever grateful for her patience and for our lasting friendship.

Chapter 1
Introduction

1.1 PURPOSE

The year is 1953. The first color televisions are sprouting up in homes across the United States, and one of those marvelous Carrier air-conditioning systems was just installed at the new movie theater across town.

It's early evening now; all the windows of your ranch house are open – and maybe even the front door – when a merciful splash of cool air forges a path through the hallway, past the kitchen, and into the living room where it laps at the sweat beading-up on your forehead. How pleasant the chilling breeze feels on your body after a long, hot, sweat-filled day at the factory.

Later, as you drift into sleep under a thin cotton sheet ever-so gently touched by the cool breeze, the neighbor's cat screams out a moan that rattles even the retinas in your eyes. You jolt to the open window next to your bed and slam it down; anything to silence these haunting screams of feline passion. This act, however, proves a fatal mistake as you lay back in bed and realize that even without the cotton sheet over your body, your skin is drowning in a sticky layer of sweat now that you've locked the breeze outside. If only you could install one of those new Carrier air-conditioner systems right in your home like they do at the movie theater, so you could close the window and still be comfortable.

The evolution of mechanical air-conditioning systems over the last century (the Carrier Corporation was founded in 1915) has helped people realize the dream of having thermal comfort without sacrificing acoustic privacy. In fact, building occupants today expect and demand acoustic privacy along with thermal comfort. Air-conditioning, however, is only one solution for ensuring thermal comfort and acoustic privacy in buildings. For the sake of energy conservation, a better solution would utilize natural ventilation and solve the noise privacy problems associated with it. That "better" solution is the goal of this thesis.

1.2 BACKGROUND

This work evolved from an MIT class project for designing energy-efficient apartment buildings in several Chinese cities. The proposed building designs utilized natural ventilation to reduce energy use, and required residents to open windows and doors to allow airflow through apartments and common hallways. The building developers in China opposed natural ventilation because of the poor noise privacy of natural ventilation. This opposition sparked interest in designing wall openings that allow airflow but block noise (dubbed *aero-acoustic wall openings*). Instead of operable doors and windows, these wall openings provide a dedicated path for airflow, leaving windows to transmit light and doors to transmit people (figure 1.1).

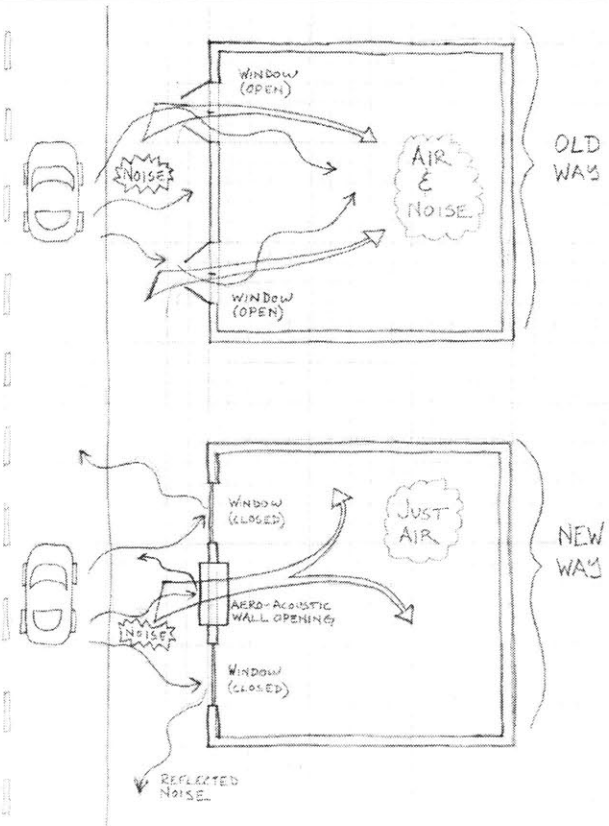

Figure 1.1 – Illustration of the old way of designing natural ventilation vs. the "new way."

Before describing the design process of these wall openings, the sections below provide a brief overview of natural ventilation and acoustics, discuss past work in the field of aero-acoustics, and present currently available aero-acoustic technology.

1.3 NATURAL VENTILATION BASICS

Natural ventilation is the flow of fresh air through a building, driven by naturally occurring forces, and is used to maintain indoor air quality and to cool occupants in indoor climates. Two common naturally occurring "forces" are wind pressure and buoyancy pressure, called *cross ventilation* and *stack-effect ventilation* respectively when used to induce ventilation. (Allard, et. al. 1998)

During cross ventilation (figure 1.2), wind creates a pressure difference between the windward side and the leeward side of a building, thus driving air through wall openings (such as open windows or doors) from the windward side (high pressure) to the leeward side (low pressure). The amount of airflow depends on the overall pressure difference caused by the wind and the overall pressure resistance of the airflow-path (caused by pressure drops through wall openings and over obstacles).

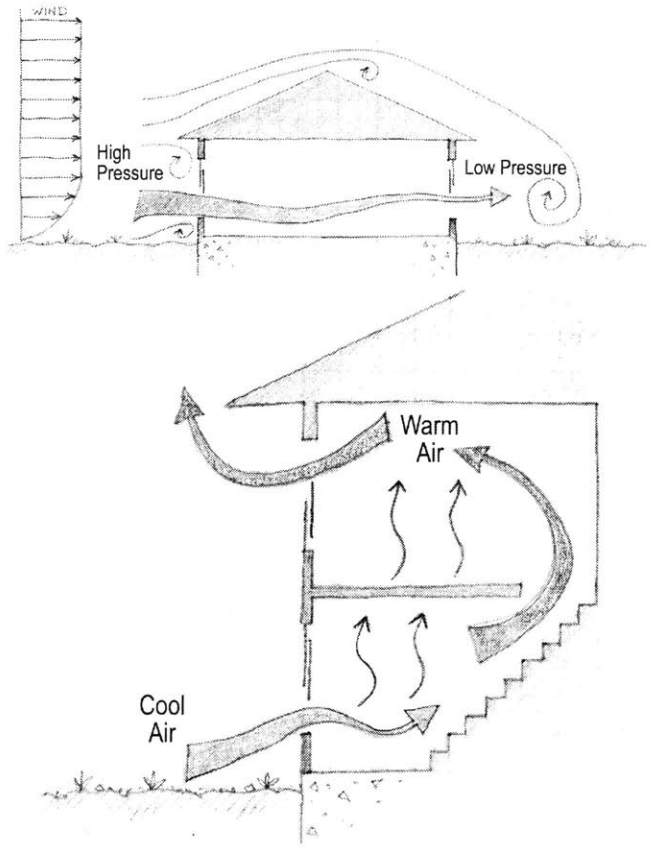

Figure 1.2 – Illustrations of cross ventilation (top) and stack-effect ventilation (bottom).

During stack-effect ventilation (figure 1.2), less dense (warm) air from inside a building

moves upward and is replaced at the bottom by the cooler outside air. As long as a vertical path exists (through stairwells, windows, and doors for example), cool air will enter at an opening near the bottom and warm air will leave at an opening near the top. While aero-acoustic wall openings apply for both cross ventilation and stack-effect ventilation, this thesis limits the examples to cross ventilation, for simplicity. General equations for cross ventilation along with a simple example, in Chapter 2, help illustrate the concept of natural cross ventilation in more detail.

1.4 ACOUSTICS BASICS

Every study of noise consists of these three elements: a source, a path, and a receiver. For example, traffic, barking dogs, and household appliances are noise sources. The noise they create travels along a path through open windows and doors to a human ear, the receiver.

The human ear is a complex device that "hears" noise in a non-linear fashion. Both the 'pitch' (frequency) and 'loudness' (sound power) fall on logarithmic scales according to the response of human hearing. For example, doubling a frequency creates a change of one octave (say from a middle-C to a high-C on a piano); and what sounds twice as loud actually has 10 times more sound power. Because of this behavior, logarithmic scales are used to describe sound.

Equation 1 defines sound level (for "loudness" measurements):

$$\mathbf{L = 10Log(ratio)} \tag{1}$$

where:
L = sound level, decibels (dB),
ratio = a ratio of sound power at a location versus a reference sound power.

The "ratio" term can be a ratio of actual sound power (in watts) – giving sound-power level – or it can be a ratio of sound intensities (watts per area) – giving sound-intensity level – or it can be a ratio of sound pressures squared (Pascal squared) – giving sound-pressure level. All sound levels use

decibels (dB) as a descriptor, and though they are proportional, they are not equal to one another. Furthermore, the reference value can be any value, so a sound level value must explicitly state which reference value it used. Since microphones directly measure sound pressure, a commonly used sound level is the sound-pressure level. The standard reference pressure for sound-pressure levels is 20E-6 Pascal, which is approximately the threshold of human hearing in young adults. Therefore, equation 2 describes sound pressure level:

$$\mathbf{L_p = 10Log}\left(\mathbf{p^2 / p_0^2}\right) \qquad (2)$$

where:
L_p = sound-pressure level, dB,
p = sound pressure measured at a certain location, Pa,
p_o = reference sound pressure, Pa (typically equals 20E-6 Pa).

If a sound has a very narrow frequency band, it is a "pure tone" and sounds like a distinct musical note. If a sound has a broad and even frequency band, it is "white noise" and sounds indistinct and noisy.

Measuring sound-pressure level versus frequency gives the spectrum of a sound. To measure the spectrum of a sound, the sound pressure level in each frequency band is determined and plotted as a function of the frequency at the center of each band. The spectrum is measured in

Octave Band Frequency (Hz)	1/3-Octave Band Frequency (Hz)
16	12.5
	16
	20
31.5	25
	31.5
	40
63	50
	63
	80
125	100
	125
	160
250	200
	250
	315
500	400
	500
	630
1000	800
	1000
	1250
2000	1600
	2000
	2500
4000	3150
	4000
	5000
8000	6300
	8000
	10000

Figure 1.3 – octave-band center frequencies and 1/3-octave band center frequencies.

octave bands or one-third octave bands (with center frequencies indicated in figure 1.3), or as a narrow band (single frequency).

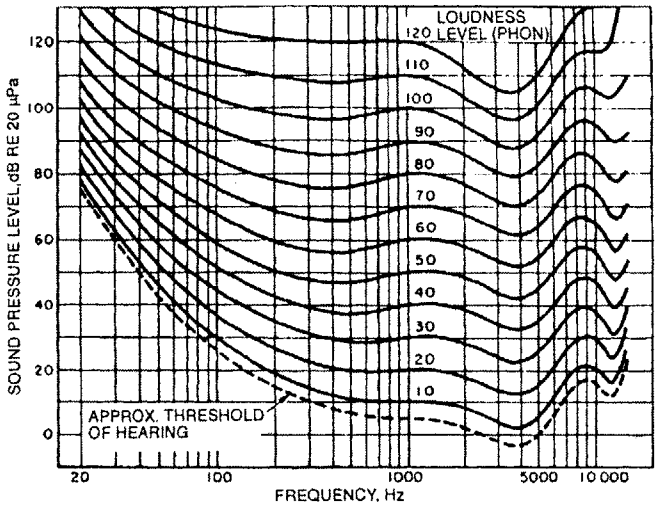

Figure 1.4 – Perceived Loudness Curves (Robinson and Dadson. 1956).

Human hearing is more sensitive to certain frequencies than others. Perceived loudness curves (figure 1.4) show the rated loudness of pure tones at different frequencies and for different sound levels. The graph shows that humans are most sensitive to sound between 100Hz and 10,000Hz, with the peak of sensitivity at 4000Hz.

Often, sound spectra are summarized by a single value that indicates the perceived loudness of the spectra. The *overall level* results from adding (logarithmically) the values of all the frequency bands, and gives a good indication of the overall noise power. The A-weighted value (determined by adding or subtracting decibels, according to figure 1.5, from the noise level at each frequency, and then adding for the overall level) is a generally accepted technique of representing normal human hearing response.

Noise transmission loss is a measure of how well a wall (or other barrier in the noise field) blocks noise at each frequency. Equation 3 defines transmission loss:

$$\mathbf{TL} = 10\mathbf{Log}(1/\tau) \qquad (3)$$

where:
τ = the fraction of sound power incident on a surface that transmits through a partition and re-radiates from the opposite surface.

Frequency (Hz)	A-Weighting Adjustment (dB)
25	-44.7
31.5	-39.4
40	-34.6
50	-30.2
63	-26.2
80	-22.5
100	-19.1
125	-16.1
160	-13.4
200	-10.9
250	-8.6
315	-6.6
400	-4.8
500	-3.2
630	-1.9
800	-0.8
1000	0.0
1250	+0.6
1600	+1.0
2000	+1.2
2500	+1.3
3150	+1.2
4000	+1.0
5000	+0.5
6300	-0.1
8000	-1.1
10000	-2.5

Figure 1.5 – A-Weighting adjustments.

Similar to A-weighting, sound transmission class (STC) is a weighted adjustment of transmission loss for human hearing and uses a single value to describe a barrier's behavior. Defined by ASTM Standard E413–87(99), sound transmission class is a method of illustrating "single-number acoustical ratings for laboratory and field measurements of sound transmission obtained in one-third octave bands." The method fits a curve of a specified shape to the transmission loss data of a partition (at each one-third octave band) so that no data point lies more than 8 dB below the curve and so the sum of the difference between the curve and all data points below the curve is equal to or less than 32 dB. Once fit, the value of the curve at 500 Hz is the STC rating of the partition (figure 1.6 illustrates the curve-fit process). STC curves are valid for noise sources with similar spectra to human speech. Analysis of other sources (traffic, machinery, etc.) should look at the transmission loss at each frequency separately for an accurate indication of transmission loss.

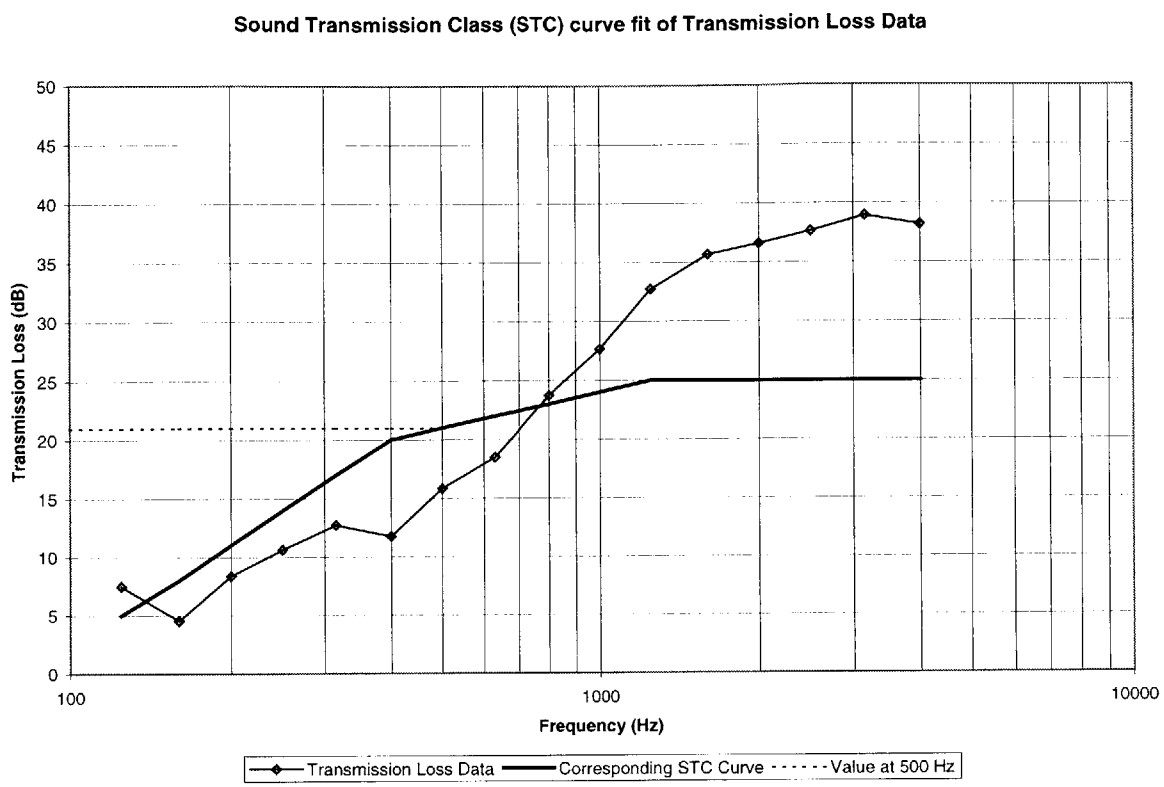

Figure 1.6 – Sound transmission class (STC) curve-fit of sample transmission loss data, showing an STC-21 rated spectrum.

Noise privacy is another issue that is difficult to quantify since each person has different sensitivity to noise. In general, A-weighted values predict human sensitivity to noise. Work on acceptable noise limits for residential spaces summarizes the maximum acceptable noise level in a residence as <45dBA in a kitchen or bathroom, <40dBA in a living or dining room, <35dBA in bedrooms (National Research Council Canada).

1.5 EXISTING TECHNOLOGY

The two previous sections provide a general overview of acoustics and natural ventilation; this section details more specific work on aero-acoustics (the combined study of acoustics and airflow).

Work in the area of aero-acoustics has developed both complex theoretical modeling and

more simple empirical prediction techniques. Beranek (1992), Vér (1972), Mechel (1976), and Kurze (1972) have developed theoretical prediction methods for aero-acoustic devices including lined ducts and duct silencers. Lippert (1954) and Miles (1947) looked at theoretical noise flow through a duct with a right-angle bend. Kuntz and Hoover (1984) modified the empirical prediction methods for sound attenuation in lined ducts developed over time by Parkinson (1937), Sabine (1940), Rogers (1940), and Vér (1978). The ASHRAE Fundamentals Handbook (1997), commonly used by building designers, recommends the Kuntz and Hoover method.

On the airflow side, Idel'Chik et. al. (1994) have looked at fluid flow in channels and ducts, extensively compiling experimental pressure loss data for various duct components. Where experimental data is limited to experiments that have already been performed, computational methods apply for a wide range of duct components. Computational Fluid Dynamics (CFD) software tools, including CHAM's PHOENICS program, solve discretized fluid mechanics equations to give averaged solutions to complex flow problems beyond those tested with experiments (CHAM, 2000).

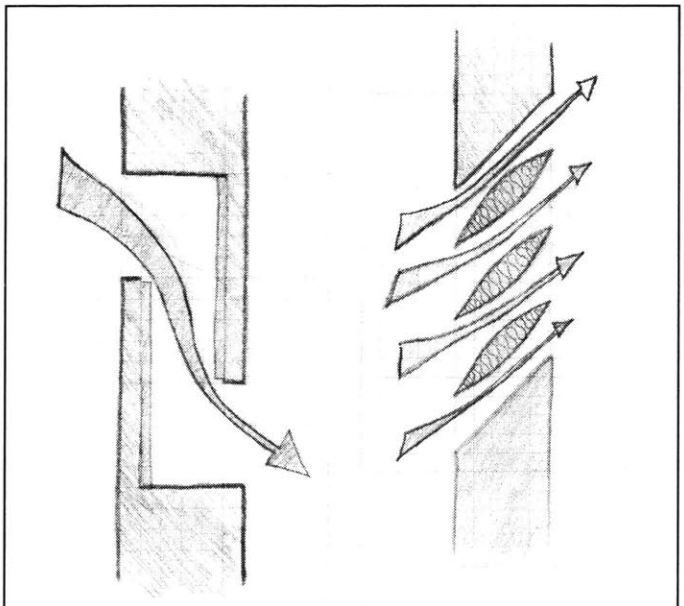

Figure 1.7 – Transfer ducts (left) and acoustical louvers (right) are currently available.

There are several manufactured aero-acoustic devices currently available on the market. Duct lining, duct silencers, and plenum silencers are used in the heating, ventilating, and air-conditioning (HVAC) field to quiet airflow in ducts. Two specific products have already attempted to provide airflow through a wall

while reducing noise transmission: acoustical louvers and transfer ducts. Acoustical louvers often enclose mechanical rooms and rooftop cooling units, while transfer ducts often link two air-conditioned offices that share a single air-return.

Neither of the above products, however, specifically targets noise control for natural ventilation. Not surprisingly, then, sound attenuation and pressure loss data indicates that neither design will perform well in a natural ventilation application. The transfer ducts simply have too much resistance to airflow, while the acoustical louvers do not provide adequate sound reduction. Section 2.3 includes a detailed explanation of why neither design works for natural ventilation, and lists the manufacturer's test data.

1.6 POSSIBILITIES

Architects, homeowners, apartment dwellers, and office workers alike will benefit from the proper development of aero-acoustic wall openings. Ultimately, the increased use of natural ventilation will help reduce the energy requirements of buildings worldwide, and the possible energy savings of ventilation versus air-conditioning are significant (up to 80% savings on annual cooling load, see figure 2.4 in chapter 2), as implied by a comprehensive investigation (Kammerud, et. al., 1984).

Before natural ventilation realizes all these possible energy savings, however, its traditional shortcomings including noise privacy, high humidity, and air quality must disappear. The work in this thesis tackles the noise privacy issue so that natural ventilation will be more attractive to architects, homeowners, apartment dwellers, and office workers alike. Once all the hurdles disappear, the full energy-saving benefits of natural ventilation will materialize.

Today, designers of naturally ventilated buildings must carefully design floor plans so that internal walls do not restrict airflow. This restriction often leads to open floor plans with poor

acoustic privacy, or very thin buildings without common hallways, or other limited designs. Further, many natural ventilation designs will not work properly if building occupants shut the "wrong" doors or windows and, thus, block the air-path. Aero-acoustic wall openings will allow architects to incorporate natural ventilation into more traditional floor plans for homes, apartment buildings, and office buildings that previously required exclusive use of mechanical air-conditioners.

With properly designed aero-acoustic wall openings, building occupants will enjoy the comfort and energy-savings of natural ventilation without losing the acoustic privacy they have learned to expect. A homeowner will not need to close the windows and turn on the air-conditioning on a hot summer night to silence the noisy cat outside his window. Instead, he will enjoy the natural evening breeze passing through aero-acoustic wall openings while he drifts off to sleep in peace and quiet. The next morning, his child can watch cartoons in the living room without waking him because he closed the bedroom door last night without cutting off the airflow through the house.

In an apartment building across town, a resident will stay cool because a buoyancy induced breeze enters his apartment from outside and exits up through the public stairwell. Yet, the sounds from the busy street outside and from the newlywed couple staging a fight in the stairwell will not disturb him.

A worker in an office building downtown will enjoy the privacy of a closed office, without losing the benefits of cross ventilation previously found only in open-plan offices. She will not hear the photocopier in the hallway because her door is closed; yet she will stay cool without air conditioning.

Aero-acoustic wall openings will change the way the public perceives (and architects design) naturally ventilated buildings. No longer do naturally ventilated buildings require overly

constrained design or lower acoustic privacy standards. With up to 80% cooling load reductions possible in most U.S. climates by using ventilation versus air-conditioning (Kammerud et. al. 1984), it is a shame to leave natural ventilation out of a design solely because of noise privacy concerns. Now, there is no need to. This thesis details the design process for two aero-acoustic wall openings that will encourage wider-spread use of natural ventilation.

1.7 OVERVIEW

The design process begins, in chapter two, by setting design goals for noise transmission loss and airflow restriction. It defines and describes prediction methods for airflow and acoustics, and proposes initial prototype designs. Then, chapter three presents the experimental procedure and results for each prototype design. The next step in the design process, chapter four, defines refined prediction methods based on the experimental results and proposes refined design ideas for several natural ventilation applications. Using the final designs, case studies and examples illustrate the practicality of the designs for architecture and natural ventilation in chapter five. Costs and life-cycle performance factor into the discussion as it explores the integration of aero-acoustic wall opening technology into naturally ventilated architecture. The final chapter concludes the thesis with a vision of the future for aero-acoustic wall openings in naturally ventilated buildings.

Chapter 2
Prototype Design

2.1 REFERENCE CASE

Illustrating the effectiveness of a wall opening in natural ventilation is a complex task. Simply giving the pressure loss coefficient (k) of each wall opening is not sufficient because the total airflow through the building also depends on the floor plan, the number of walls in series, the total pressure gradient, and the open area in each wall. Each building design is unique and each will perform differently. Therefore, a sample apartment (figure 2.2) serves as a

Wall #	Wall Area	Window & Door Areas	Net Available Wall Area
1	30 m^2	12 m^2	18 m^2
2	30 m^2	6 m^2	24 m^2
3	21 m^2	3 m^2	18 m^2
4	21 m^2	6 m^2	15 m^2

Figure 2.1 – Table showing wall area available for aero-acoustic wall openings.

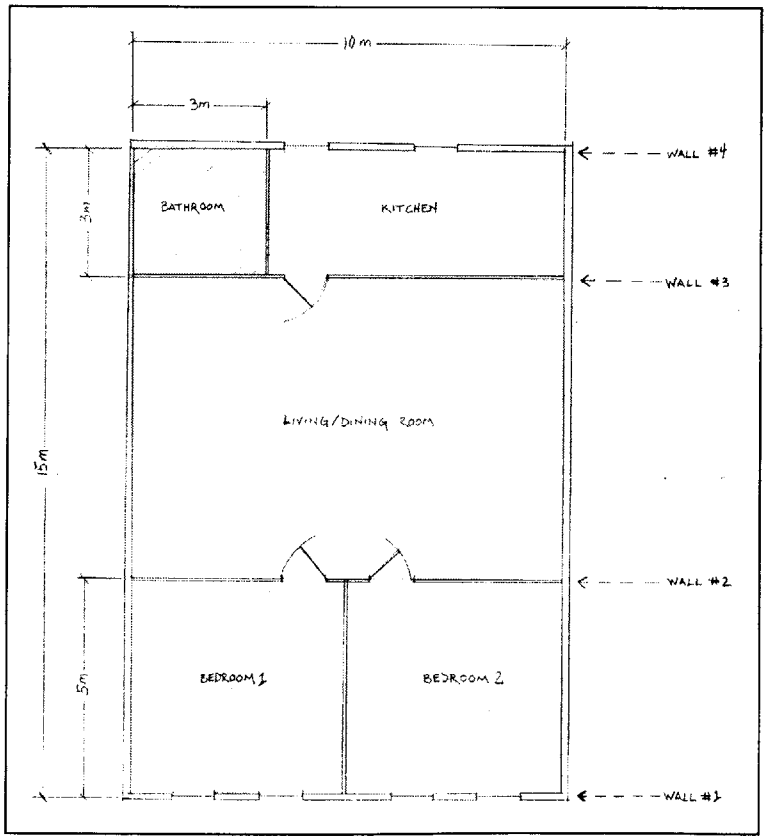

Figure 2.2 – Reference apartment floor plan.

- Floor area – 150 m^2 (1615 $ft.^2$) (single-level, two bed, one bath, kitchen, living/dining)
- Volume – 450 m^3 (10m x 15m x 3m) (15,892 ft^3) (33ft x 49ft x 9.8ft)

reference for judging the effectiveness of natural ventilation throughout this thesis. Figure 2.1 is a table showing the wall area available for the aero-acoustic wall openings to use.

Ultimately the aero-acoustic wall openings should not use the entire available wall area (for aesthetic and logistic reasons). Further, since the geometry is not considered, this "wall area method" serves only as a rough indication of how well a device will fit in the walls. It is also important to note that this reference apartment is a "worst-case" design example for natural ventilation purposes. Section 5.1 provides three more examples (apartment plans and office plans) demonstrating how aero-acoustic wall openings are actually designed into the wall, and how the layout of the floor plan effects the performance of the devices.

2.2 DESIGN GOALS

The first step of the design process establishes design goals for noise and airflow. For noise, the wall openings should provide at least the same noise reduction as the doors and windows they will replace. Test data by the National Research Council Canada gives transmission loss data for various partitions (figure 2.3). A single pane of glass (without a frame, just the glass) has a sound transmission class (STC) rating of 29 (see section 1.4 for a definition

Partition Type	**STC**
1/2" (13mm) gypsum board on both sides of 2 x 4" (40 x 90mm) wood studs	33
4" (90mm) concrete block [30 lb/ft^2 (147kg/m^2)]	37
6" (140mm) concrete block [41 lb/ft^2 (202kg/m^2)]	45
1/8" (3mm) glass (no frame)	29
1/8" (3mm) glass (double glazed) and 1/4" (6mm) air-space (with metal frame)	28
Solid core wood door [4.9lb/ft^2 (24kg/m^2)] (no seals)	22
Solid core wood door (w/ foam tape seals around perimeter)	26
Hollow core steel door (18 gauge steel faces, no seals)	17
Hollow core steel door (18 gauge steel faces, foam tape seals)	28
Minimum design goal for aero-acoustic wall opening	***25***

Figure 2.3 – Table of STC ratings for various walls, windows, and doors. All tests were performed by the National Research Council Canada. For complete spectral data, see Harris (1994).

of STC rating), and a double paned window (with a metal frame, including the seal) has an STC rating of 28. Performance of doors range from STC-17 for a hollow steel door to STC-26 for a well-sealed solid-wood door.

Based on the average performance of these windows and doors, the minimum design goal for the aero-acoustic wall-openings calls for an STC rating of 25. For reference, typical wood-stud walls with gypsum on both sides have an STC rating around 30-40 and concrete block walls have an STC rating around 40-50. While replacing a large wall area (with a high STC rating) with aero-acoustic wall openings (with a lower STC rating) will degrade the overall STC of the wall, it will not be significantly worse than the degradation that windows and doors already create (due to logarithmic addition of transmission loss). Each 10dB sound reduction sounds like a 50% reduction in volume, so an STC-25 rated partition will create about 80% in noise volume reduction.

The airflow goal is a bit more complex because there are three major variables: wall area, airflow rate, and pressure loss per wall. If the device needs to be larger than the available wall area to pass enough air, the design will not work; if the airflow rate is too low, natural ventilation will be ineffective; and if the pressure loss per wall is too great, then mechanical fans may be required. If considering all these variables simultaneously, establishing an airflow design goal is a complex and daunting task.

For simplicity, the airflow design goal uses the sample case (defined in section 2.1) as an indicator of expected performance. Essentially, an air change rate of 10 air changes per hour (ACH) must flow through the sample floor plan when a pressure gradient of 10 Pascal exists between one side of the building and the other, and the aero-acoustic wall openings take up no more wall area than is available. While it is unreasonable for the aero-acoustic wall openings to occupy the entire available wall area (and geometry limitations will further restrict the design),

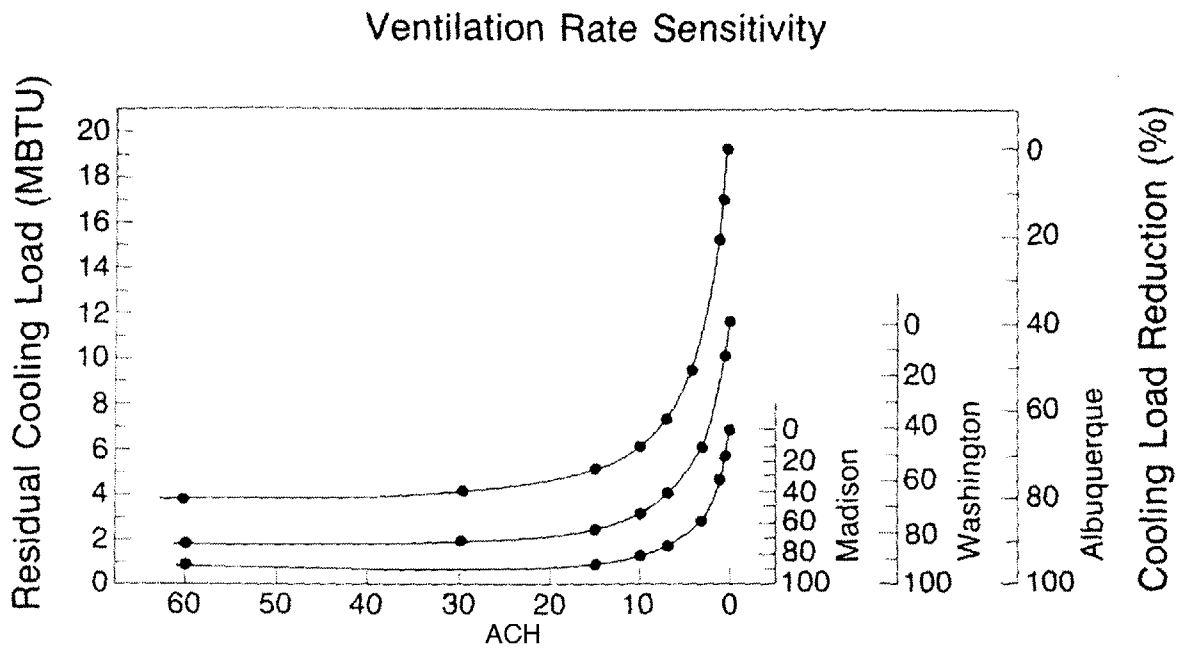

Figure 2.4 – Energy savings possibilities determined by Kammerud, et. al. (1984) for three U.S. Cities.

the percentage of wall area occupied by the device gives a good indication of the design's feasibility. Section 5.1 discusses how the designs will actually fit into the wall.

An air change rate of 10 ACH is chosen for the design goal because it will provide substantial cooling load reductions (up to 80%) in most U.S. climates according to Kammerud et. al. (1984). Figure 2.4 shows the effective cooling load reduction (for an entire cooling season) as a function of ACH for a standard 109m^2 x 2.5m (1173ft^2 x 8.2ft) home in three U.S. cities (Madison [43.13 N latitude], Washington D.C. [38.85 N], and Albuquerque [35.05 N]). The graph indicates that an air change rate greater than a critical value (near 10ACH for the typical apartment used) does not help reduce the cooling load beyond a maximum savings of about 80%. The critical ACH value will change based on the heat load inside the building (solar, internal, etc.), but 10ACH is a conservative number based on the relatively large cooling loads used in the study. The Kammerud study used BLAST for its calculations, an energy-load software program developed by the U.S. Department of Energy. Details of the building used in the Kammerud study

are reproduced in appendix B, along with baseline energy requirements and cooling season definitions for the various cities tested. A table of the total energy savings for each city is also reproduced in appendix B.

City	Country	Summertime Mean Wind Speed mph (m/s)
Albuquerque, NM	USA	10 (4.5)
Beijing	China	7 (3.1)
Berlin	Germany	8 (3.6)
Boston, MA	USA	14 (6.3)
Edmonton, Alberta	Canada	9 (4.0)
London	England	10 (4.5)
Madison, WI	USA	12 (5.4)
Paris	France	9 (4.0)
Shanghai	China	8 (3.6)
Washington, D.C.	USA	11 (4.9)

Figure 2.5 – Chart of average wind speeds during summer (ASHRAE Handbook, Fundamentals. 1997)

A total pressure gradient of 10 Pascal is chosen for the design goal because a constant outdoor wind at 4m/s (9mph) flowing around a building will produce it. Figure 2.5 shows the average summertime wind speeds for several cities (many of which are above 4 m/s). Other pressure sources, such as buoyant forces or mechanical fans, may also provide 10Pa, or higher, pressure gradients.

In the last part of the design goal, the maximum wall area used for the devices may not exceed the available wall area of the sample case as defined by figure 2.2 in section 2.1. Each wall in the sample case has an available wall area for the aero-acoustic wall openings (total area minus area of doors and windows). If a wall opening needs more than this area in order to achieve the required flowrate (10ACH under a 10Pa pressure gradient), it will not meet the design goal. While geometry restrictions are not considered in the airflow design goal, the wall area requirement is simply an indication of how much area the devices will need. Section 2.3 contains a detailed example of the design goal calculations for airflow, and section 5.1 shows how the designs are actually designed into the walls of several example buildings.

Manufacturer	Model	Description	% open area	K-value	STC
Airolite	T9206	6", airfoil	26	0.95	17
Airolite	T9106	6", architectural	29	1.74	18
Airolite	T9208	8", airfoil	28	1.24	19
NCA	ACSLJ-6	6", architectural	25	1.69	18
NCA	ACSLJ-8	8", architectural	22	1.69	20
NCA	ACSLJAF-12	12", airfoil	20	0.82	17
NCA	ACSLJ-12	12", architectural	21	1.75	20
Arrow United Industries	FS-401-LF	4", architectural, lower freq.	-	3.05	11
Arrow United Industries	FS-401-HF	4", architectural, higher freq.	-	3.05	13
Industrial Acoustics (IAC)	Slimshield 4"	4", architectural	-	-	16
Industrial Acoustics (IAC)	Slimshield 6"	6", architectural	-	-	21
Industrial Acoustics (IAC)	Noishield 12"	12", airfoil (LP model)	-	-	15
Industrial Acoustics (IAC)	Quiet-Vent "W"	transfer duct	16	14.8	46

Figure 2.6 – Table of sound transmission class (STC) ratings and pressure loss coefficient (k-value) data from manufacturers (for acoustical louvers and transfer ducts).

2.3 EXISTING TECHNOLOGY – PERFORMANCE

The existing aero-acoustic products (acoustical louvers and transfer ducts) do not meet the design goals for noise and airflow. In fact, the designs seem to disregard optimal sound and airflow design altogether. Some acoustical louver products were fitted with "aerodynamic" blades to help improve the airflow that, instead of improving the flow, reduced the open area of the device and choked the flow; the transfer duct has sharp corners and overly-thick lining that greatly increase their pressure loss characteristics. The geometry of the products, also, seems arbitrary with little or no consideration for proper duct length or cross-sectional aspect ratio.

Published manufacturer test data indicates the performance of each product for air-pressure loss and sound attenuation. Each manufacturer states that their tests adhere to ASTM standards E90-97 and E413-87 for noise attenuation and to AMCA standard 500-L-99 for air-pressure loss (though the AMCA standard is not applicable for the transfer duct, it is used regardless). The figure includes twelve different acoustical louver models from four manufacturers and one transfer duct model (transfer duct products are not widely available, as are acoustical louvers).

The pressure loss coefficient (k), equation 4, helps compare pressure loss performance:

$$\mathbf{k} = \frac{\Delta \mathbf{P}}{\frac{1}{2}\boldsymbol{\rho}\mathbf{u}^2} \tag{4}$$

where:
k = pressure loss coefficient of the device,
ΔP = pressure drop from the inlet of the device to the outlet, Pa,
ρ = air density, kg/m^3,
u = mean air velocity through the device of constant cross-section, m/s.

The k-values range from 0.82 to 3.05 for the louvers (see figure 2.6). The k-value of the transfer duct is 14.8. The k-values for transfer ducts will differ significantly depending on their mounting and the percentage of wall area they occupy, but the AMCA testing standard does not consider these variations (and the results of the test, therefore, give artificially high k-value results). Figure 2.6 is a table showing the STC ratings and k-values for each product, given by the manufacturer of each product. Not one of the acoustical louvers meets the minimum sound requirement of STC-25, but the transfer duct far exceeds it (without laboratory verification, however, these STC ratings are somewhat questionable).

Using an adjusted k-value of 10 (and area ratio of 16%) for a typical transfer duct and a k-value of 1.5 (and area ratio of 25%) for a typical acoustical louver, the sample case (defined in chapter 1) illustrates how well each design will perform in a natural ventilation application. The following steps show the calculation process used to determine the required wall area for an aero-acoustic wall opening, and ultimately determine whether it meets the airflow design goal. The calculation assumes an airflow rate of 10ACH and an overall pressure gradient of 10Pa, then solves for the wall area required by the aero-acoustic device:

EXAMPLE: Finding Wall Area Required by Aero-Acoustic Wall Openings

The total pressure gradient across all four walls is 10 Pascal. Assuming an even pressure-loss distribution, each wall will cause 2.5 (10 divided by 4) Pascal of pressure drop.

Knowing the k-value of the aero-acoustic wall openings in each wall (k = 10 for the transfer duct and 1.5 for the louver), the velocity through each opening is defined by:

$$\mathbf{u} = \sqrt{\frac{2\Delta \mathbf{P}}{\rho \mathbf{k}}}$$

where:
ΔP = pressure loss through each wall (1.5 Pa),
u = average velocity through the cross section area of the opening, m/s,
ρ = air density, kg/m^3,
k = pressure loss coefficient.

The total occupied wall area for each wall is determined by the volume flow rate and the area ratio. The volume flow rate is defined by:

$$\dot{\mathbf{V}} = \frac{\mathbf{ACH}}{3600} \cdot \mathbf{V}$$

where:
V = total volume (450 m^3),
$\dot{\mathbf{V}}$ = volume flow rate through apartment, m^3/s,
ACH = air changes per hour (10).

Finally, the total area occupied by the aero-acoustic wall openings is defined by:

$$\mathbf{A} = \frac{\dot{\mathbf{V}}}{\mathbf{u}(\mathbf{area\_ratio})}$$

where:
A = total occupied wall area (in each wall), m^2,
area_ratio = ratio of open cross section flow area to total occupied wall area.

Figure 2.7 shows the results of the above calculation in a table of the wall area required by the device (to pass 10ACH with a 10Pa pressure gradient) versus the wall area available in each wall of the reference case. The transfer duct requires more wall area ($17m^2$) than is available ($15m^2$) so it fails, while the acoustical louver requires less wall area than is available in each wall so it passes.

	k-value	Wall Area Needed	Wall Area Available	Pass or Fail
Transfer Duct	10	17 m^2	15 m^2	fail
Acoustical Louver	1.5	4.3 m^2	15 m^2	pass

Figure 2.7 – results of wall area test on existing aero-acoustic wall openings.

An aero-acoustic wall opening that meets both the airflow and the acoustic design goals must carefully balance the contradictory requirements of blocking noise and permitting airflow. Along with modifying the two existing designs, the process included brainstorming for new ideas.

2.4 DESIGN IDEAS

New design ideas evolved from the existing product designs (acoustical louvers and transfer duct). Figure 2.8 shows just a few of the ideas conceived during brainstorming. The two designs showing the best promise for both airflow and acoustic performance are the transfer duct (modified for improved airflow) and the U-shaped duct (shown in the lower part of figure 2.8). The design process then expanded the two design ideas and modified them to meet both th e airflow and the acoustic design goals.

The design of an aero-acoustic wall opening must evolve from an understanding of how it will perform as several variables change simultaneously. Acoustic and fluid mechanic theory combined with empirical data in the following section provide prediction models for noise transmission loss and airflow resistance of the two designs noted above.

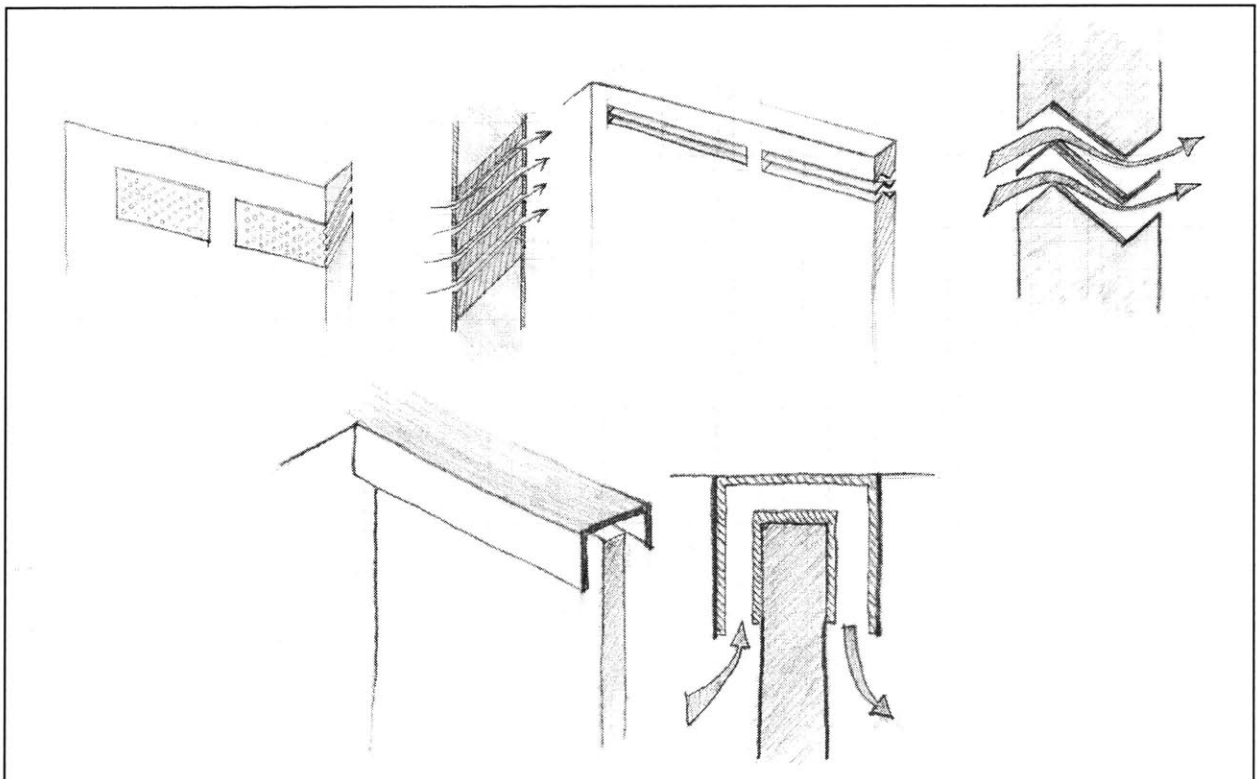

Figure 2.8 – Sketches of initial brainstorm ideas, in addition to transfer duct and louvers.

2.5 ACOUSTIC PREDICTION

Complex acoustic theory could predict the exact transmission loss through an aero-acoustic wall opening (Vér, Scott, Beranek, Mechel, et. al.), but would require a detailed analysis with complex math and exact material properties not covered in this thesis. Instead, empirical methods for each component of the opening (entrance, bends, and straight duct) superimpose onto one another giving an estimate for the transmission loss through the entire opening (the noise attenuation through the solid wall, perpendicular to the duct, is so much larger than through the open duct, that it may be ignored). Chapter 4 presents revised prediction methods derived using the experimental results (the methods below were used to get a "first-cut" estimate so that test prototypes could be built).

Both designs have these three common duct components: an entrance and exit, one or two lengths of straight lined duct, and two bends. Beranek and Vér (1992) propose a simple method for finding entrance and exit losses according to the graph in figure 2.9 (where the sound reduction, dB, at the entrance or exit is a function of wavelength, λ, and cross-sectional height, h). Lippert (1954) proposed an experimental validation of theoretical acoustics to find the sound loss through a 90 degree bend, due to end reflections, though his method does not apply to these aero-acoustic designs because of the short entrance and exit regions surrounding their bends (analysis in Chapter 4 shows that this loss may, in fact, be neglected). Kuntz and Hoover (1987) proposed a method of predicting sound loss in straight lined ducts. It turns out,

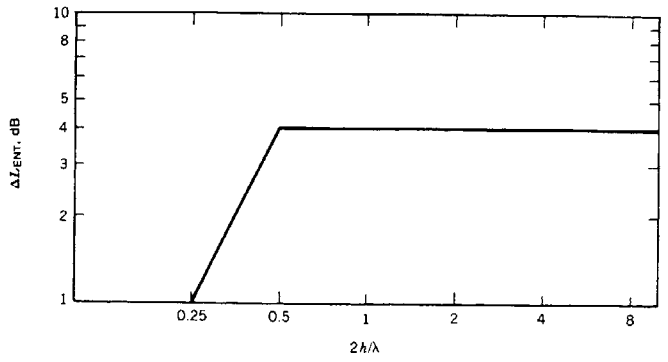

Figure 2.9 – entrance loss due to sound reflection (h is the smaller cross section dimension).

as shown in Chapter 4, that the lined duct portion of the designs contributes almost exclusively to the overall sound transmission loss.

According to Kuntz and Hoover, equations 5 and 6 predict the transmission loss of a straight duct with acoustic lining on all sides:

$$\mathbf{TL} = \frac{\mathbf{a_o}^{0.748}\mathbf{h}^{0.356}(\mathbf{P/A})\mathbf{L}\cdot\mathbf{f}^{(1.17+\mathbf{K_2 d})}}{\mathbf{K_1 d}^{2.3}} \text{ dB } (125 \text{ Hz} < f < 800 \text{ Hz}) \tag{5}$$

$$\mathbf{TL} = \frac{\mathbf{K_4}(\mathbf{P/A})\mathbf{L}\cdot\mathbf{f}^{(\mathbf{K_5}-1.61\log(\mathbf{P/A}))}}{\mathbf{w}^{2.3}\mathbf{h}^{2.7}} \text{dB } (800 \text{ Hz} < f < 10{,}000 \text{ Hz}) \tag{6}$$

where,

a_o = normal random absorption coefficient of the lining (not incident absorption),
h = smallest inside cross-section dimension (mm)
P = inside cross-section perimeter (mm)
A = cross-section area (mm2)
L = length of duct (m)
f = frequency (Hz)
d = density of lining (kg/m3)
w = larger cross-section dimension (mm)
K_1 = 0.0214
K_2 = 0.19
K_4 = 3.32E18
K_5 = -3.79

The above prediction model is empirical and is, therefore, limited in application to test cases similar to those tested in the experiments. Testing of the formulae reveals that the curve becomes discontinuous if the aspect ratio (w/h) is large (Kuntz and Hoover base their method on tests of three cross sections with a maximum aspect ratio of 2).

Theoretically, transmission loss in a duct is linearly proportional to length and lined perimeter, and inversely proportional to cross sectional area:

$$\mathbf{TL} = \mathbf{L}\left(\frac{\mathbf{P}}{\mathbf{A}}\right)\theta_{\text{geometry}} \tag{7}$$

where $\theta_{geometry}$ is some complex function that depends on the geometry of the duct (aspect ratio),

the properties of the lining, the sound frequency, and the air temperature. Kuntz and Hoover maintain this relationship in their prediction method, using two complex equations for $\theta_{geometry}$ in each frequency range. Obviously, then, the goal is to maximize length and perimeter while minimizing cross sectional area. Further, according to Kuntz and Hoover, designs should also use a lining with low density and a large absorption coefficient.

It is not enough, however, to design an aero-acoustic wall opening that only optimizes sound transmission loss (if that were the case, a solid wall would suffice). Instead, the two designs must strike a balance for airflow and acoustic performance so that they meet both design goals.

2.6 AIRFLOW PREDICTION

The two designs comprise these four components: an entrance, an exit, one or more bends, and one or more lengths of straight lined duct.

Pressure loss for incompressible fluid flow through a duct system is the sum of the pressure losses through each component of the system, assuming the components are spaced far enough apart so that their streams do not mix (i.e. – entrance, exit, length of straight duct, bend, expansion, contraction, etc.):

$$\Delta P_{total} = \sum_{i=1 \rightarrow n} \tfrac{1}{2} k_i \rho u_i^{\,2} \tag{8}$$

where:

ΔP = total pressure loss through all components of the duct system, Pa,
n = number of components in the duct system,
u_i = mean velocity through the cross section at each component, m/s,
k_i = $k_{local} + k_{friction}$ = overall pressure loss coefficient for each component,
k_{local} = local dynamic pressure loss coefficient,
$k_{friction}$ = viscous pressure loss coefficient,

Each opening, bend, or length of duct has a characteristic pressure-loss coefficient (k) that determines its pressure loss behavior. That overall k-value is the sum of a local dynamic pressure loss coefficient (k_{local}) and a viscous pressure loss coefficient ($k_{friction}$). Idel'Chik (1994)

compiled an expansive set of empirical pressure loss data for various duct components and geometries. The results of his work are "sufficiently basic to allow application to nearly any shape of flow passage encountered in engineering practice," (Editor's preface to the third edition). Simple addition of the pressure loss coefficients for each component provides, with limited accuracy, an estimate of the overall pressure loss coefficient through the duct system. The data provides a first-order understanding of how geometry will affect the overall airflow performance of the transfer duct and U-shaped duct. This analysis refined and verified in chapter 3 by a computational fluid dynamics (CFD) analysis.

Transfer Duct

For the transfer duct, the sum of three component pressure losses indicates the overall pressure loss: dynamic pressure loss at an entrance that immediately goes into an angle, friction pressure loss of a straight duct, and dynamic pressure loss at an exit that immediately follows a bend. The data below describes the losses as functions of duct geometry.

Entrance Component (into an Angle)

The entrance into the transfer duct is approximately the same as an entrance that is flush and at an angle of 20 degrees with the wall as shown in figure 2.11 (20 degrees is the smallest angle tested). The aspect ratio, w/h, is the variable of interest (h is the height of the opening in the plane of the bend, and w is the width of the opening).

As seen, a large aspect ratio (w/h) gives a lower pressure loss coefficient. This estimate for entrance loss,

w/h	∞	1	0.5	0.2
k (at 20 degrees)	0.85	0.96	1.04	1.58

Figure 2.10 – k-values for angled inlet at 20 degrees.

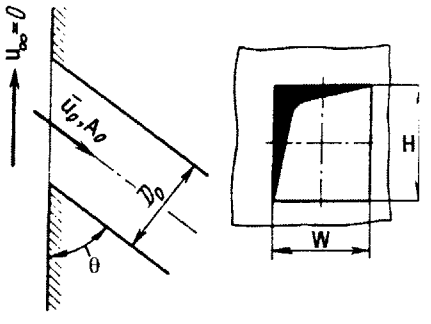

Figure 2.11 – angled inlet.

however, is a likely source of error since the actual geometry of a transfer duct entrance (i.e. – a sharp bend) is not an angled inlet.

Straight Duct Component (friction)

Similar to the commonly used Moody chart, Idel'Chik has assembled data for the pressure loss coefficient of ducts as a function of roughness, Reynolds number, and hydraulic diameter. The duct lining has an equivalent sand grain roughness of approximately 2mm (derived from Johns Manville Corporation literature). The following equations assist in deriving the overall k-value from the charts below (figures 2.12 and 2.13).

$$\mathbf{k_{friction} = \lambda' \frac{L}{D_h}}$$

$$\mathbf{\lambda' = C\lambda}$$

$$\mathbf{Re = \frac{\rho u D_h}{\mu}}$$

$$\mathbf{D_h = 4\frac{A}{P}}$$

$$\mathbf{\overline{\Delta} = \frac{\Delta}{D_h}}$$

where:

$k_{friction}$ = viscous pressure loss coefficient through straight duct,
L = length of duct, m,
C = correction factor for rectangular ducts,
λ = function of Reynolds number and average surface roughness (in chart),
Re = Reynolds number,
U = average velocity through cross section, m/s,
μ = dynamic viscosity, Ns/m^2,
D_h = hydraulic diameter, m,
A = cross section area, m^2,
P = wetted perimeter, m,
Δ = sand grain roughness, m.

Values of λ	Re								
$\overline{\Delta}$	3×10^3	4×10^3	6×10^3	10^4	2×10^4	4×10^4	6×10^4	10^5	2×10^5
0.05	0.077	0.076	0.074	0.073	0.072	0.072	0.072	0.072	0.072
0.04	0.072	0.071	0.068	0.067	0.065	0.065	0.065	0.065	0.065
0.03	0.065	0.064	0.062	0.061	0.059	0.057	0.057	0.057	0.057
0.02	0.059	0.057	0.054	0.052	0.051	0.050	0.049	0.049	0.049
0.015	0.055	0.053	0.050	0.048	0.046	0.045	0.044	0.044	0.044
0.010	0.052	0.049	0.046	0.043	0.041	0.040	0.039	0.038	0.038
0.008	0.050	0.047	0.044	0.041	0.038	0.037	0.036	0.035	0.035
0.006	0.049	0.046	0.042	0.039	0.036	0.034	0.033	0.033	0.032

Figure 2.12 – Table of λ versus Reynolds number and surface roughness for circular ducts.

w/h	10	5	2.5	1.67	1.25	1.0
C	1.08	1.06	1.04	1.02	1.01	1.00

Figure 2.13 – Table of correction factor, C, for rectangular ducts versus aspect ratio.

Figure 2.12 shows that larger Reynolds numbers and larger hydraulic diameters give smaller values for λ, and thus a smaller k-value. Further, smaller aspect ratios produce a slightly smaller correction factor (figure 2.13).

Exit Component (after a bend)

For an exit that immediately follows a sharp 90-degree bend (figure 2.14), figure 2.15 gives the k-value as a function of the cross-sectional aspect ratio (w/h), and the height ratio.

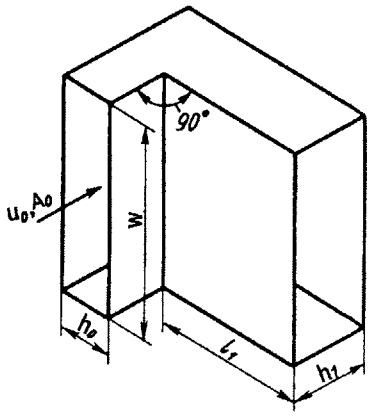

Figure 2.14 – exit after a bend.

Value of k	w/h		
h_{in}/h_{out}	4.0	1.0	0.25
0.5	9.9	9.0	8.8
1.0	3.2	2.9	2.7
1.4	2.0	2.0	1.8
2.0	1.3	1.3	1.3

Figure 2.15 – Table of k-values for an exit component immediately following a bend.

Overall, the exit losses of the transfer duct are most significant (compared to the other two components), and increasing the flow area at the exit bend by making its height twice that of the internal cross section will minimize the pressure loss.

U-Shaped Duct

For the U-shaped duct, four component pressure losses from Idel'Chik (1994) add to give the overall pressure loss: dynamic pressure loss at an entrance with one side tangent to the wall, friction pressure loss of the straight duct, dynamic pressure loss at a 180 degree bend, and dynamic pressure loss at an exit with one side tangent to the wall.

Entrance Component (along a wall)

Idel'Chik gives the pressure loss coefficient, k, for a duct mounted flush on a wall as 0.63 regardless of geometry (shown in figure 2.16).

Straight Duct Component

The straight duct component losses are the same as they are for the transfer duct, above.

Bend Component (180 degrees)

The pressure loss coefficient in a 180-degree bend depends on the geometry of the bends and whether the corners are sharp or rounded. Figure 2.17 shows the sharp bend and figure 2.18 shows the rounded bend. (h_k in figure 2.18 is the same dimension as h_{el} in figure 2.17.)

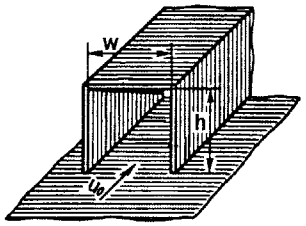

Figure 2.16 – entrance flush with the wall.

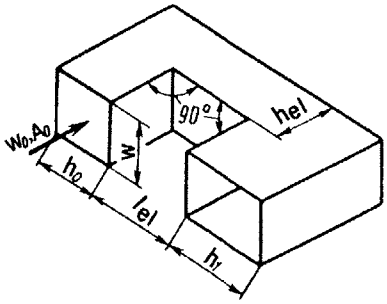

Figure 2.17 – sharp U-bend.

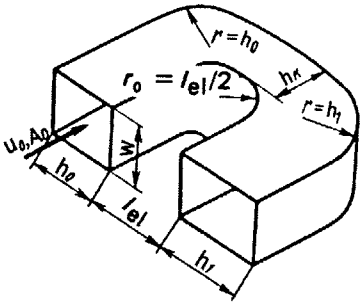

Figure 2.18 – rounded U-bend.

Values of k	L_{elbow}/h_0										
h_{elbow}/h_0	**0.0**	**0.2**	**0.4**	**0.6**	**0.8**	**1.0**	**1.2**	**1.4**	**1.6**	**1.8**	**2.0**
0.5	7.9	6.9	6.1	5.4	4.7	4.3	4.2	4.3	4.4	4.6	4.8
0.73	4.5	3.6	2.0	2.5	2.4	2.3	2.3	2.3	2.4	2.6	2.7
1.0	3.6	2.5	1.8	1.4	1.3	1.2	1.2	1.3	1.4	1.5	1.6
2.0	3.9	2.4	1.5	1.0	0.8	0.7	0.7	0.6	0.6	0.6	0.6

Figure 2.19 – Table of k-values for 180-degree bend with sharp corners

Values of k	L_{elbow}/h_0									
h_{elbow}/h_0	**0.2**	**0.4**	**0.6**	**0.8**	**1.0**	**1.2**	**1.4**	**1.6**	**1.8**	**2.0**
0.5	4.5	2.6	1.9	1.7	1.5	1.3	1.2	1.1	1.0	0.9
0.73	2.5	1.5	0.9	0.7	0.5	0.5	0.4	0.4	0.4	0.3
1.0	1.6	0.9	0.5	0.3	0.3	0.3	0.2	0.2	0.2	0.3
2.0	1.6	1.0	0.8	0.7	0.6	0.5	0.5	0.4	0.4	0.4

Figure 2.20 – Table of k-values for 180-degree bend with rounded corners. (The amount of rounding is a function of the other dimensions, shown in figure 2.18.)

Figures 2.19 and 2.20 show the k-values, as a function of duct geometry, for the sharp U-bend and the rounded U-bend, respectively. For both bends, it is critical to ensure that h_{elbow} is at least as large as h_0. If the bend has sharp corners h_{elbow}/h_0 should be equal to 2.0 and L_{elbow}/h_0 should be between 1.0 and 1.4. If the bend has rounded corners, h_{elbow}/h_0 should be equal to 1.0 and L_{elbow}/h_0 should be between 1.0 and 1.4. Under these conditions, rounded corners will halve the k-value versus sharp corners (0.3 versus 0.7), but either case gives an adequately low k-value.

Exit Component (along wall)

While Idel'Chik (1994) does not specifically identify data for an exit along a wall, it will have a pressure loss coefficient no greater than about 1.0 (that of a standard open-duct discharge) and no less than about 0.5 (that of an optimum baffled exit). There is not much room for improvement at the exit without adding baffles, so the pressure coefficient of the exit will likely be closer to 1.0.

Chapter 3
Experiments

3.1 EXPERIMENTAL SETUP

Based on the acoustic prediction models the prototype designs should maximize duct length, cross-sectional aspect ratio, and the lining's absorption coefficient while minimizing the lining's density. Fortunately, the airflow prediction model indicates that a large cross-sectional aspect ratio will reduce pressure loss at the entrance and the straight duct components while not significantly increasing pressure loss at any other component, and that increasing duct length will only slightly increase pressure loss.

Two specific prototype designs emerge from the above results. Figure 3.1 details the U-shaped duct prototype (as-built) and figure 3.2 details the U-shaped duct prototype (as-built).

For consistency, both prototype designs have the same cross-section dimensions and use the same materials. Both have a cross-section with dimensions: h=2.5 inches

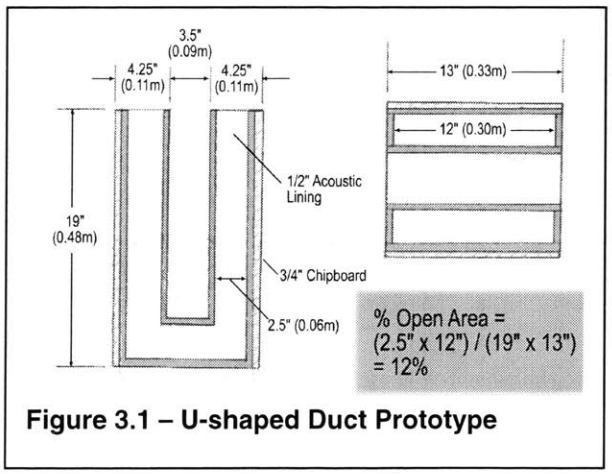

Figure 3.1 – U-shaped Duct Prototype

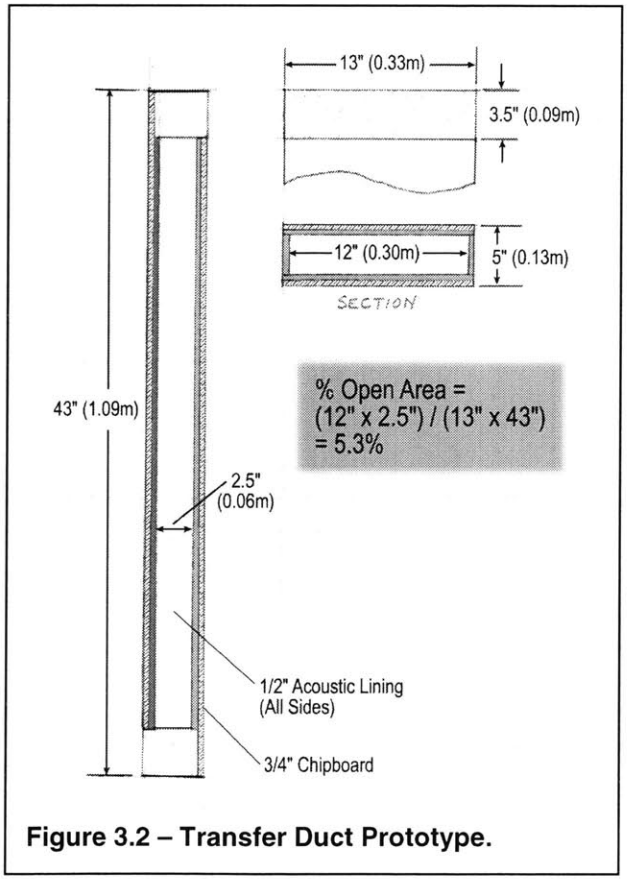

Figure 3.2 – Transfer Duct Prototype.

(0.0635m) and w=12 inches (0.3048m) as measured from the inside perimeter of the lining surface (giving an aspect ratio [w/h] of 5). The 'h' dimension is chosen so that the transfer duct will fit inside a standard 2"x4" stud-construction wall. The U-duct fits over the outside surfaces of the wall, so it does not need to be as narrow (though, for aesthetics, it should not protrude too far away from the wall). The combined length of straight lined duct is 3 feet (0.9144m) for both prototypes. Three-quarter inch chip board makes up the wall faces (its mass is similar to gypsum board, but is easier to work with during experiments); all ductwork uses sheet metal and is sealed with duct tape; ½" Permacoat Linacoustic lining by Johns Manville (found to have the highest absorption to density ratio of popular linings on the market) was attached to the ducts using adhesive "Stick-Clips™." Joints were sealed with "Diversi-Gum™," a high-density clay-like compound, and covered with duct tape. Figure 3.3 shows the test section (seen from inside the source room) before the U-shaped duct prototype is installed.

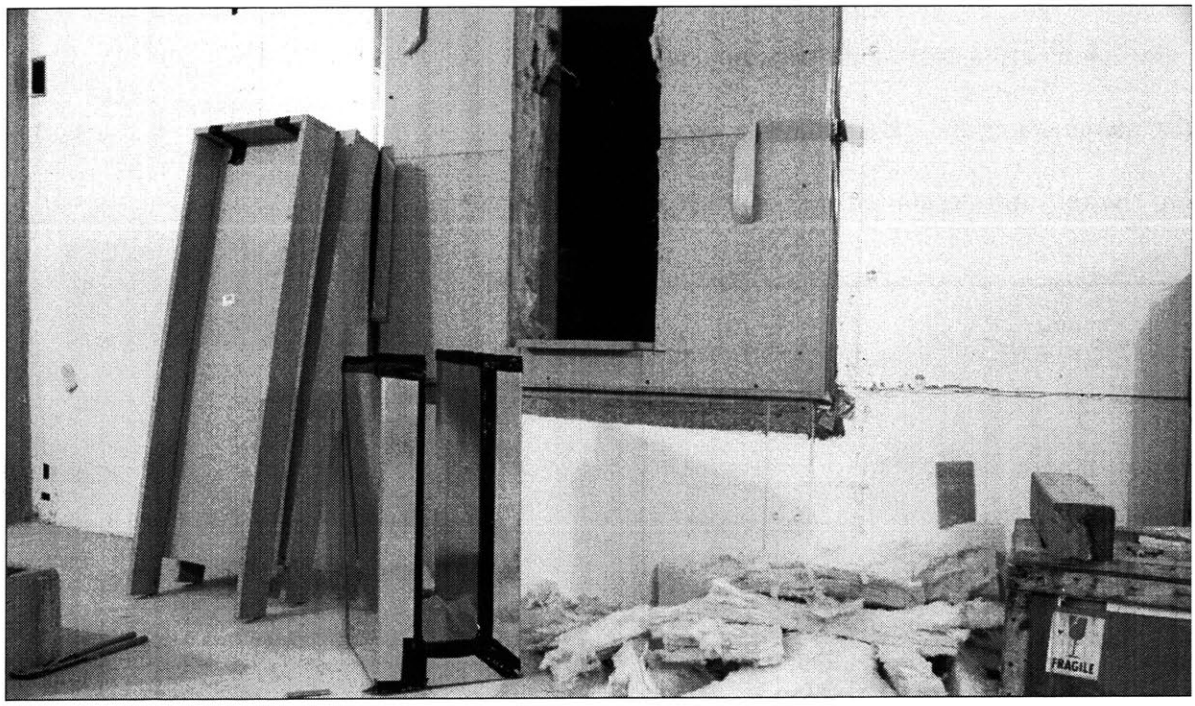

Figure 3.3 – Test section (seen from the source room) during installation of the U-shaped duct.

According to the acoustic predictions, both prototypes should significantly fail to meet the design goal of a sound transmission class (STC) rating of 25 (see section 1.4 for a definition of STC). The predictions indicate an STC rating of only 8, because of poor predicted performance at higher frequencies. This, in fact, is not true, and experimental results reveal (in section 3.2) that the acoustic prediction method drastically under-predicts high frequency transmission loss, so the above result can be ignored for now.

The airflow prediction method indicates that the transfer duct will have an overall k-value of $k_{entrance}(0.85) + k_{friction}(0.5) + k_{exit}(1.3) = 2.65$. The open area of the transfer duct prototype is 4.6%. The U-shaped duct will have an overall k-value of $k_{entrance}(0.63) + k_{bend}(0.7) + k_{friction}(0.5) + k_{exit}(1.0) = 2.83$. The open area of the U-shaped duct prototype is 12%.

When the predicted k-values are plugged into the reference apartment for airflow performance (detailed in section 2.1), the U-shaped duct will meet the airflow design goal (set in section 2.2), but the transfer duct will not. Figure 3.4 details the results ("wall area required" is the area occupied by the devices to pass 10 ACH with a total pressure gradient of 10Pa). Further testing and investigation are necessary to fully understand the performance of both designs and to derive solid conclusions. Chapter 4, Refined Designs, further explores the designs and their performances.

	k-value	%open area	Wall area required by device	Wall area available	Pass/fail?
Transfer Duct	2.65	5.3%	18.9 m^2	15 m^2	Fail
U-shaped Duct	2.83	12%	8.6 m^2	15 m^2	Pass

Figure 3.4 – summary of airflow prediction results for the "as-built" prototypes.

3.2 ACOUSTIC EXPERIMENTS

3.2.1 Procedure

Testing the noise transmission loss (TL) of the prototypes according to ASTM Standard E90-97 provides quantitative results of noise performance for the prototypes. BBN Laboratories in Cambridge, Massachusetts provided reverberant test chambers for the experiments. The facility comprises two "reverberant" rooms (a source room and a receiver room, each with minimal acoustic absorption) connected by a concrete wall with a removable section for mounting test specimens (figures 3.5, 3.7, and 3.8). A centrifugal sound source (Bruel & Kjaer type 4204, figure 3.6) creates a uniform sound field near 90 dBA (between 100 Hz to 10,000 Hz) in the source room. The sound travels through the test specimen into the receiver room where the room absorbs some sound while the rest produces a uniform sound field. A sound analyzer (B&K 2260 Investigator) measures the sound spectrum at six spatial points in the source room and at six spatial points in the receiver room (figure 3.5).

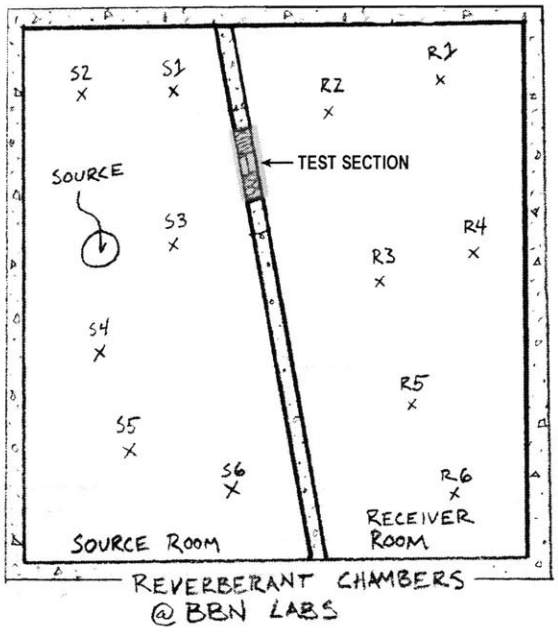

Figure 3.5 - Plan Drawing of Test Chambers. "S" points are microphone locations in the source room, and "R" points are microphone positions in the receiver room.

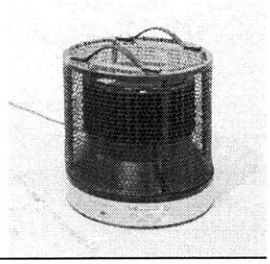

Figure 3.6 - B&K centrifugal sound source (type 4204) and its average spectrum as measured in the source room.

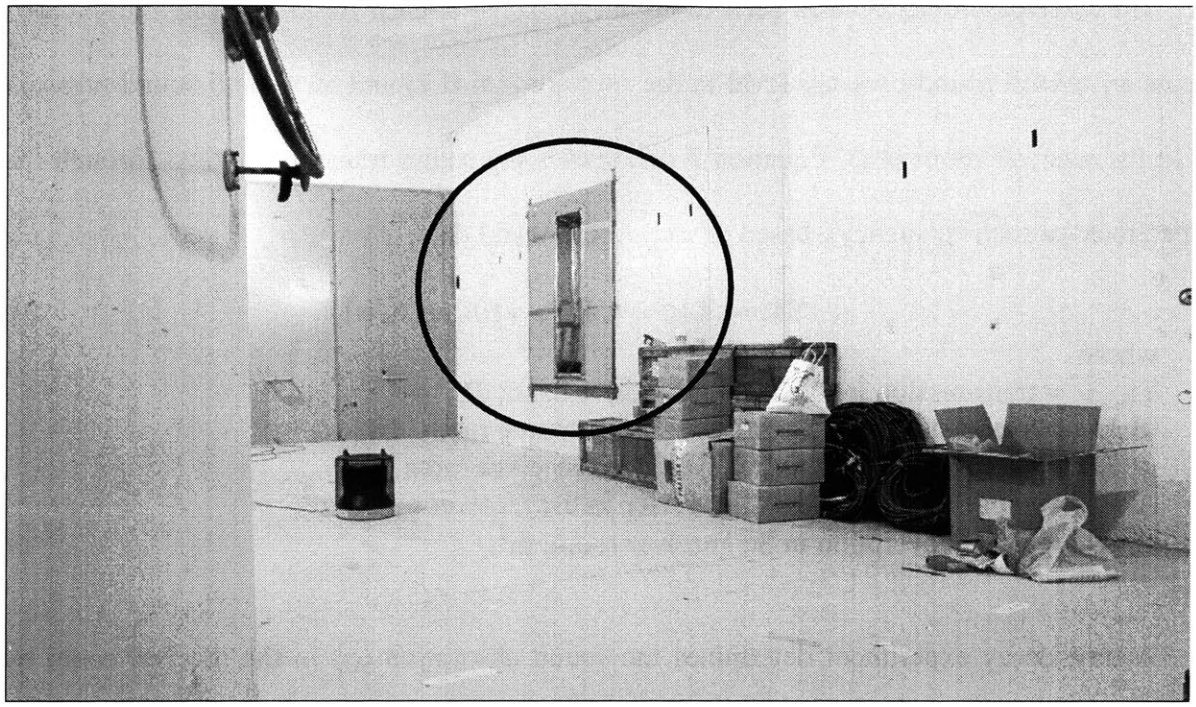

Figure 3.7 – Picture of source room with transfer duct prototype fully mounted in test section.

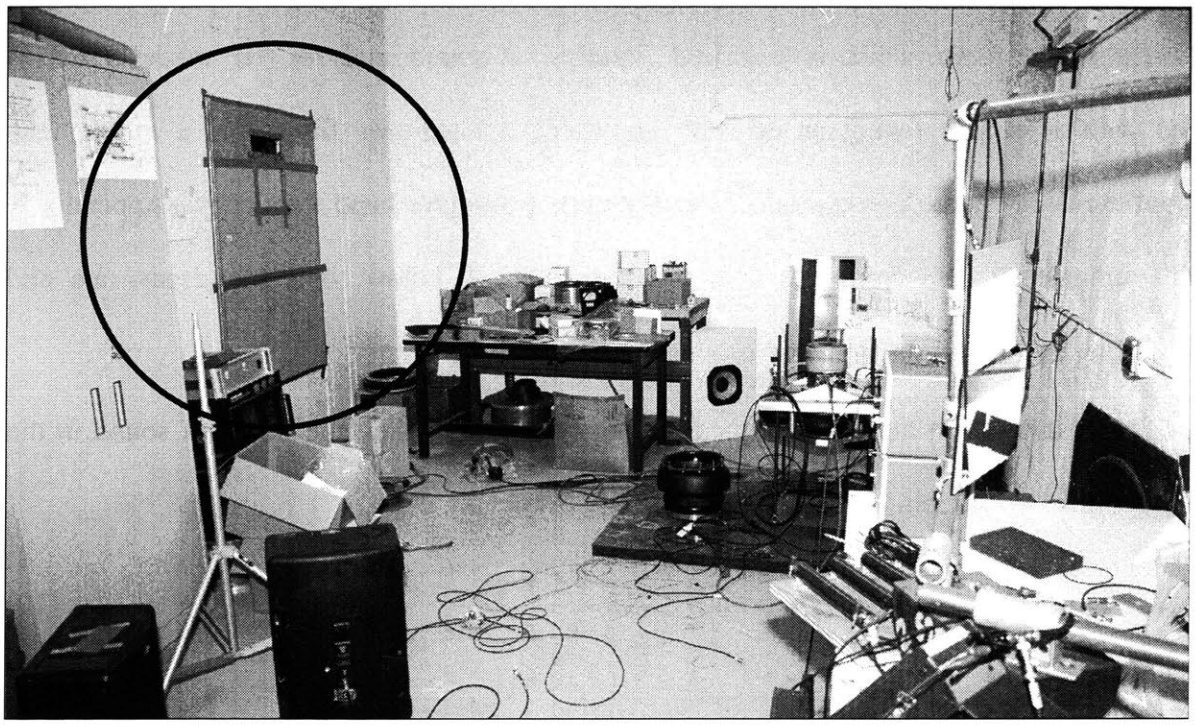

Figure 3.8 – Picture of receiver room with transfer duct prototype fully mounted in test section.

The six measurements from each room are averaged at each frequency (logarithmically) to create an overall sound-pressure level in the source room (L1) and an overall sound-pressure level in the receiver room (L2). Equation 9 determines the sound transmission loss through the test specimen (at each frequency), based on the experimental data:

$$\mathbf{TL} = <\mathbf{L1}> - <\mathbf{L2}> + 10\mathrm{Log}(\mathbf{A}/\boldsymbol{\alpha}) \tag{9}$$

where:
TL = transmission loss at each 1/3-octave band, dB,
<L1> = average sound pressure level in the source room, dB,
<L2> = average sound pressure level in the receiver room, dB,
A = wall area occupied by the device in the receiver room, m^2,
α = sound absorption in the receiver room, m^2.

A time-decay experiment determines the sound absorption (α) in the receiver room by measuring how quickly a uniform sound field decays at each frequency after the sound source stops (the source room's absorption is not important to know because it only effects the sound field in the source room, which is measured directly). A sound analyzer (HP model 35670A) coupled with a speaker (using an 80-watt amplifier), a band-pass filter, and a microphone measured the decay rate (dB/second) of sound at each 1/3-octave band frequency. Appendix A contains time-decay data from the tests while figure 3.9, below, lists the decay rate and corresponding absorption (α) at each frequency.

The absorption in the room at each frequency relates to the time decay of sound in the room according to equation 10 (ASTM Standard E90-97):

$$\mathbf{a} = 0.921\left(\frac{\mathbf{Vd}}{\mathbf{c}}\right) \tag{10}$$

where:
a = sound absorption in the room, m^2 or Sabines,
V = volume of the room, m^3 (87.8 m^3 in receiver room),
c = speed of sound in air, m/s (343.3 m/s at 20°C), and
d = decay rate of the sound pressure level in the room, dB/second.

Frequency (Hz)	100	125	160	200	250	320	400	500	640	800	1,000
Decay rate (dB/s)	41	44	104	53	61	51	56	48	63	52	60
Absorption (m^2)	9.7	10.4	24.7	12.5	14.3	11.9	13.3	11.2	14.7	12.3	14.1

(continued)	1,250	1,600	2,000	2,500	3,150	4,000	5,000	6,300	8,000	10,000
Decay rate (dB/s)	56	56	58	62	61	64	75	86	105	124
Absorption (m^2)	13.2	13.2	13.7	14.5	14.4	15.2	17.6	20.3	24.7	29.3

Figure 3.9 – Decay rate measurements and corresponding absorption for receiver room.

After finding the absorption values, work began on the actual transmission loss experiments. Initial transmission loss experiments on straight, lined ducts provide data for comparison with manufacturer's data and with the prediction methods. Two straight ducts (12" x 12" x 48", and 2.5" x 12" x 36" – inside dimensions) lined with 1/2" acoustic lining (Johns Manville Permacoat Linacoustic brand) were tested. The ducts (detailed in figure 3.10) fit in the specimen wall so they are flush with the source room wall and protrude into the receiver room.

The final transmission loss experiments called for mounting the two prototypes in the specimen wall. Figure 3.11 shows the installed transfer duct prototype, and figure 3.12 shows the installed U-shaped duct prototype.

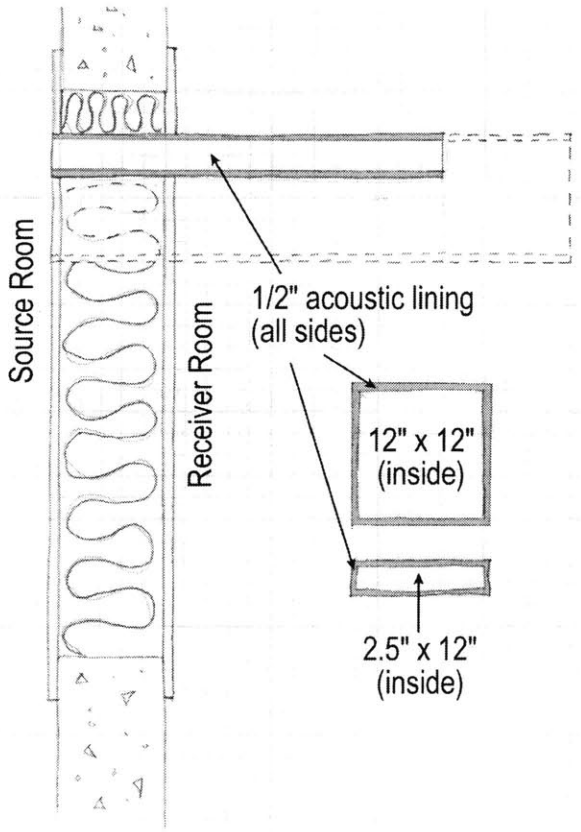

Figure 3.10 – Detail of straight ducts, as mounted for testing (12"x12" and 2.5"x12" inside cross sections).

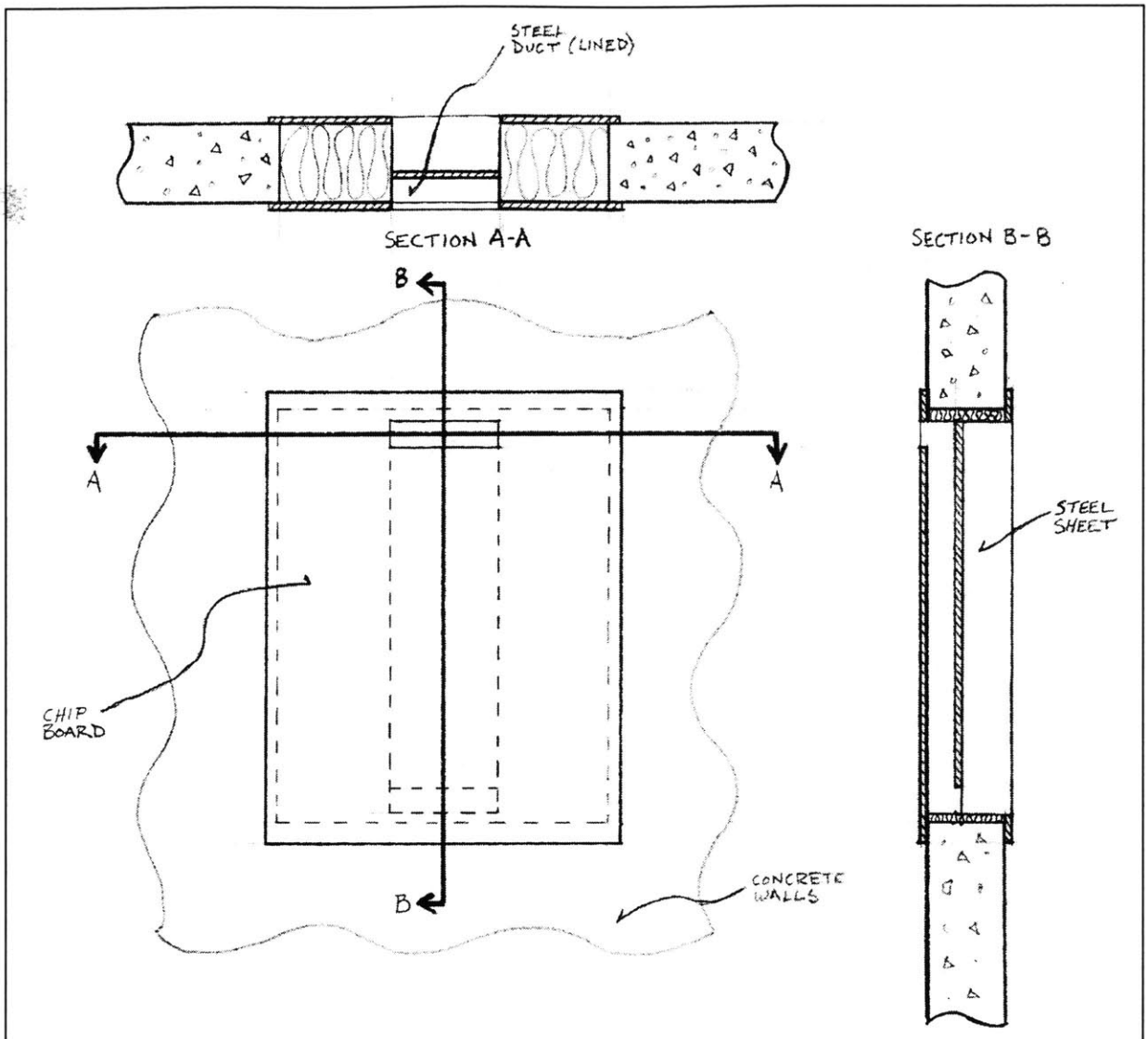

Figure 3.11 – Detail of the transfer duct prototype installed in the test section. Duct dimensions are given in figure 3.2.

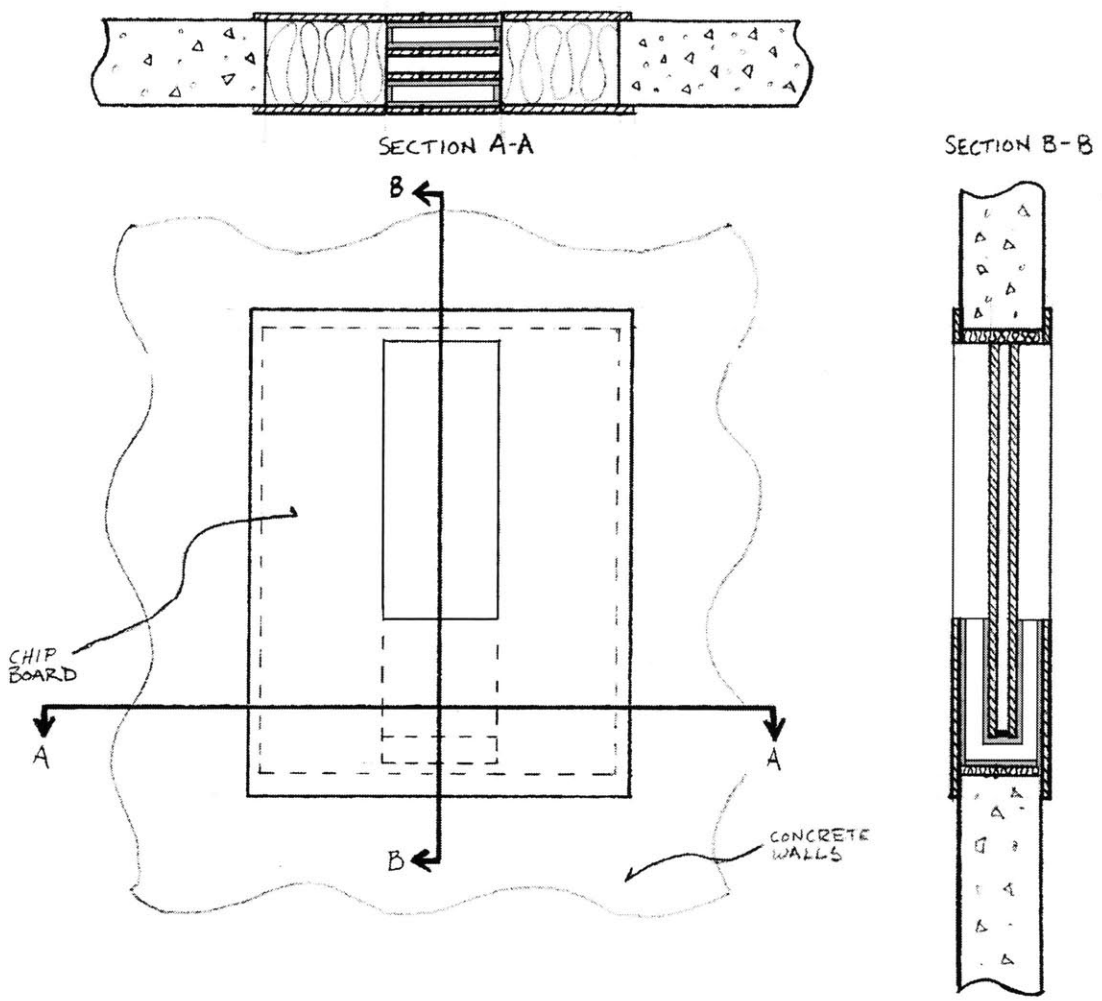

Figure 3.12 – Detail of the U-shaped duct prototype installed in the test section. Duct dimensions are given in figure 3.1.

3.2.2 Results

The straight duct tests reveal that the two cross-sections (12"x12" and 2.5"x12") behave quite differently. Figure 3.13 shows the experimental results from the two straight-duct tests along with the predicted results (Kuntz and Hoover, 1987) for both duct cross sections. Kuntz and Hoover's (1987) prediction method (from chapter 2) represents the square duct's performance (12"x12") fairly well, but fails for the rectangular duct (2.5"x12") especially at frequencies above 1000 Hz. (*Appendix A includes complete data for all the experiments in this section.*)

The prototypes exhibit similar noise transmission-loss curves as the 2.5"x12" straight duct (experimental data). Figure 3.14 plots the experimental data for both prototypes along with the experimental data for the straight duct. The transfer duct produces a sound transmission class

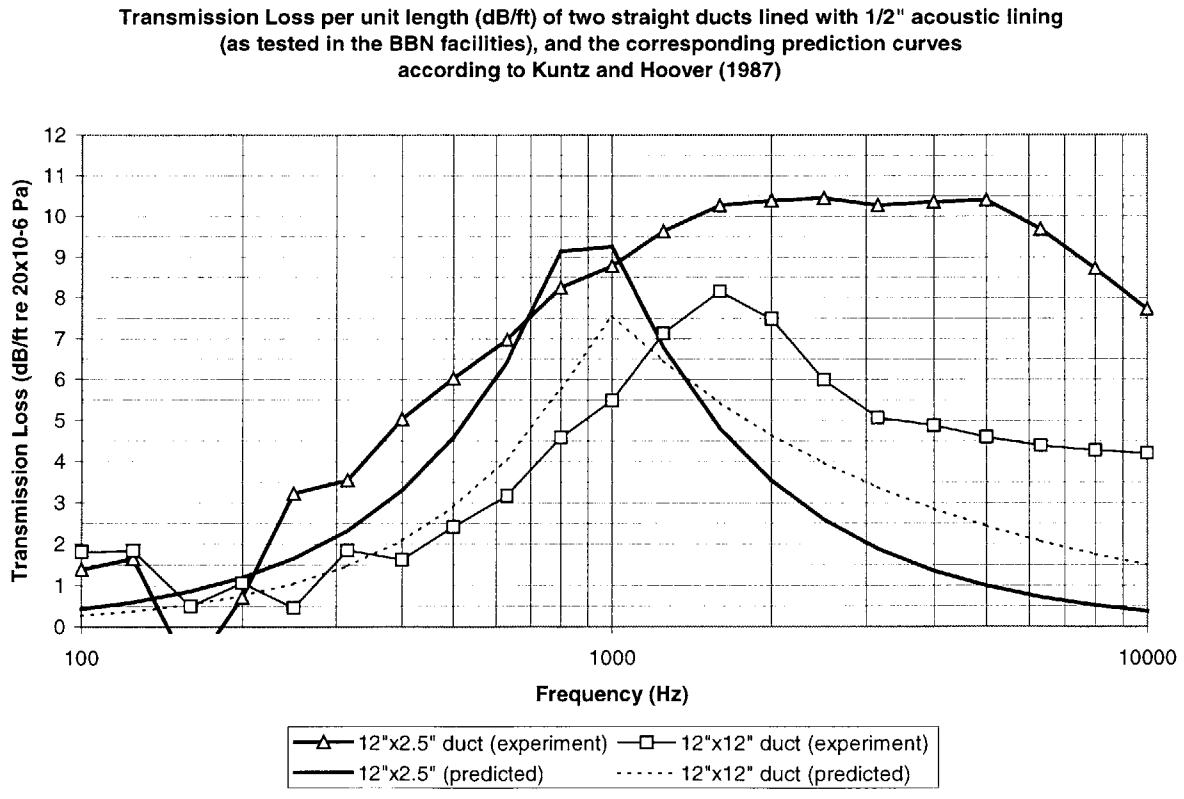

Figure 3.13 – Experimental transmission loss (dB) of straight ducts (as detailed in figure 3.10) plotted along with prediction curves for each duct.

(STC) rating of 21 (see description of STC in *Chapter 1, Introduction*), while the U-shaped duct produces an STC rating of 23. Figure 3.15 shows the STC-23 curve plotted against the transmission loss spectrum of the U-shaped duct. One should note that the critical deviation occurs at the lower frequencies (this is also true for the transfer duct); therefore, improvements in the design will target low-frequency performance to increase STC rating.

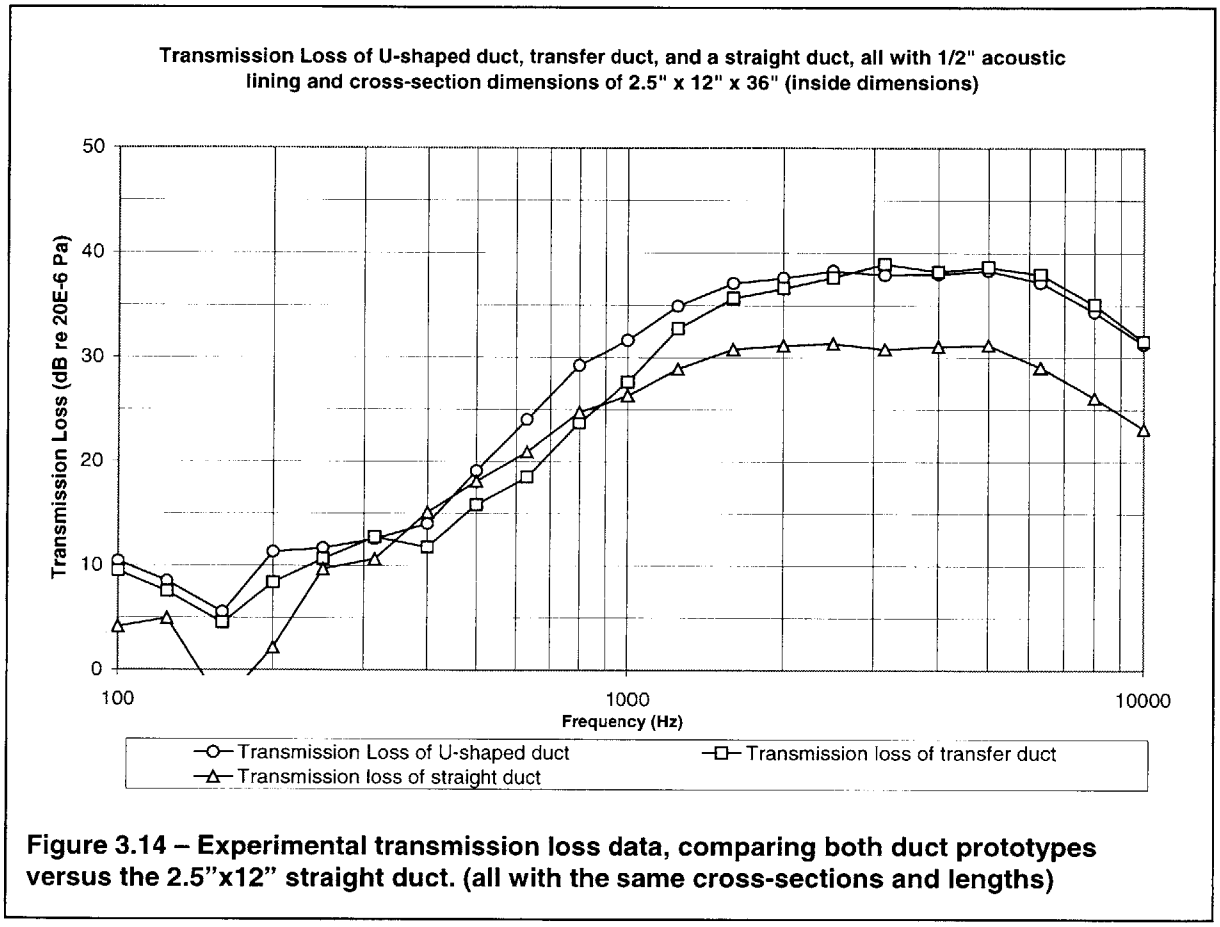

Figure 3.14 – Experimental transmission loss data, comparing both duct prototypes versus the 2.5"x12" straight duct. (all with the same cross-sections and lengths)

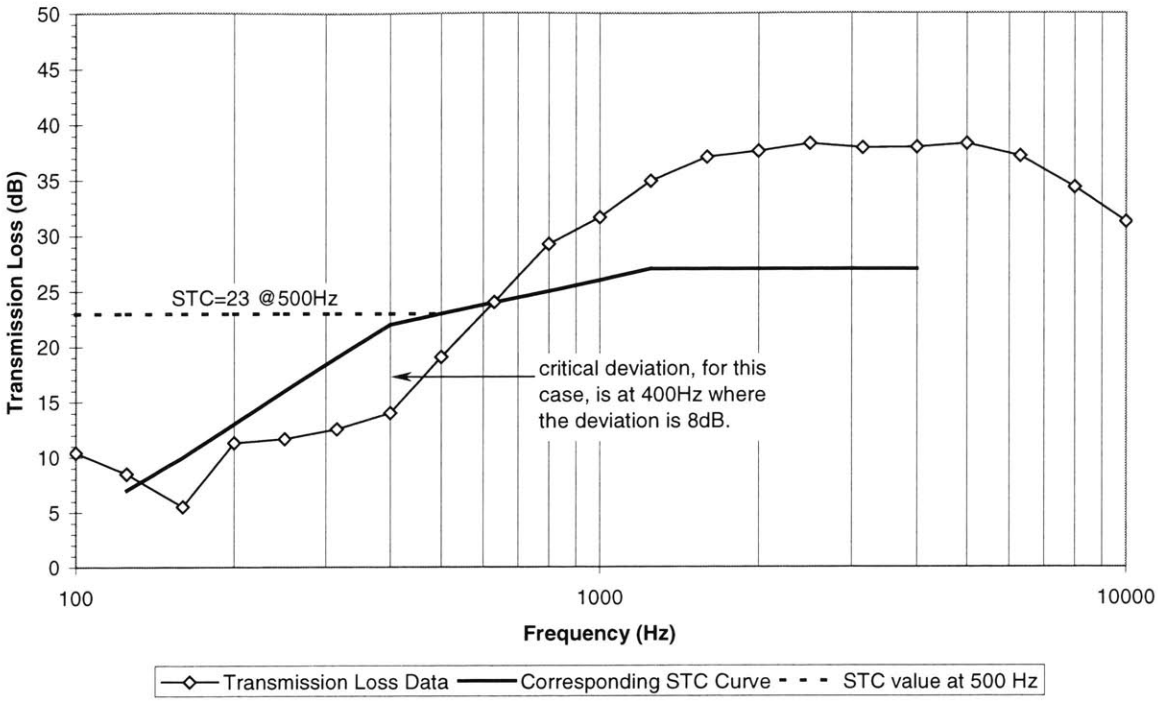

Figure 3.15 – STC-23 curve-fit of U-shaped duct transmission loss curve.

In figure 3.17, for the transfer duct, one curve shows transmission loss when all sides of the duct are lined, and the other curve shows the transmission loss when just one side is lined.

In figure 3.18, for the U-shaped duct, one curve shows transmission loss when the corners of the duct-bends are sharp and fully lined, and the second curve shows transmission loss when a curved piece of unlined sheet metal is installed at the base of the bend (as illustrated in figure 3.16).

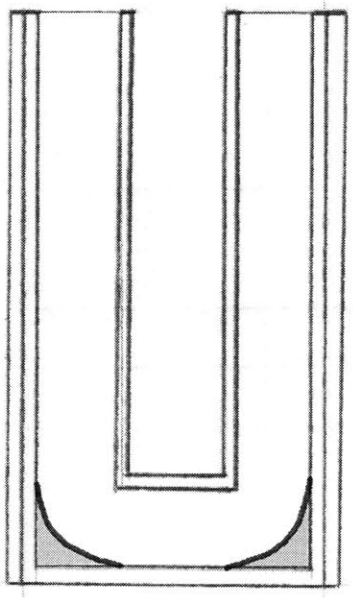

Figure 3.16 – Corners of U-shaped duct are rounded with a piece of curved sheet metal (fiber glass is inserted behind metal).

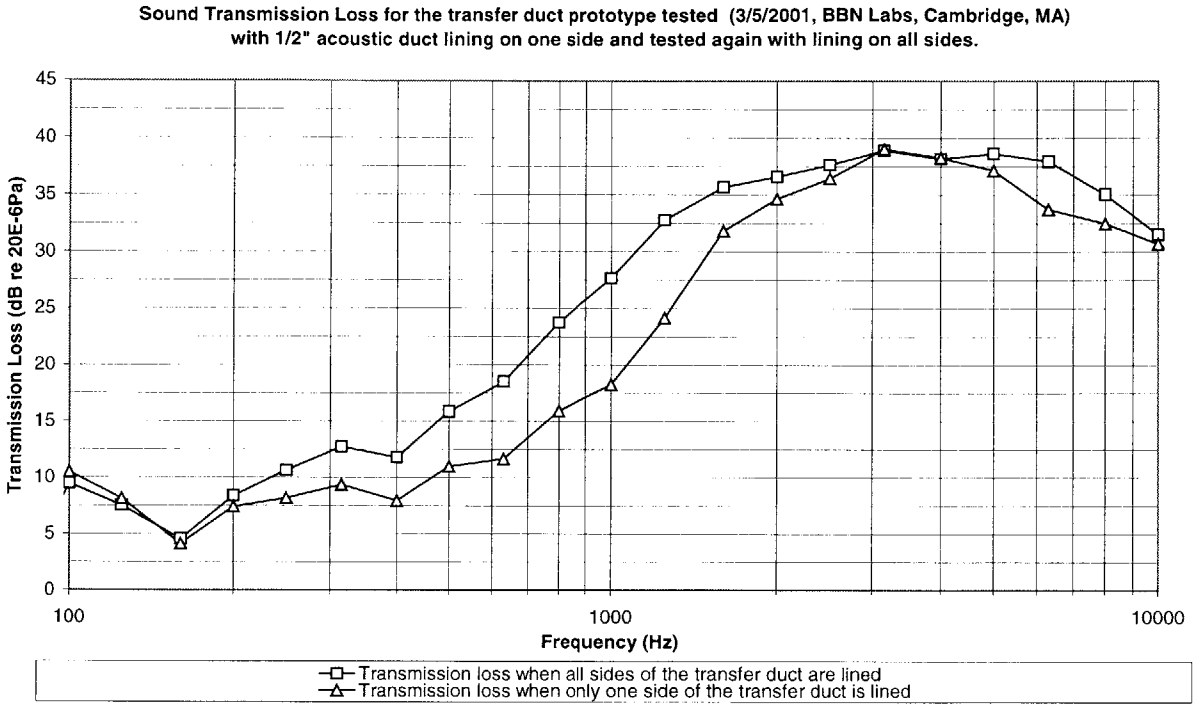

Figure 3.17 – Experimental transmission loss curves for the transfer duct, tested with acoustic lining on just one side and again with lining on all sides.

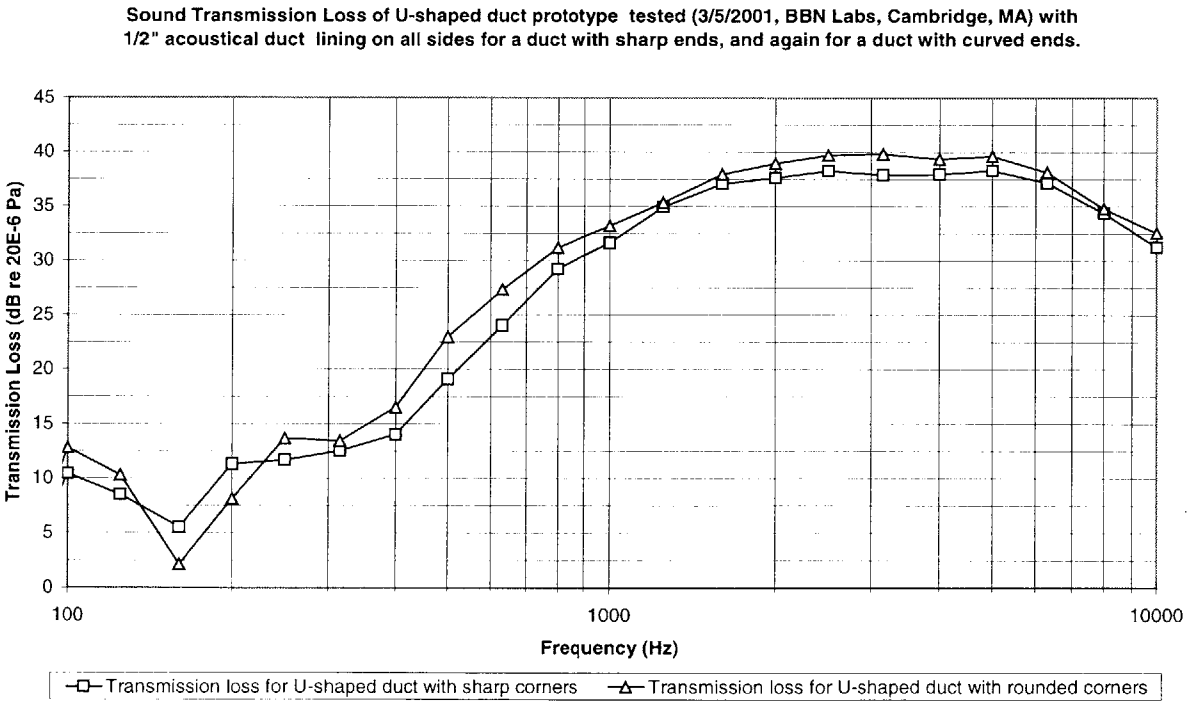

Figure 3.18 – Experimental transmission loss curves for the U-shaped duct, tested with sharp bends and again with rounded bends.

Based on these results, the overall transmission loss through either a transfer duct or a U-shaped duct is determined almost exclusively by the transmission loss through the straight lined section of duct, while any bends, entrances, or exits have only a minor effect. Later, in section 4.1, the refined acoustic prediction method utilizes this idea – that the total transmission loss of these aero-acoustic wall openings is primarily driven by the length of lined duct.

3.2.3 Discussion

The experiments provide four important conclusions:

- Both prototypes nearly meet the design goal of an STC-25 rating for noise transmission loss (the transfer duct has an STC rating of 21 and the U-shaped duct has an STC rating of 23).
- Lining just one side of a duct reduces the low-frequency (<2000 Hz) transmission loss of the duct by approximately 2-4 dB/ft. (which is significant since low-frequency transmission loss is already a problem area).
- A curved corner does not notably degrade the transmission loss versus a sharp corner.
- The prediction method proposed by Kuntz and Hoover (1987) predicts the 2.5"x12" duct completely wrong, and predicts the 12"x12" duct well at lower frequencies but only marginally well at higher frequencies.

Kuntz and Hoover is the currently accepted ASHRAE method, but is only verified for square cross-sections. The results above indicate that Kuntz and Hoover is not valid for ducts that have cross sections with large aspect ratios. Further modeling and prediction for the design of aero-acoustic wall openings will use alternative prediction methods described in section 4.1.

3.3 AIRFLOW COMPUTATION

3.3.1 Procedure

A Computational Fluid Dynamics (CFD) software program (PHOENICS 3.1) finds the pressure loss coefficient (k) of the prototypes (as built). The program uses discretized fluid mechanics equations and conservation of mass principles to find average velocity vectors at each grid point. Turbulent airflow is modeled using the k-ε turbulence model.

The prototypes are modeled in the software by "mounting" them in the center of a solid wall (3m x 3m x 0.1016m [9.8ft x 9.8ft x 4in]) that sits perpendicular to the flow in an enclosed channel (30m x 3m x 3m [98ft x 9.8ft x 9.8ft]) at 12m (39ft) downstream from a fixed volume-flow source (0.01 m^3/s [21cfm]) and upstream from a zero-pressure outlet (figure 3.19). A smooth, no-slip condition defines the boundary of the channel walls. The duct lining is modeled using an equivalent sand-grain roughness of 2mm. Effectively, all the airflow from the fixed source flows through the prototype in the perpendicular wall and out through the zero-pressure outlet. The grid design (figure 3.20) is sufficiently fine to provide accurate results, yet coarse enough to allow timely solutions on a desktop computer with 500MHz computing speed (the average computing time for the given models and grid is approximately 10 hours).

The prototypes are modeled as detailed in figures 3.1 and 3.2 of section 3.1. Additional tests were performed on slightly altered designs to show the effect of rounding the corners of the

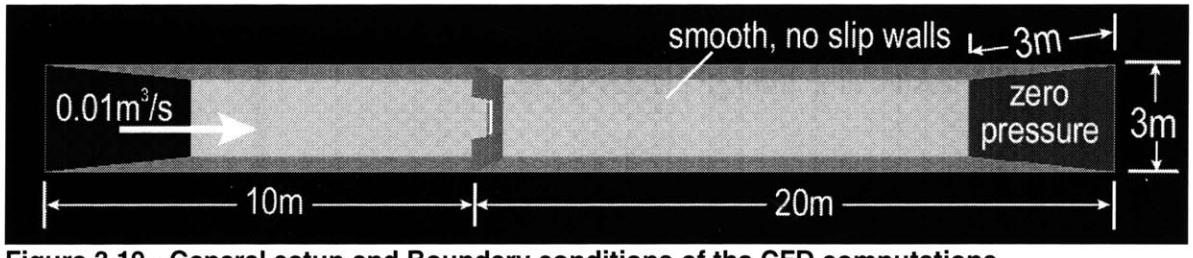

Figure 3.19 - General setup and Boundary conditions of the CFD computations.

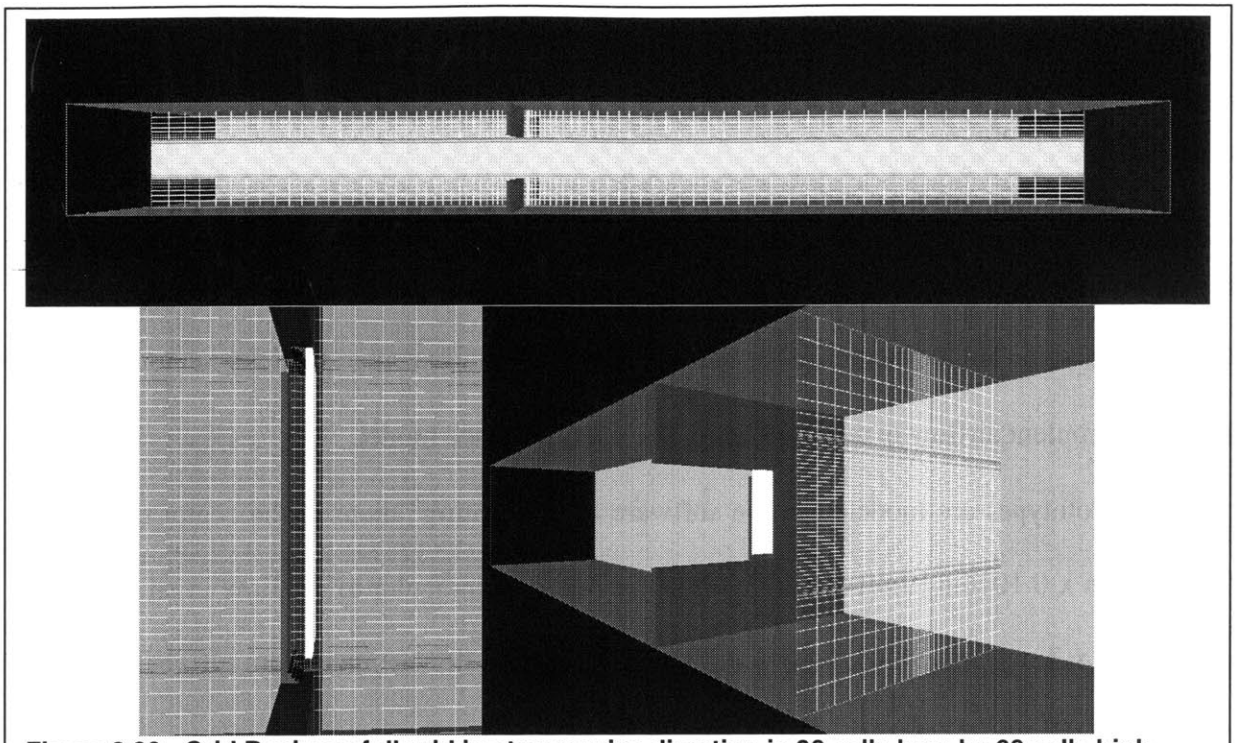

Figure 3.20 - Grid Designs: full grid in stream-wise direction is 90 cells long by 60 cells high (top), close-up of grid near the transfer duct, with rounded corners, in the stream-wise direction (left), full grid normal to stream-wise direction is 30 cells deep by 60 cells tall (right).

U-shaped duct, rounding the corners of the transfer duct, increasing the entrance and exit areas of the transfer duct, and locating the transfer duct near the floor. Figure 3.17 summarizes all of the results.

The overall pressure difference (measured as the difference in pressure near the source and near the outlet) helps calculate the overall pressure loss coefficient (k) of the prototype, using equation 11:

$$\Delta \mathbf{P} = \tfrac{1}{2}\rho \mathbf{k} \mathbf{V}^2 \qquad (11)$$

where:

ρ = density of air, kg/m^3,
k = pressure loss coefficient, dimensionless,
V = average velocity through the cross-section, m/s,
ΔP = total pressure drop through the device, Pa.

The density of air is 1.204 kg/m^3, and since the cross-sectional area of the ducts is 0.0194 m^2 ($30in^2$), the average velocity (volume flow/area) is 0.52 m/s (1.16mph) for a volume flow rate

of 0.01 m^3/s (21cfm) (giving a Reynolds Number ~ 2400, which makes the flow transitionally turbulent inside the duct).

3.3.2 Results

As designed, the transfer duct prototype has a pressure-loss coefficient (k) of 2.80 (pressure loss of 0.3869 Pa) and the U-shaped duct has a pressure loss coefficient of 2.71 (pressure loss of 0.3752 Pa). Rounding the corners of the transfer duct lowers its k-value to 2.53; doubling the entrance and exit areas of the transfer duct lowers its k-value to 1.99; both doubling the entrance and exit areas and rounding the corners of the transfer duct lowers its k-value to 1.73; rounding the corners of the U-shaped duct lowers its k-value to 2.31; and increasing the height of the bend in the U-shaped duct lowers its k-value to 2.68.

	Average Velocity (m/s)	Pressure Drop (Pa)	k-value (CFD)	k-value (Idel'Chik)	% difference
U-shaped Duct Prototype	0.48	0.45	2.71	2.83	4%
Transfer Duct Prototype	0.48	0.39	2.80	2.65	5%
Transfer Duct (at floor level)	0.48	0.46	3.31	N/A	N/A
Transfer duct (round corners)	0.48	0.35	2.53	N/A	N/A
Transfer duct (large exit and entrance)	0.48	0.28	1.99	1.98	0.5%
Transfer duct (large exit/entrance and round corners)	0.48	0.24	1.73	N/A	N/A
U-shaped Duct (round corners)	0.48	0.35	2.31	2.43	5%
U-shaped Duct (large height in bend)	0.48	0.37	2.68	2.83	6%
Square Orifice (4" thick)	0.48	0.20	1.43	1.50	5%

Figure 3.21 – Table of CFD computation results compared with Idel'Chik's predictions.

Additionally, a test of the transfer duct placed in the lower part of the wall showed the effect of wall placement on the pressure loss. The transfer duct was located at floor level so that the outlet stream bends sharply at the floor, and the pressure loss coefficient increased to 3.31 (compared to the 2.80 k-value when centered vertically in the wall). Figure 3.17 summarizes the CFD results and compares them to the prediction results (from section 2.6). Appendix A presents graphics CFD outputs showing the pressure and velocity distributions for each duct tested.

3.3.3 Discussion

The CFD results and the prediction method results (using Idel'Chik's data) are similar for all cases (within 0.5% and 5% of each other). Therefore, further refinement and design may use either method to predict the k-value. However, the CFD model considers the walls, floor, and ceiling orientations, while the Idel'Chik method assumes an infinite wall. Therefore, the CFD method is used from this point on.

Plugging the calculated k-values into the reference apartment case detailed in section 2.1 indicates that the U-shaped duct will meet the design goal for airflow (passing 10ACH through the apartment with a 10Pa pressure gradient), but the transfer duct will not (figure 3.22 summarizes the results; "wall area required" is the area needed by the device to pass the required airflow).

	k-value	%open area	Wall area required by device	Wall area available	Pass/fail?
Transfer Duct	2.80	5.3%	19.4 m^2	15 m^2	Fail
U-shaped Duct	2.71	12%	8.4 m^2	15 m^2	Pass

Figure 3.22 – summary of airflow prediction results with respect to the design goal.

Since these aero-acoustic wall openings will replace windows and doors as the air-path for natural ventilation, it is useful to compare the wall areas needed for each to pass equal airflows. Using equation 8 from section 2.6, equating the pressure drop and volume flow rate for the device

and a standard orifice, and solving for the resulting area ratio yields:

$$\Delta P_{orifice} = \Delta P_{device}$$

$$\tfrac{1}{2}\rho k_{orifice} V_{orifice}^{\ 2} = \tfrac{1}{2}\rho k_{device} V_{device}^{\ 2}$$

$$k_{orifice}\left(\dot{V}/A_{orifice}\right)^2 = k_{device}\left(\dot{V}/A_{device}\right)^2$$

$$\sqrt{\frac{k_{device}}{k_{orifice}}} = \frac{A_{device}}{A_{orifice}} \qquad (12)$$

where:

$\dot{V}$ = volume flow rate, m^3/s,
A = cross-section area open to free airflow, m^2,
k = pressure loss coefficient, dimensionless.

The area ratio ($A_{device}/A_{orifice}$) indicates how much area an aero-acoustic wall opening needs compared to a typical orifice opening (window or door) to pass the same volume flow of air under the same pressure drop. The orifice has a pressure loss coefficient of 1.43 (according to CFD) or 1.50 (according to Idel'Chik). Using the CFD value for consistency, the prototype designs both have area ratios near 1.4, indicating that the prototypes need between ~40% more open area than windows and doors to pass the same airflow.

Considering the percentage open area, further helps determine the actual wall area ratio (wall area needed by a window versus the wall area needed by the aero-acoustic wall openings). Windows have nearly 100% open area, so the wall area ratio is found by dividing the area ratio (from equation 12) by the percent open area of each design. It turns out that the U-shaped duct needs 11 times more wall area than a fully open window, and the transfer duct needs 26 times more wall area than a fully open window. This indicates that these aero-acoustic designs will likely call for large amounts of wall area to meet the airflow passed by a conventional open-

window system. Ultimately, however, the integration of these aero-acoustic wall openings into "real" architecture will determine their success. Section 5.1 demonstrates that the U-shaped duct can be effectively integrated into the walls (using several sample floor plans) to meet the airflow design goal while also meeting aesthetic standards.

Room for improvement in pressure loss exists in making the air-path more streamlined and increasing the cross-section area at the bends. The acoustic experiments (section 3.2) revealed that the suggested modifications will not greatly degrade acoustic performance. The following chapter, *Refined Designs*, investigates modifications to the designs that improve the pressure-loss characteristics, while maintaining the acoustic performance.

Chapter 4
Refined Designs

4.1 REFINED PREDICTION METHODS

The experiments above indicate that the acoustic prediction method is inadequate, while Idel'Chik's airflow prediction method and the CFD computations agree closely with each other (difference of 5% or less). Therefore, changes to the acoustic prediction method are necessary before final design revisions are finalized (the two airflow methods effectively verify each other).

The Kuntz and Hoover (1987) method for predicting sound transmission loss in a lined duct is not valid for ducts with large aspect ratios, as shown in chapter 5. Ideally, a simple equation would predict transmission loss for all geometries, but there currently is no such equation (short of complex theoretical analysis). Instead, the experimental curve for the tested duct (2.5" x 12" inside cross section with ½" lining) may be scaled for length (i.e. – the per length transmission loss may be simply multiplied by the length to get the predicted transmission loss). Unfortunately, this method is restrictive as it is valid only for duct/lining combinations that have already been tested (so that the transmission loss curve is known).

A fifth order regression curve-fit of the data (2.5"x12" cross section with 1/2" acoustic lining) yields an estimate of transmission loss (TL per meter) as a function of frequency (between 100 Hz and 10,000 Hz):

$$\mathbf{TL} = 0.056 + 0.001\mathbf{f} - 3.93\times10^{-7}\mathbf{f}^2 + 6.98\times10^{-11}\mathbf{f}^3 - 5.96\times10^{-15}\mathbf{f}^4 + 1.94\times10^{-19}\mathbf{f}^5 \quad (13)$$

Equation 13 then multiplies by the length of the duct to predict the total transmission loss of the duct.

4.2 REFINED PROTOTYPES

Using sound transmission class (STC) to gauge sound transmission loss shows that the prototype designs have room for improvement at low frequencies (below 1000Hz). Equation 7 in section 2.5 indicates that duct length is the most effective way to increase transmission loss at low frequencies. The modified prediction method (using equation 13) for sound found that a lined duct at least 1.1m long is required to meet an STC-25 rating. This length of 1.1m, then, is set as the minimum length of lined duct for both designs (excluding length due to entrance, exit, and bends). Any contribution to the transmission loss by the bends, entrances, or exits only increases the transmission loss. Figure 4.1 shows the predicted sound transmission loss spectra for the designs (based on a 1.1m long lined duct) and the corresponding sound transmission class

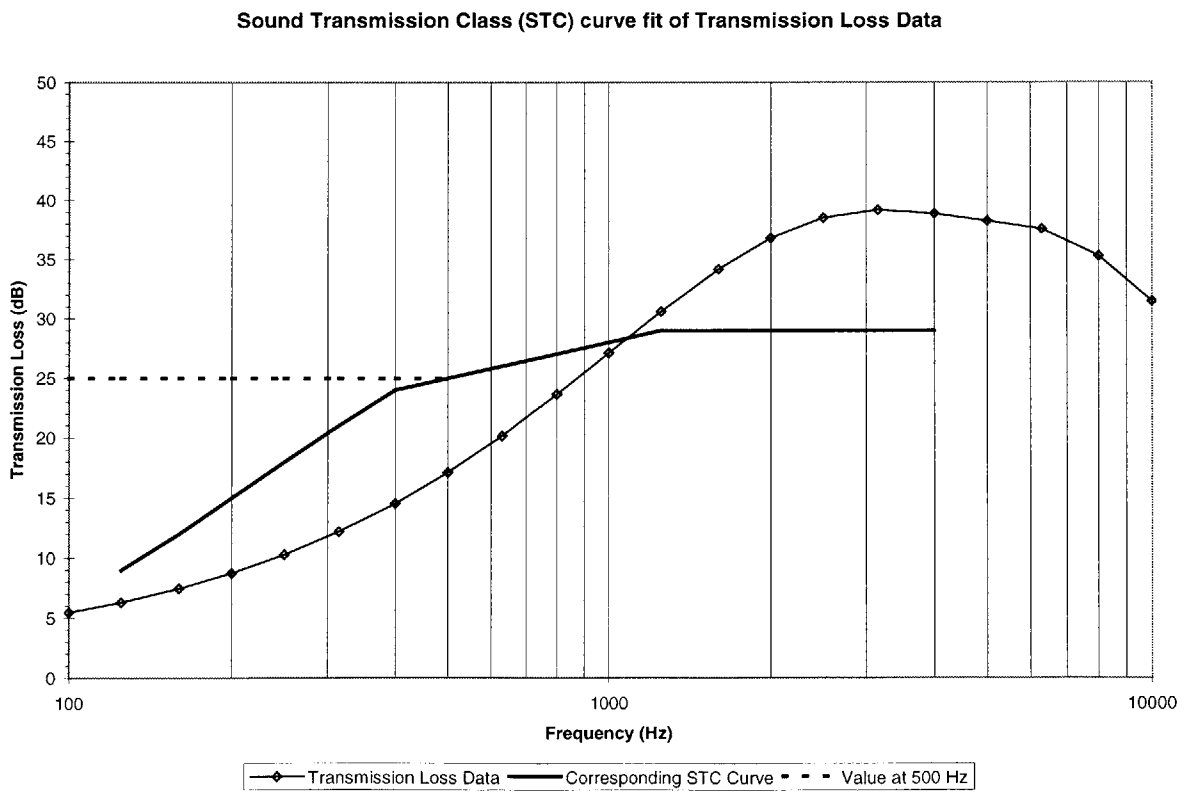

Figure 4.1 – Predicted sound transmission loss spectra for both refined designs (they will have very similar curves because they both have 1.1m of lined duct), plotted with the corresponding sound transmission class (STC-25) curve.

(STC-25) curve. Both designs have the same predicted transmission loss curve because they both have 1.1m of lined duct (though the U-shaped duct may have a slightly better STC rating, based on its better experimental performance in section 3.2).

The airflow pressure loss of both prototypes is not ideal, especially for the U-shaped duct. Idel'Chik's data from chapter 2 provides a guide for improving the airflow characteristics further, and several modifications were already tested with the CFD computations in section 3.3 (figure 3.21). The acoustic model verified that the modifications (adding bends and increasing entrance and exit areas) will not adversely effect the noise attenuation, as long as the length of lined

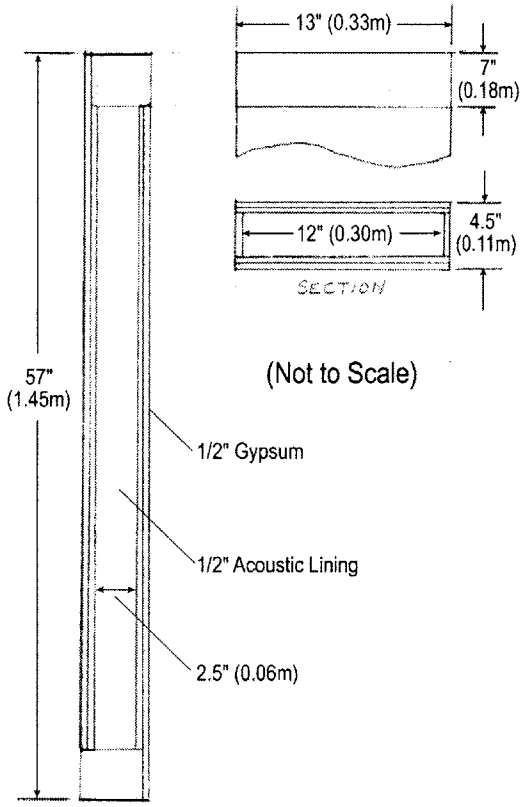

Figure 4.2 – Refined transfer duct design.

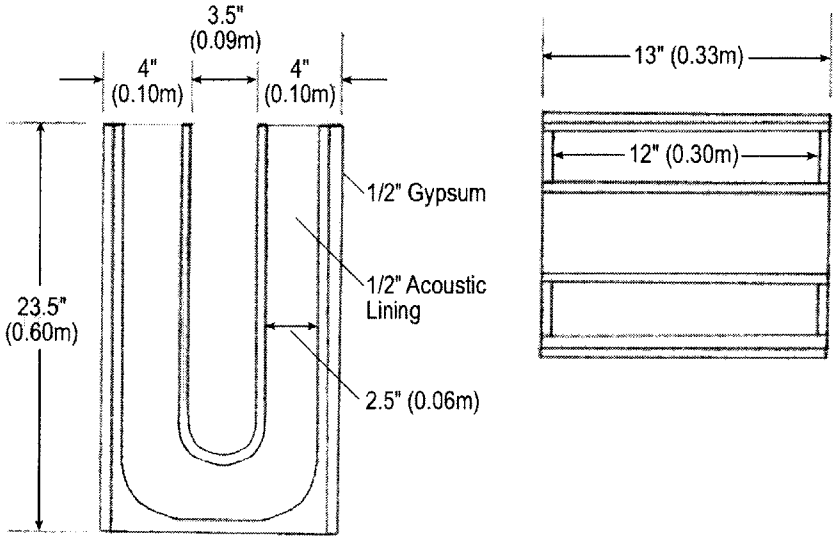

Figure 4.3 – Refined U-shaped Duct (top) and transfer duct.

duct is equal to or greater than 1.1m. The changes to improve the airflow without reducing the transmission loss are: rounded corners on the U-shaped duct; rounded corners and doubled entrance and exit areas on the transfer duct. Figures 4.2 and 4.3 detail the modified design suggestions.

The two designs, detailed above, are just a sample of what the design of an effective aero-acoustic wall opening could become. The specific design of a transfer duct or U-shaped duct will depend on the exact needs of each installation, so each design will be different. The designs may be changed and altered, according to the results in this section (and the discussion in section 6.1), to suit each application (e.g. – to get more sound transmission loss, the length should be increased, or to produce a cheaper version where airflow resistance is not critical, the bends can be replaced by sharp corners).

The CFD results (from section 3.2) show that the k-values are 1.73 for the transfer duct and 2.31 for the U-shaped duct. The open area of the refined transfer duct is 4% and the open area of the refined U-shaped duct is 10% (open area is calculated as the percentage of open cross-section area to total frontal wall area occupied by the device).

Plugging the predicted k-values into the reference case detailed in section 2.1, indicates that the U-shaped duct will still meet the airflow design goal (of passing 10ACH with a 10Pa pressure gradient), and the transfer duct still will not (figure 4.4 summarizes the results). This confirms that the transfer duct is a less feasible design when the wall area occupied by the devices is the limiting factor. The U-shaped duct emerges as the most promising design for aero-acoustic wall openings for natural ventilation applications. Chapter 5 further investigates its integration into naturally ventilated architecture, showing how it is actually sized and positioned in each wall to meet the airflow design goals along with aesthetic standards.

	k-value	%open area	Wall area required by device	Wall area available	Pass/fail?
Transfer Duct	1.73	4%	20.2 m^2	15 m^2	Fail
U-shaped Duct	2.31	10%	9.3 m^2	15 m^2	Pass

Figure 4.4 – Summary of airflow prediction results with respect to the design goal, for the refined designs (as detailed in figures 4.2 and 4.3).

Chapter 5
Discussion

5.1 INTEGRATION INTO ARCHITECTURE

Without a vision of how these wall-openings will be incorporated into building design, this work is incomplete. The sample case (detailed in section 2.1) used throughout this thesis provides only limited insight into how well these devices will fit into a wall (using wall area estimates to predict whether or not the device will fit). This section proposes actual building designs and illustrates how the U-shaped duct will be installed in the designs to achieve the desired airflow rates and noise transmission loss. When natural ventilation, alone, does not provide enough airflow (as in case 1, below), fans are introduced in the designs (as one option for meeting the needed pressure gradient).

Architects must be able to utilize an aero-acoustic wall-opening without limiting aesthetic freedom, and these devices are intended to free the architects from the noise privacy constraint of natural ventilation design. Below are four sample cases that illustrate how these devices can be incorporated into architectural design. Architects are free to then derive an endless supply of other imaginative solutions.

All four cases use the refined U-shaped duct (as defined in section 4.2), installed at the top of the wall so that windows and doors fit below it (the height of the wall is 3 meters). In the apartments (cases one and two) the wall and ceiling are both 3 meters tall (giving a slightly taller space than normal, that permits installation of the U-shaped duct above doors and windows). In the offices (cases three and four) a drop ceiling is installed 0.5 meters below the top of the 3 meter-tall wall, creating a plenum. The height of the U-shaped duct is 0.6 meters in all cases.

Figures 5.1 and 5.2 illustrate how the U-shaped duct may be installed for the apartments and the offices, respectfully. Of course, other creative installations and ideas are possible and encouraged.

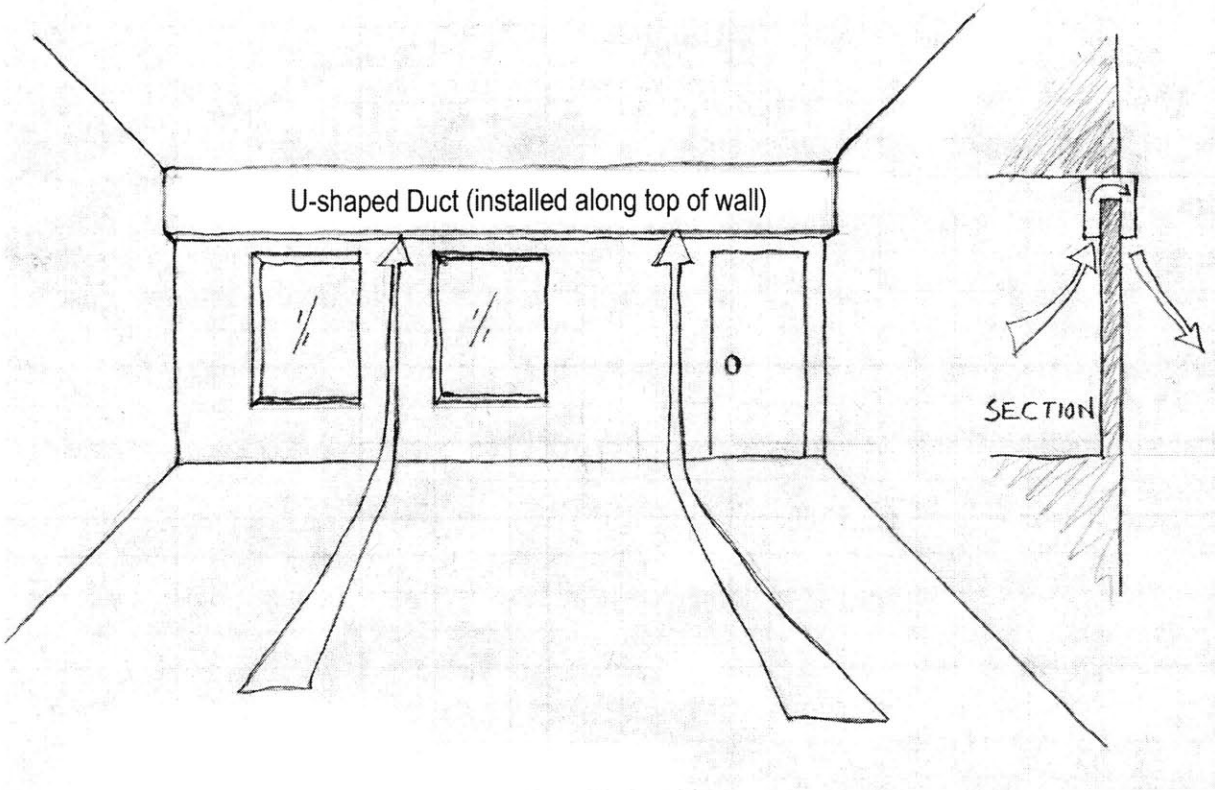

Figure 5.1 – Illustration of U-shaped duct installation for apartments (cases 1&2).

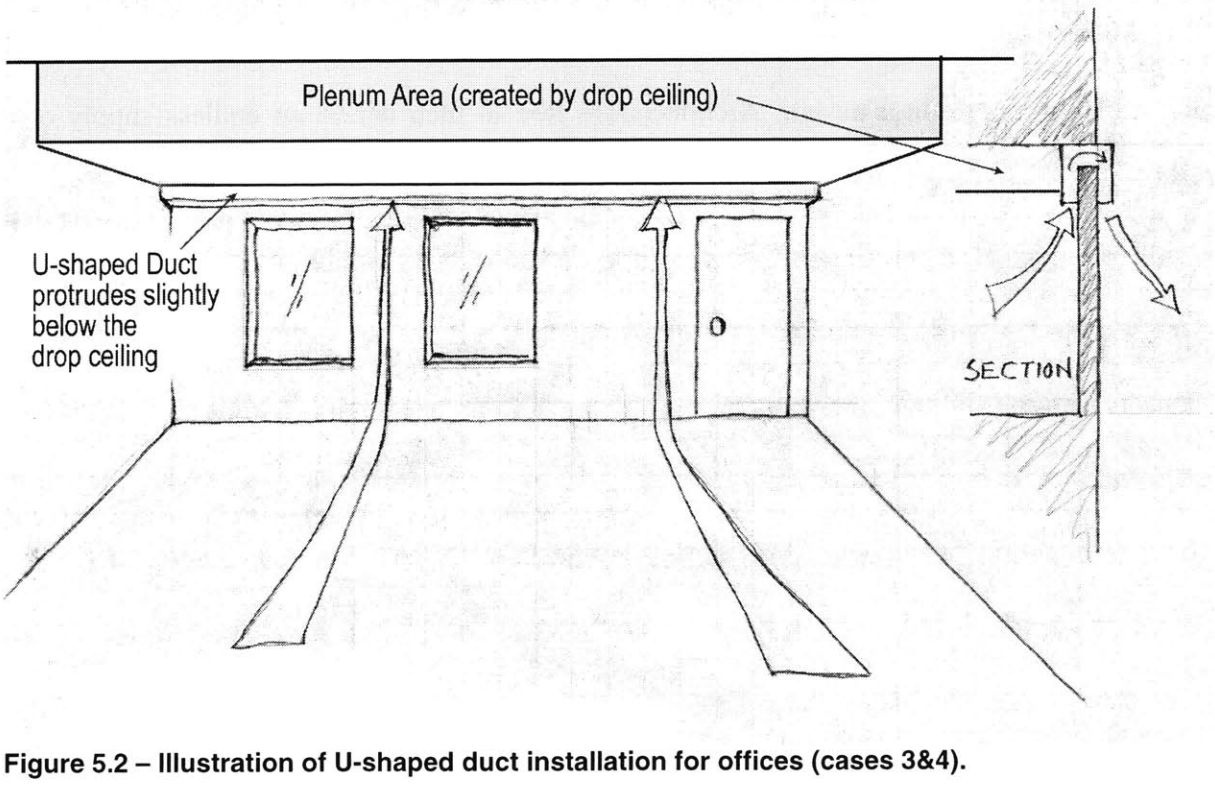

Figure 5.2 – Illustration of U-shaped duct installation for offices (cases 3&4).

Case 1: *Residential Apartment Building (same as reference case)*

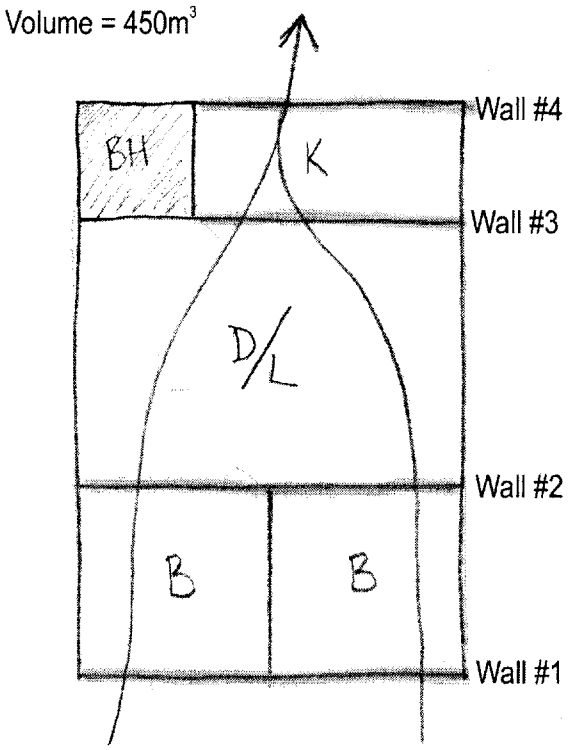

This residential apartment is 10 meters (33ft) wide by 15 meters (49ft) deep by 3 meters tall (9.8ft), giving a total volume of $450m^3$ ($15{,}892ft^3$). The U-shaped duct is installed along the top of the four walls (figure 5.1) that are perpendicular to the airflow (walls 1-4 above), so that the windows and door fit below it. This allows the U-shaped duct to utilize the full wall length (without worrying about doors and windows getting in the way). For aesthetic reasons, the U-shaped duct is installed only along the top of the wall, and is not allowed to occupy any other part of the wall.

Since walls 3 and 4 are smaller than walls 1 and 2, they limit the maximum length of the U-shaped duct (to seven meters). The U-shaped duct extends 0.6m (2ft) down from the ceiling and protrudes 0.1m (4in) out from the wall.

In order for the apartment to achieve a ventilation rate of 10 air changes per hour (ACH) with only 7 meters (23ft) of installed U-shaped duct, a total pressure gradient of nearly 50 Pascal

(12.5Pa per wall) must exist between wall 1 and wall 4 (see the example in section 2.2 for equations to calculate pressure loss, wall area, and airflow rate). That pressure could theoretically be caused by a wind speed of approximately 9m/s (20mph). Figure 2.5 (in chapter 2) shows, however, that an average summertime wind speed of 9 m/s is rarely seen (Boston has one of the highest average summertime wind speeds in the world, at 6.3m/s [14mph]). Therefore, a 50Pa pressure difference is unreasonable for natural ventilation. Fan-assisted ventilation, however, can produce enough pressure to drive the 10 ACH ventilation rate and will use relatively little energy doing so. For example, to drive 10 ACH with a 50Pa pressure drop, a 50% total-efficiency (electric efficiency plus hydraulic efficiency) fan will use approximately 125 watts of electric power. If the fan runs 24 hours a day for the three months of a cooling season, it will add approximately 270kWh of energy to the electric bill – approximately 10% of the energy that would have been used if air-conditioning was used exclusively. At an average electric billing rate of $0.10/kWh, the fan would cost around $27 each year to operate (versus about $130 a year to run the air-conditioner just to meet the cooling load, not 24 hours a day).

Case 2: *Modified Apartment Building (for better natural ventilation)*

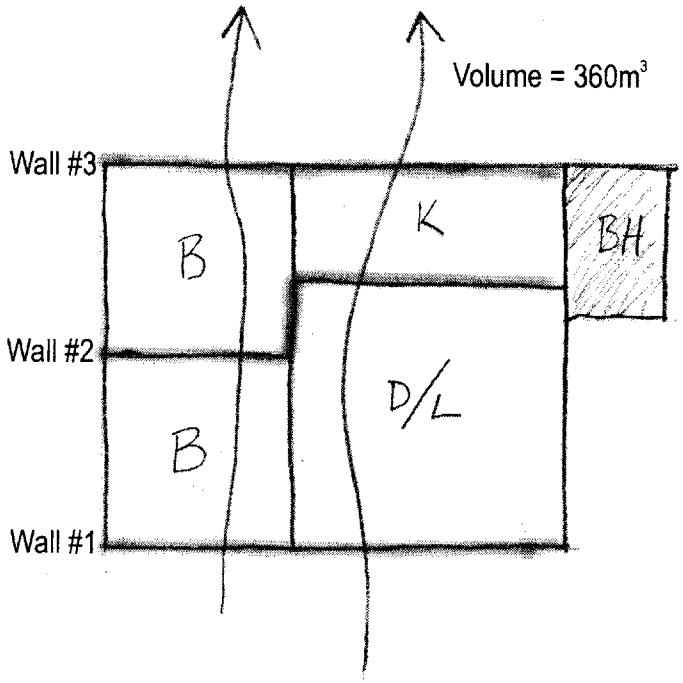

The design of a building and its internal spaces are important in natural ventilation. This case demonstrates how a better-designed apartment can achieve superior natural ventilation performance compared to the reference apartment in case 1. This also illustrates how case 1 (used throughout the thesis) is, in fact, a "worst case" scenario.

First, the volume of the apartment is reduced to $360m^3$ ($12{,}713ft^3$) (12m x 10m x 3m [39ft x 33ft x 9.8ft]), so that less volume flow is needed to create the same air change rate. The orientation of the apartment is shifted so that the area of windward and leeward walls is larger, allowing more wall area for installing the U-shaped duct. Lastly, the walls are oriented so that only three walls (in series) are perpendicular to the flow (versus four walls in case 1).

All walls are the same area, and they limit the maximum length of the U-shaped duct to 12 meters (39ft). The U-shaped duct extends 0.6m (2ft) down from the ceiling and protrudes

0.1m (4in) out from the wall (just as in case 1).

In order for the apartment to achieve a ventilation rate of 10 air changes per hour (ACH) with 12 meters (39ft) of installed U-shaped duct, a total pressure gradient of only 8 Pascal (~2.67Pa per wall) must exist between wall 1 and wall 3. A wind speed of approximately 3.65m/s (8mph) could theoretically create the required pressure gradient. Figure 2.5 (in chapter 2) indicates that many locations around the world have an average summertime wind speed greater than 3.65m/s. Therefore, this modified apartment plan is well-posed to utilize natural ventilation without any further work.

Case 3: *Office Building (two walls, open plan)*

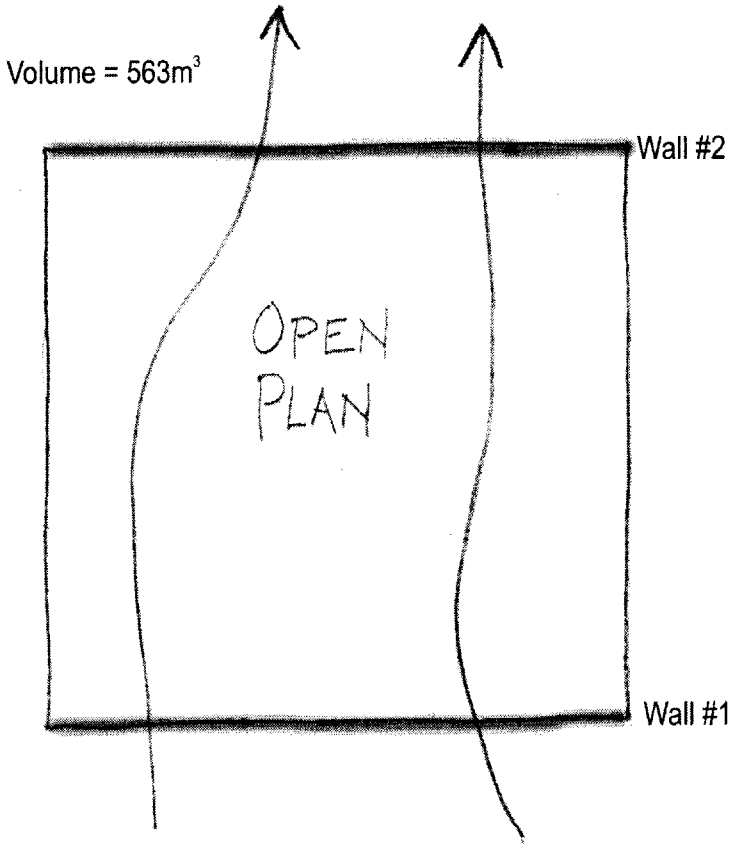

Natural ventilation is certainly not restricted to apartment buildings. Any building with normal cooling loads can utilize natural ventilation. This case presents a standard office building

with an open-plan design (no internal walls). The volume of the space is 562.5m^3 (19,865ft^3) (15m x 15m x 2.5m [49ft x 49ft x 8ft]). A 0.5m (1.6ft) tall drop ceiling is installed, and the total wall height is 3m (9.8ft) (2.5m in the space plus 0.5m in the drop ceiling). The U-shaped duct is installed in the drop-ceiling space along the wall and protrudes 0.1m (4in) past the drop ceiling into the space (figure 5.2, above), so that it is just visible in the space.

Both perpendicular walls are the same area, and they limit the maximum length of the U-shaped duct to 15 meters (49ft).

In order for the office space to achieve a ventilation rate of 10 air changes per hour (ACH) with 15 meters of installed U-shaped duct over two walls, a total pressure gradient of only 8 Pascal (4Pa per wall) must exist. A wind speed of approximately 3.65m/s (8mph) could theoretically create the required pressure gradient. Figure 2.5 (in chapter 2) indicates that many locations around the world have an average summertime wind speed greater than 3.65m/s. Therefore, this open-plan office space is well-posed to utilize natural ventilation without any further work.

Case 4: *Office Building (three walls, closed offices and open plan space)*

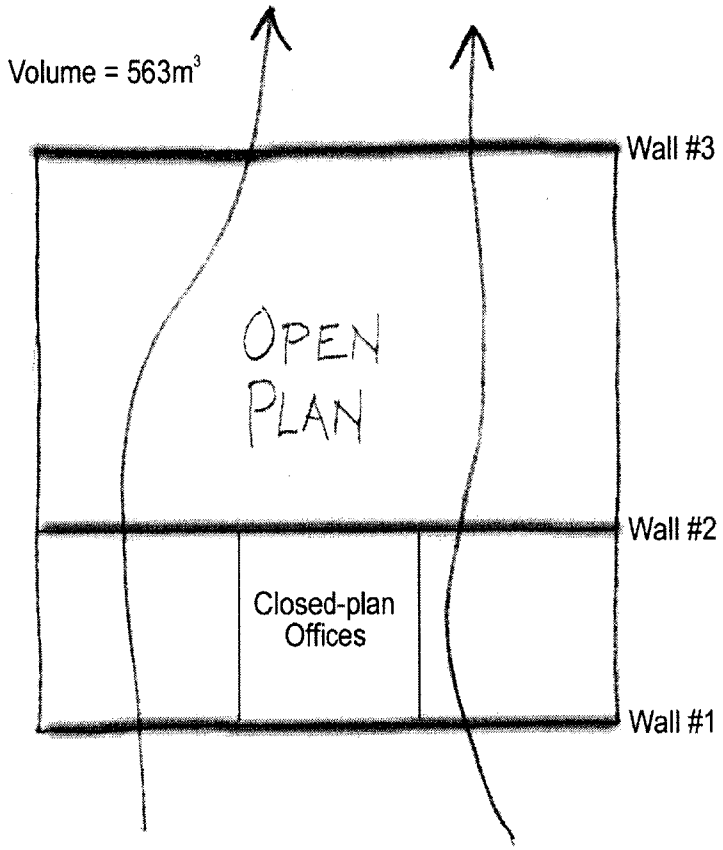

Open plan offices, however, are often undesirable for noise privacy reasons. Case 4 is a slightly modified idea for an office space that has individual closed offices and an open-plan area adjacent to one another. The volume, dimensions, and drop ceiling are the same as for the previous case, except there are three walls perpendicular to the flow (instead of two). The walls, again, limit the maximum length of U-shaped duct to 15m (49ft).

In order for the office space to achieve a ventilation rate of 10 air changes per hour (ACH) with 15 meters of installed U-shaped duct over two walls, a total pressure gradient of about 12 Pascal (4Pa per wall) must exist. A wind speed of approximately 4.5m/s (10mph) could theoretically create the required pressure gradient. Figure 2.5 (in chapter 2) indicates that a few locations around the world have an average summertime wind speed greater than 4.5m/s. Therefore, this mixed-plan

office space is well-posed to utilize natural ventilation without any further work.

All the above cases are simply design ideas that utilize the U-shaped duct to achieve natural ventilation without losing noise privacy. Architects should follow these three design guidelines to create creative new floor plan designs that optimize natural ventilation:

- The wall length normal to the airflow direction should be large compared to the wall length parallel to the flow (so that more wall length is available for the U-shaped duct),
- Tall ceilings (3m high) should be used so that the U-shaped duct (0.6m high) can fit in the wall above any doors and windows,
- The U-shaped duct should be oriented downward (so that rain, dust, etc. can not enter it).

5.2 PRACTICALITY FOR APPLICATIONS

5.2.1 Cost

The costs of this type of device come from materials, off-site labor, and on-site labor. If pre-fabricated, the on-site labor of installing these systems will be approximately equal to standard wall construction (so can be neglected). The prototypes, as-built, used approximately $15-$20 worth of material each (~3 feet of liner at $110 per 100 feet; 3 feet of metal duct at ~$4 per foot; and ~4 square feet of fiber board at $1 per square foot). The material cost of the production will be less (perhaps about 50% of the prototype material cost, or $8-$10 per device). Fabrication time of each device will be low because of the relative simplicity in the designs (automated fabrication time for one device is estimated between 0.1 and 0.25 man-hours, from procurement to packaging). Assuming a combined overhead (labor, materials, and taxes) of 25-50% and a cost of $20 per man-hour, each device will cost between $12.50 and $22.50.

5.2.2 Performance

When installed to compliment air-conditioning during off-peak times, these devices can save

up to 80% on annual cooling-energy load (if supplying a constant air change rate of 10 ACH), according to the study by Kammerud et. al. (1984). Assuming a conservative savings of just 40% (based on utilization effectiveness, effect of latent heat loads on ventilation usage, and fluxuations in actual air change rate), an unventilated seasonal cooling load of 4000 kWh (for an average 110m^2 [1184ft^2] building between June 1st and September 30th, Kammerud [1984]), a COP-3 air-conditioner, and the current electricity rate in Boston ($0.14/kWh), one will save almost $75 each year ($111 for annual cooling costs versus $186 when air-conditioning is used all the time – ~40% savings).

The percentage of cooling load savings from natural ventilation will convert to approximately an equal percentage in savings on cooling energy cost for most buildings in most climates, according to Kammerud (1984). Therefore, the estimated cost savings of utilizing these aero-acoustic devices will be between 40% and 80% of the total air-conditioning costs for any "normal-load" building in most climates.

5.2.3 Pay-back Period and Pricing

For most climates these devices will not be able to replace air-conditioning for peak loads, but will save energy costs at other times when air-conditioning would otherwise be necessary. Therefore, total initial cost will be higher (initial cost of air-conditioning is the same, while cost of construction increases because of device installation). Using the sample case discussed in section 5.1.2 (annual savings of $75) that has four walls and a desired pay-back period of 5 years, the price of installing aero-acoustic wall openings for each wall should be near $375. Assuming each wall needs approximately five devices, the per device price will be near $75 (since building size and cooling load savings scale linearly with each other, this per device price should be relatively constant for all normal-load buildings).

Since the per device cost (from section 5.1.1) is estimated between $12.50 and $22.50, the total profit will be around $50 per device (70% - 83% gross profit margin). This estimate is based on a five year pay-back period. A more conservative three-year pay-back period warrants a price of approximately $45 per device (50% - 72% gross profit margin). This opportunity for profit is good, and allows some flexibility in pricing to promote the new product. Overall, the economics of bringing these types of products to market are promising.

5.3 FUTURE EXPLORATION

Noise is only one problem of natural ventilation, and this work proposes a fix for noise and visual privacy. Other concerns including humidity, pollution, and meeting assorted building codes are left for future study and design.

In addition to future design work on aero-acoustic wall openings, the modeling and prediction methods warrant more attention. The current straight lined-duct attenuation prediction method recommended by ASHRAE (Kuntz and Hoover, 1987) does not work for ducts with large aspect ratios. A more general empirical prediction technique that considers the properties of the duct lining as well as the cross section geometry will be helpful in optimizing these aero-acoustic wall openings (and lined duct systems in general).

Chapter 6
Conclusion

6.1 REVIEW

The designs of two aero-acoustic wall openings (a U-shaped duct and a transfer duct) slowly developed throughout this thesis. In the end, the U-shaped duct prevails as the most promising design for use in naturally ventilated buildings because it uses wall area more effectively than the transfer duct. According to work by Kammerud, et. al. (1984), when used properly to provide a constant air change rate of 10 ACH, the aero-acoustic wall openings can save up to 80% on annual cooling load for many climates. The profit margin possibilities of these devices is promising, and the market should be explored further.

While the specific designs detailed in this thesis are supported by experiment and modeling, the information in the above chapters will support the exploration of design modifications and further optimization for natural ventilation (and other) applications. These important general ideas should carry through for all aero-acoustic wall opening designs:

- The straight portion of the lined duct dictates the total sound transmission loss;
- The pressure loss coefficient (k-value) of a design is less important than its percent open area (k-value is proportional to wall area squared, but percent open area is proportional to wall area). So, designs like the U-shaped duct that reduce the required wall area are best even though they may have higher k-values. Along similar lines, rounding corners and otherwise streamlining the flow may cost more than they are worth and should be investigated further.
- Improvements to transmission loss should focus on low-frequency noise. The high-

frequency transmission loss is apparently driven by the cross-sectional dimensions (larger dimensions equals less attenuation), and the low-frequency attenuation is driven by lined duct length. Therefore, a duct with larger cross-sectional dimensions but similar lengths (than the design detailed above) may improve the airflow without severely affecting the sound attenuation.

6.2 VISION OF THE FUTURE

As energy demand continues increasing throughout the world, conventional energy supplies will start running low. While alternative energy sources may help ease the ensuing trouble, energy conservation methods must also be adopted. With buildings using approximately 35% of the total energy consumed in the United States (U.S. Energy Information Administration, 1995), it makes sense to target energy conservation strategies at buildings. Natural ventilation is a proven way to ease cooling energy load, and is gaining popularity in Europe and elsewhere (where energy costs are much greater than in the U.S.). However, issues such as privacy, air quality, and safety are hindering its popular adoption in buildings.

This thesis proposes a way to improve the privacy characteristics of natural ventilation. Hopefully, further work and innovative design will follow and eventually the stumbling blocks of natural ventilation will be knocked down to clear the way for more energy efficient buildings.

References

- Allard, F., et. al. 1998. Natural Ventilation in Buildings, a Design Handbook. James & James Ltd., London.
- AMCA Standard 500-L-99. "Laboratory Methods of Testing Louvers for Rating."
- American Society of Heating, Refrigerating and Air-Conditioning Engineers. 1997. ASHRAE Handbook, Fundamentals.
- ASTM Standard E413-87(99). "Classification for Rating Sound Insulation."
- ASTM Standard E90-97. "Standard Test Method for Laboratory Measurement of Airborne Sound Transmission Loss of Building Partitions and Elements."
- Beranek and Vér. 1992. Noise and Vibration Control Engineering.
- CHAM, PHOENICS v3.1. 2000. Concentration, Heat, and Momentum, Ltd. Bakery House, 40 high St., Wimbledon Village, London, SW19 5AU, England.
- Harris, et. al. 1994. Noise Control in Buildings. McGraw-Hill
- Idel'Chik, I.E., et. al. 1994. Handbook of Hydraulic Resistance. CRC Press
- Johns Manville Corporation. Internal Report 491-T-102. "Airflow Resistance and Sound Absorption of Manville Linacoustic Duct Liners." (confidential – not for general distribution or republication)
- Johns Manville Corporation. Internal Report 491-T-99. "Sound Insertion Loss Properties of Manville Linacoustic Duct Liners." (confidential – not for general distribution or republication)
- Kammerud, Ceballos, Curtis, Place, and Anderson. 1984. "Ventilation Cooling of Residential Buildings." ASHRAE Transactions, Vol 90, pt. 1B, AT-84-05 No.2
- Kuntz and Hoover. 1987. "The Interrelationships Between the Physical Properties of Fibrous Duct Lining Materials and Lined Duct Sound Attenuation." ASHRAE Transactions, No. 3082 (RP-487).
- Kurze, U.J. and Vér, I.L. 1972. "Sound Attenuation in Ducts Lined with Non-Isotropic Material," J. Sound Vib. Vol.24, pp177-187
- Lippert, W.K.R. 1954. "The Measurement of Sound Reflection and Transmission at Right-Angled Bends in Rectangular Tubes," Acoustica, V4, no.2, pp313-319

- Mechel, F.P. 1976. "Explicit Formulas of Sound Attenuation in Lined Rectangular Ducts," Acustica vol.34 pp289-305 (in German)

- Miles, J.W. 1947. "The Diffraction of Sound Due to Right-Angled Joints in Rectangular Tubes," J. of Acoustical Society of America, V19, pp572

- Parkinson, J.S. 1937. "Nature of Noise in Ventilating Systems." ASHVE Transactions. V43, pp95.

- Robinson, D.W. and Dadson, R.S. 1956. "A re-determination of the equal loudness relations for pure tones." British Journal of Applied Acoustics. v7 n5 p166

- Rogers, R. 1940. "The Attenuation of Sound in Tubes." J. Acoust. Soc. Am. V11 pp480-484

- Sabine, H.J. 1940. "The Absorption of Noise in Ventilating Ducts." J. Acoust. Soc. Am. V12 pp53.

- U.S. Energy Information Administration. 1995. "State energy Data Report 1995."

- Vér, I.L. 1978. "A Review of the Attenuation of Sound in Straight Lined and Unlined Ductwork of Rectangular Cross Section." ASHRAE Trans. V84, pp122-149.

Appendix A
Experimental Data

A1 – RECEIVER ROOM ABSORPTION TEST DATA

Knowing the absorption of the receiver room at each frequency is essential when measuring transmission loss. ASTM Standard E90-97 offers instructions on measuring the sound absorption of a room using reverberation time experiments. The reverberation time experiments find the rate of sound decay (dB/s) in the room at each frequency. Then, the Sabine equation (equation Ax) determines the sound absorption of the room at each frequency:

$$\mathbf{A} = 0.921\frac{\mathbf{Vd}}{\mathbf{c}} \qquad \text{(Ax)}$$

where:
A = sound absorption of the room, m^2,
c = speed of sound in air, m/s,
V = volume of the room, m^3,
d = decay rate of sound, dB/s.

The table below summarizes the absorption of the receiver room at each frequency. The graphs farther below are plots of the actual time decay data measured by the microphone and filtered for each frequency.

Absorption Calculations for BBN receiver room based on time-decay noise testing of the "as is" room on 29 November 2000 by S.D. Hamilton.

Volume	87.78	m^3
Speed of Sound	343.24	m/s

Frequency (Hz)	Slope (dB/s)	Absorption (sabins)
100.00	-40.97	9.65
125.00	-44.17	10.40
160.00	-104.72	24.67
200.00	-53.17	12.52
250.00	-60.67	14.29
315.00	-50.52	11.90
400.00	-56.28	13.26
500.00	-47.61	11.21
630.00	-62.60	14.74
800.00	-52.39	12.34
1000.00	-59.83	14.09
1250.00	-55.88	13.16
1600.00	-56.22	13.24
2000.00	-58.19	13.71
2500.00	-61.54	14.50
3150.00	-61.13	14.40
4000.00	-64.71	15.24
5000.00	-74.64	17.58
6300.00	-86.23	20.31
8000.00	-104.81	24.69
10000.00	-124.18	29.25
12500.00	-155.41	36.60

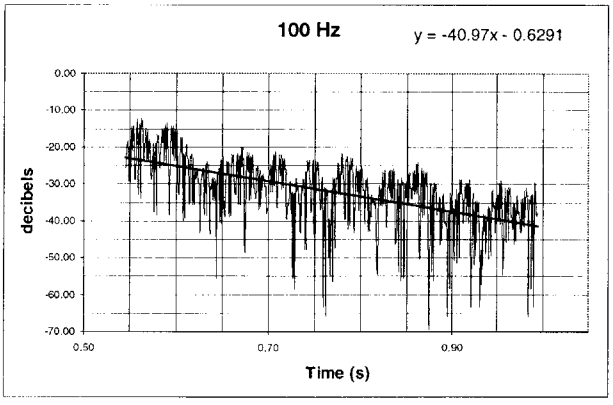

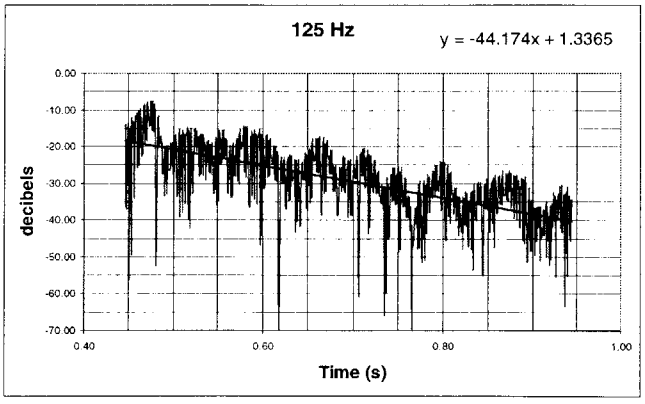

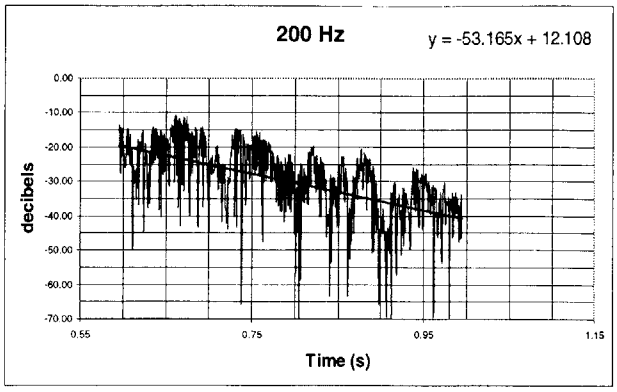
200 Hz
y = -53.165x + 12.108
decibels
0.00
-10.00
-20.00
-30.00
-40.00
-50.00
-60.00
-70.00
0.55
0.75
0.95
1.15
Time (s)

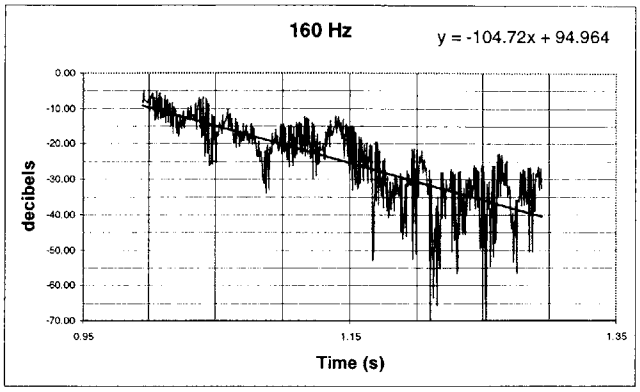
160 Hz
y = -104.72x + 94.964
decibels
0.00
-10.00
-20.00
-30.00
-40.00
-50.00
-60.00
-70.00
0.95
1.15
1.35
Time (s)

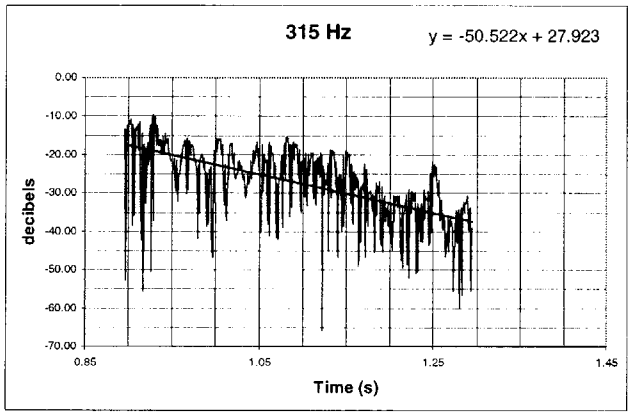
315 Hz
y = -50.522x + 27.923
decibels
0.00
-10.00
-20.00
-30.00
-40.00
-50.00
-60.00
-70.00
0.85
1.05
1.25
1.45
Time (s)

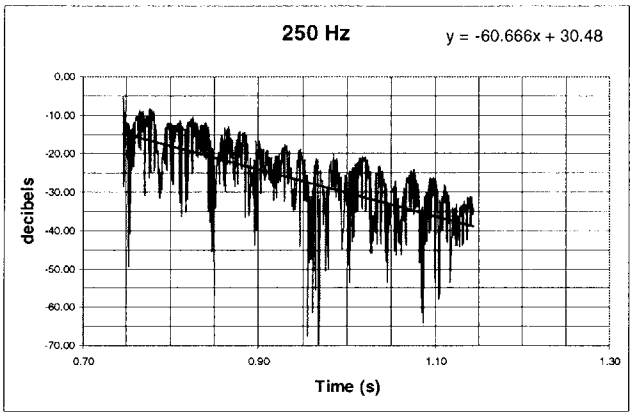
250 Hz
y = -60.666x + 30.48
decibels
0.00
-10.00
-20.00
-30.00
-40.00
-50.00
-60.00
-70.00
0.70
0.90
1.10
1.30
Time (s)

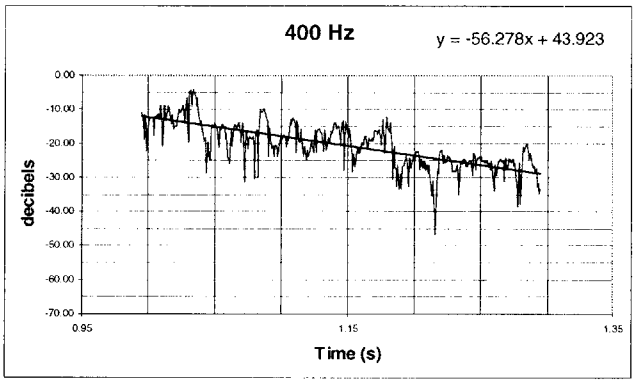
400 Hz
y = -56.278x + 43.923
decibels
0.00
-10.00
-20.00
-30.00
-40.00
-50.00
-60.00
-70.00
0.95
1.15
1.35
Time (s)

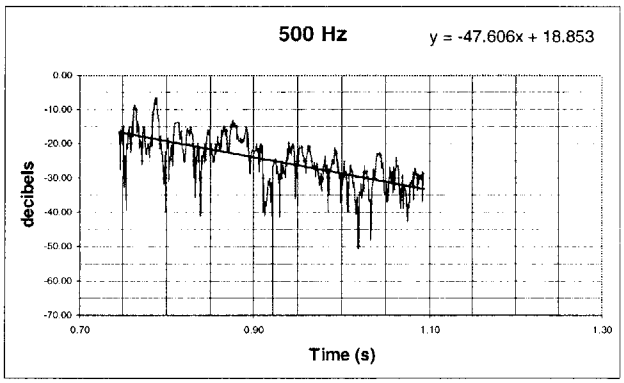
500 Hz
y = -47.606x + 18.853
decibels
0.00
-10.00
-20.00
-30.00
-40.00
-50.00
-60.00
-70.00
0.70
0.90
1.10
1.30
Time (s)

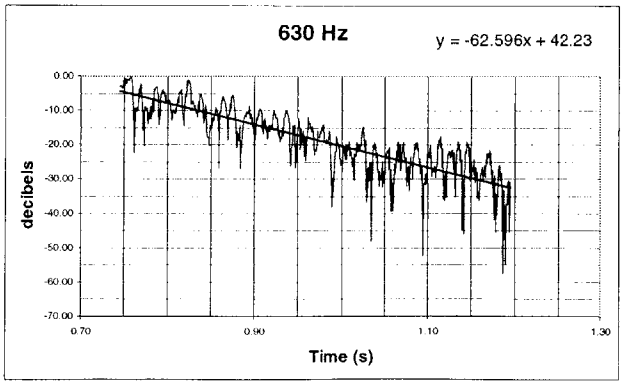
630 Hz
y = -62.596x + 42.23
decibels
0.00
-10.00
-20.00
-30.00
-40.00
-50.00
-60.00
-70.00
0.70
0.90
1.10
1.30
Time (s)

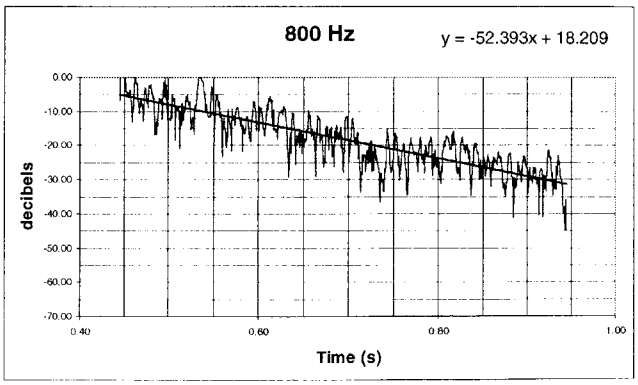
800 Hz
y = -52.393x + 18.209
decibels
0.00
-10.00
-20.00
-30.00
-40.00
-50.00
-60.00
-70.00
0.40
0.60
0.80
1.00
Time (s)

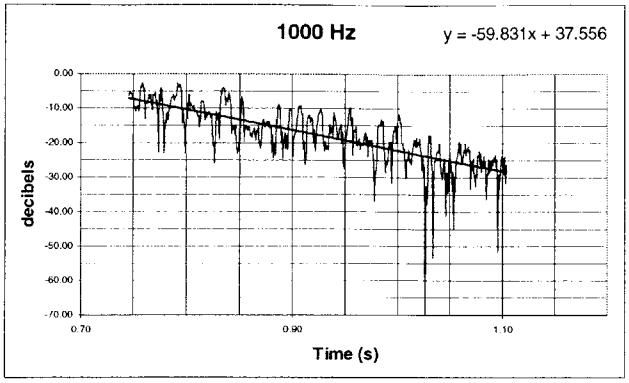
1000 Hz
y = -59.831x + 37.556
decibels
Time (s)

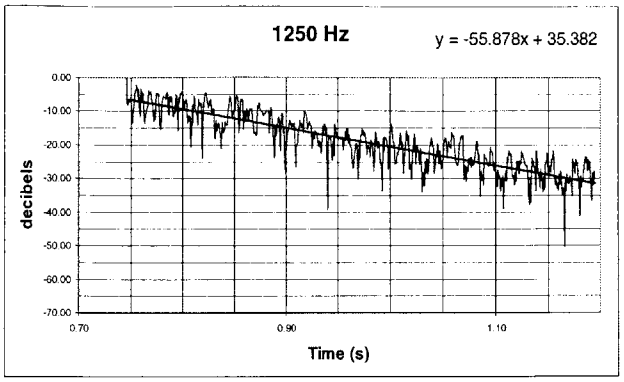
1250 Hz
y = -55.878x + 35.382
decibels
Time (s)

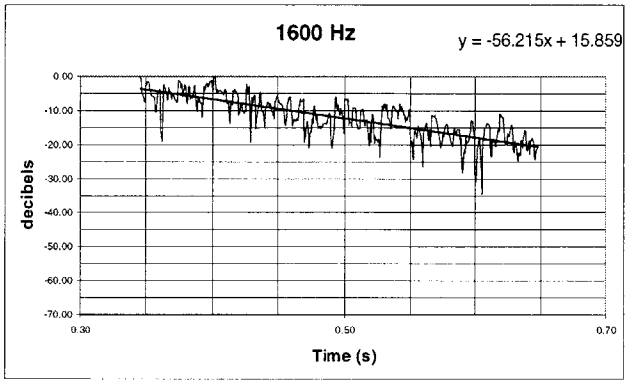
1600 Hz
y = -56.215x + 15.859
decibels
Time (s)

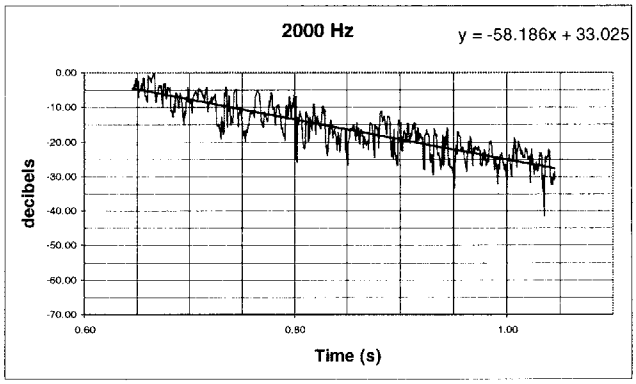
2000 Hz
y = -58.186x + 33.025
decibels
Time (s)

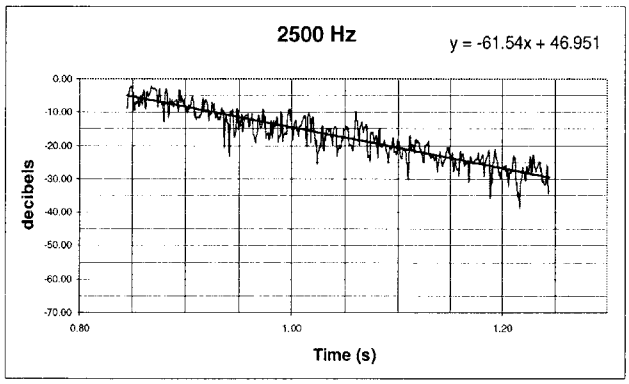
2500 Hz
y = -61.54x + 46.951
decibels
Time (s)

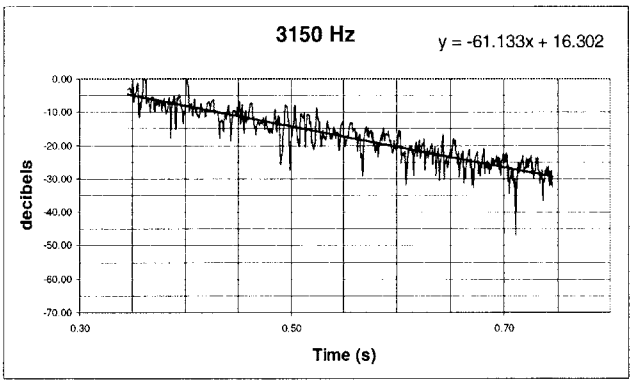
3150 Hz
y = -61.133x + 16.302
decibels
Time (s)

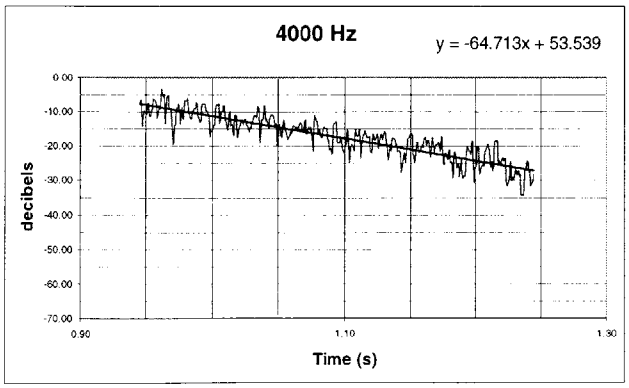
4000 Hz
y = -64.713x + 53.539
decibels
Time (s)

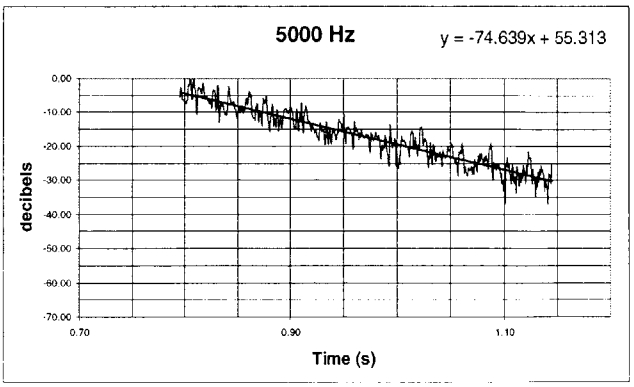
5000 Hz
y = -74.639x + 55.313
decibels
Time (s)

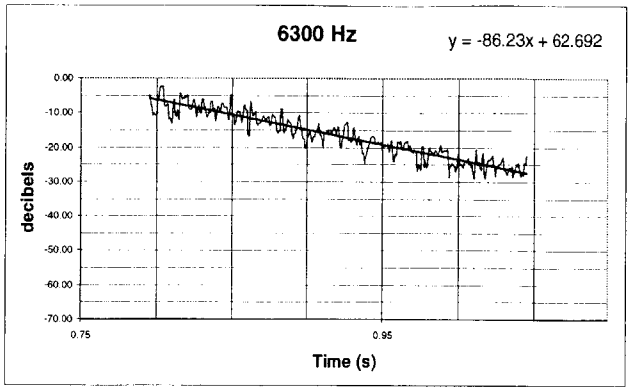
6300 Hz
y = -86.23x + 62.692
decibels
0.00
-10.00
-20.00
-30.00
-40.00
-50.00
-60.00
-70.00
0.75
0.95
Time (s)

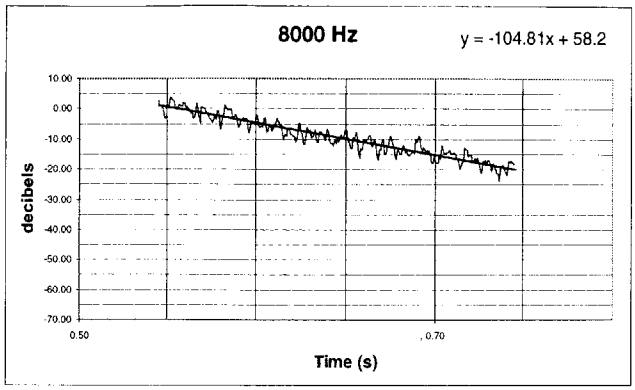
8000 Hz
y = -104.81x + 58.2
decibels
10.00
0.00
-10.00
-20.00
-30.00
-40.00
-50.00
-60.00
-70.00
0.50
0.70
Time (s)

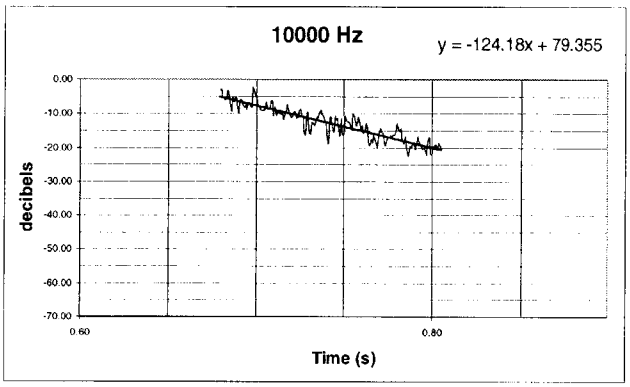
10000 Hz
y = -124.18x + 79.355
decibels
0.00
-10.00
-20.00
-30.00
-40.00
-50.00
-60.00
-70.00
0.60
0.80
Time (s)

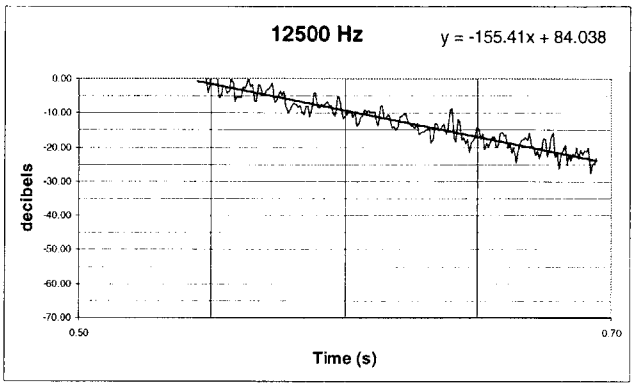
12500 Hz
y = -155.41x + 84.038
decibels
0.00
-10.00
-20.00
-30.00
-40.00
-50.00
-60.00
-70.00
0.50
0.70
Time (s)

A2 – TRANSMISSION LOSS TEST DATA FOR STRAIGHT DUCTS

Sound transmission loss tests of straight ducts were performed on 4 December 2000. A 2.5" x 12" x 36" (inside dimensions) duct and a 12" x 12" x 48" (inside dimensions) duct lined with 1/2" acoustic lining were tested.

The tables and graphs below show the data, as recorded during the experiments.

2.5" x 12" Duct

Frequency (Hz)	Source (dB)	Receiver (dB)	NR	Absorption (A2)	TL
100.0	74.3	43.9	30.36	9.65	4.136
125.0	74.6	43.1	31.50	10.40	4.950
160.0	75.0	48.1	26.97	24.67	-3.337
200.0	75.8	46.3	29.50	12.52	2.145
250.0	78.3	40.7	37.60	14.29	9.668
315.0	78.7	40.9	37.77	11.90	10.631
400.0	78.6	35.9	42.71	13.26	15.100
500.0	78.6	33.7	44.96	11.21	18.085
630.0	79.8	30.8	48.98	14.74	20.913
800.0	82.7	30.6	52.03	12.34	24.738
1000.0	83.4	29.2	54.20	14.09	26.329
1250.0	83.8	27.3	56.47	13.16	28.895
1600.0	83.1	24.7	58.39	13.24	30.792
2000.0	82.2	23.2	58.91	13.71	31.159
2500.0	80.0	20.6	59.33	14.50	31.336
3150.0	77.9	19.2	58.76	14.40	30.793
4000.0	77.5	18.2	59.28	15.24	31.063
5000.0	76.6	16.6	60.03	17.58	31.196
6300.0	74.9	16.4	58.51	20.31	29.050
8000.0	73.4	16.9	56.45	24.69	26.137
10000.0	71.9	17.7	54.21	29.25	23.162
12500.0	70.8	19.2	51.52	36.60	19.506

Sound loss measurements of a lined duct (2.5"x12"x36" inside dimensions) in the BBN reverb rooms

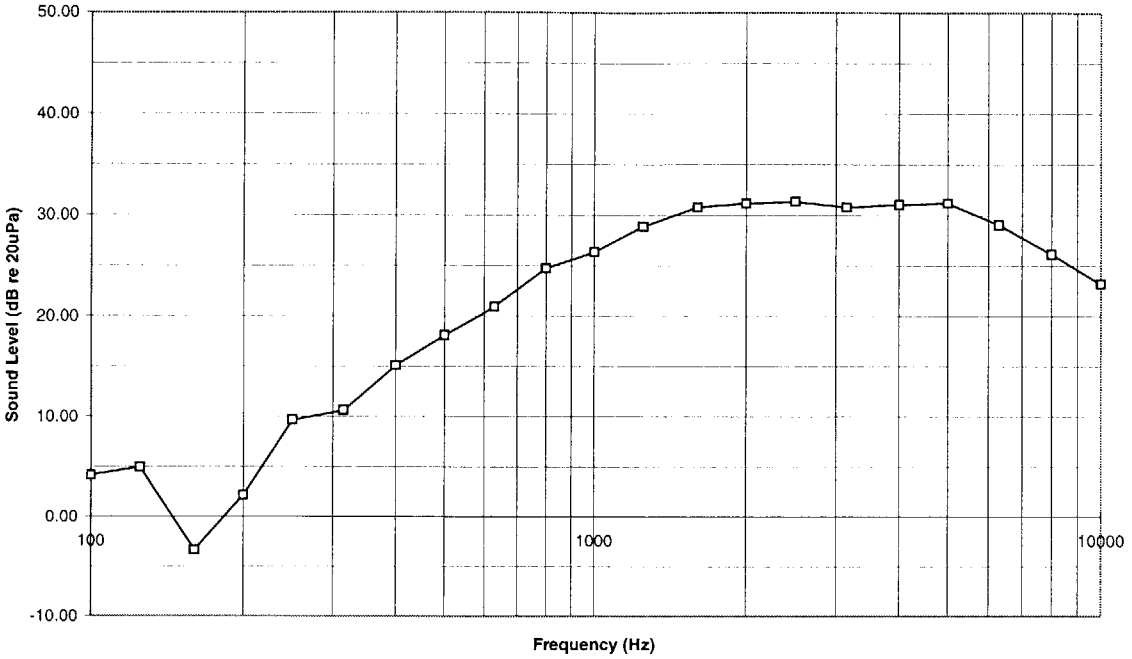

12"x12" Duct

Frequency (Hz)	Source (dB)	Receiver (dB)	NR	Absorption (A2)	TL
100.0	75.3	47.9	27.39	9.65	7.229
125.0	74.0	46.2	27.82	10.40	7.333
160.0	74.7	48.5	26.23	24.67	1.985
200.0	75.5	49.9	25.54	12.52	4.243
250.0	77.5	53.8	23.73	14.29	1.865
315.0	78.4	49.9	28.48	11.90	7.400
400.0	77.6	49.5	28.06	13.26	6.514
500.0	78.1	47.6	30.49	11.21	9.679
630.0	78.7	44.1	34.67	14.74	12.668
800.0	81.9	42.4	39.56	12.34	18.329
1000.0	82.5	38.7	43.77	14.09	21.960
1250.0	83.0	33.0	50.03	13.16	28.519
1600.0	82.4	28.3	54.16	13.24	32.622
2000.0	81.6	30.0	51.61	13.71	29.922
2500.0	79.7	33.8	45.88	14.50	23.943
3150.0	77.5	35.4	42.19	14.40	20.288
4000.0	76.8	35.1	41.67	15.24	19.518
5000.0	75.3	34.1	41.16	17.58	18.388
6300.0	72.5	31.6	40.95	20.31	17.548
8000.0	69.4	28.1	41.33	24.69	17.085
10000.0	66.0	24.2	41.76	29.25	16.779
12500.0	63.3	19.4	43.83	36.60	17.873

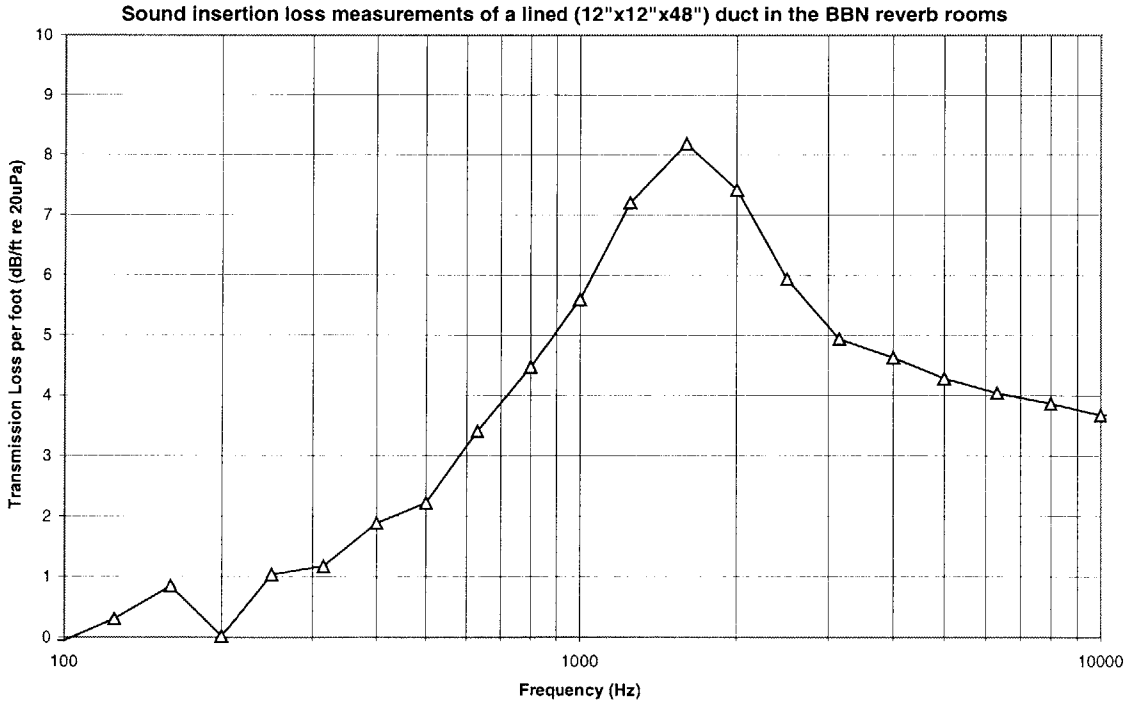

A2 – TRANSMISSION LOSS TEST DATA FOR PROTOTYPES

Sound transmission loss tests of two prototypes (as defined in chapter 3) were performed on 7 March 2001 (transfer duct) and 14 March 2001 (U-shaped duct).

The tables and graphs below show the data, as recorded during the experiments.

Transfer Duct (all sides lined)

Frequency (Hz)	Source (dB)	Receiver (dB)	NR	Absorption (A2)	TL
100.0	73.8	44.2	29.63	9.65	9.464
125.0	73.9	45.9	28.00	10.40	7.506
160.0	75.1	46.3	28.78	24.67	4.537
200.0	75.2	45.5	29.68	12.52	8.385
250.0	77.7	45.2	32.51	14.29	10.639
315.0	78.1	44.3	33.80	11.90	12.727
400.0	77.5	44.2	33.31	13.26	11.767
500.0	78.0	41.3	36.65	11.21	15.832
630.0	78.8	38.4	40.49	14.74	18.487
800.0	81.7	36.7	44.96	12.34	23.727
1000.0	82.6	33.1	49.46	14.09	27.649
1250.0	83.0	28.7	54.25	13.16	32.742
1600.0	82.1	24.9	57.21	13.24	35.673
2000.0	81.5	23.2	58.30	13.71	36.612
2500.0	79.5	19.9	59.57	14.50	37.637
3150.0	77.2	16.4	60.83	14.40	38.932
4000.0	76.4	16.0	60.35	15.24	38.199
5000.0	74.3	12.9	61.42	17.58	38.651
6300.0	71.8	10.4	61.33	20.31	37.936
8000.0	68.5	9.3	59.29	24.69	35.043
10000.0	65.3	8.8	56.49	29.25	31.513
12500.0	62.6	8.8	53.80	36.60	27.846

Transfer Duct (one side lined)

Frequency (Hz)	Source (dB)	Receiver (dB)	NR	Absorption (A2)	TL
100.0	74.9	44.9	29.97	9.65	10.496
125.0	74.4	46.5	27.93	10.40	8.131
160.0	74.9	47.3	27.65	24.67	4.107
200.0	75.1	47.1	28.00	12.52	7.396
250.0	77.3	48.0	29.33	14.29	8.156
315.0	77.7	48.0	29.74	11.90	9.362
400.0	77.8	49.0	28.77	13.26	7.921
500.0	78.2	47.1	31.09	11.21	10.968
630.0	78.8	45.8	32.95	14.74	11.642
800.0	82.0	45.6	36.45	12.34	15.911
1000.0	82.4	43.1	39.35	14.09	18.240
1250.0	83.1	38.1	44.95	13.16	24.135
1600.0	82.4	29.7	52.65	13.24	31.808
2000.0	81.5	25.9	55.64	13.71	34.640
2500.0	79.4	21.7	57.69	14.50	36.452
3150.0	77.3	17.0	60.23	14.40	39.025
4000.0	76.5	16.7	59.73	15.24	38.279
5000.0	74.4	15.2	59.23	17.58	37.160
6300.0	71.8	15.4	56.43	20.31	33.724
8000.0	68.8	12.7	56.03	24.69	32.478
10000.0	65.6	10.7	54.98	29.25	30.690
12500.0	63.1	9.6	53.59	36.60	28.335

Sound Transmission Loss for a transfer duct prototype tested (3/5/2001, BBN Labs, Cambridge, MA) with 1/2" acoustic duct lining on one side and tested again with lining on all sides.

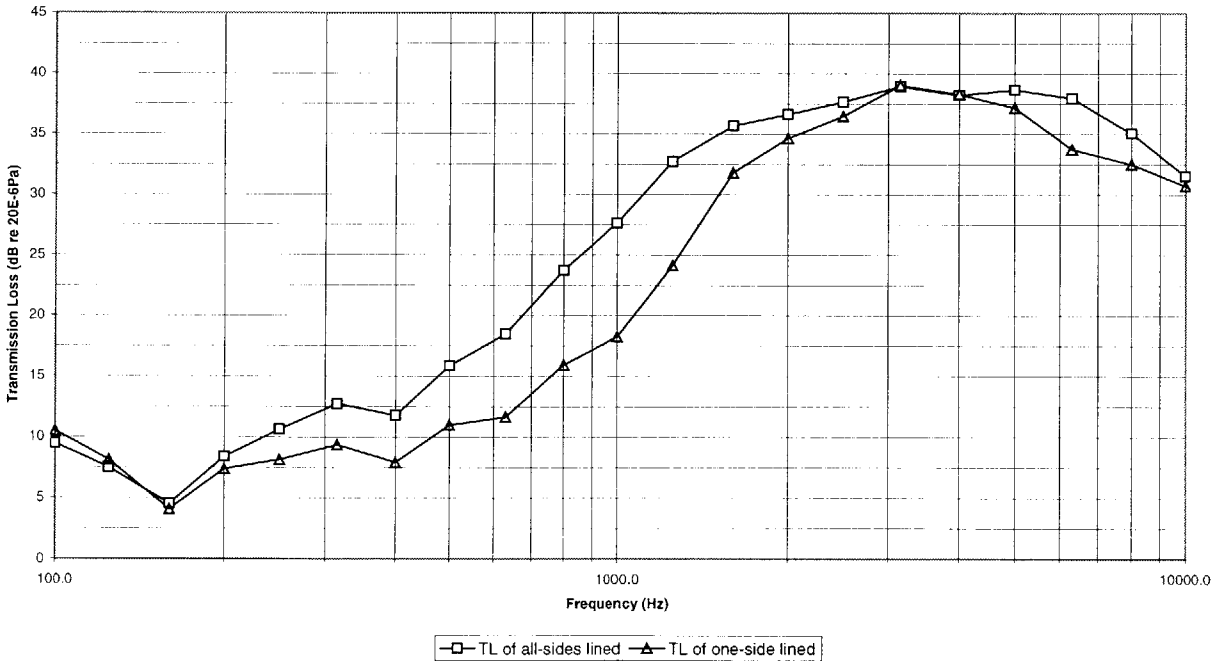

U-shaped Duct (sharp corners)

Frequency (Hz)	Source (dB)	Receiver (dB)	NR	Absorption (A2)	TL
100.0	75.6	45.0	30.58	9.65	10.418
125.0	74.9	45.9	28.99	10.40	8.497
160.0	75.2	45.5	29.77	24.67	5.529
200.0	76.6	44.0	32.60	12.52	11.305
250.0	78.1	44.6	33.54	14.29	11.671
315.0	78.5	44.9	33.62	11.90	12.549
400.0	78.7	43.2	35.56	13.26	14.012
500.0	78.8	38.9	39.90	11.21	19.086
630.0	79.1	33.1	46.02	14.74	24.017
800.0	82.7	32.2	50.46	12.34	29.228
1000.0	82.9	29.5	53.44	14.09	31.633
1250.0	83.5	27.1	56.43	13.16	34.914
1600.0	82.9	24.2	58.62	13.24	37.081
2000.0	82.1	22.8	59.30	13.71	37.613
2500.0	79.8	19.6	60.21	14.50	38.281
3150.0	77.6	17.8	59.80	14.40	37.899
4000.0	76.8	16.7	60.11	15.24	37.964
5000.0	74.8	13.8	61.06	17.58	38.292
6300.0	72.2	11.7	60.56	20.31	37.167
8000.0	69.0	10.3	58.61	24.69	34.363
10000.0	65.8	9.6	56.23	29.25	31.253
12500.0	63.2	9.5	53.66	36.60	27.710

U-shaped Duct (rounded corners)

Frequency (Hz)	Source (dB)	Receiver (dB)	NR	Absorption (A2)	TL
100.0	75.7	43.4	32.26	9.65	12.792
125.0	75.6	45.5	30.09	10.40	10.290
160.0	75.8	50.1	25.68	24.67	2.129
200.0	76.9	48.1	28.76	12.52	8.155
250.0	78.5	43.6	34.84	14.29	13.660
315.0	78.2	44.4	33.83	11.90	13.448
400.0	78.1	40.8	37.36	13.26	16.505
500.0	78.6	35.5	43.08	11.21	22.964
630.0	79.3	30.7	48.62	14.74	27.314
800.0	82.1	30.4	51.70	12.34	31.167
1000.0	83.2	28.9	54.29	14.09	33.181
1250.0	83.3	27.2	56.15	13.16	35.331
1600.0	82.9	24.1	58.79	13.24	37.950
2000.0	82.0	22.1	59.96	13.71	38.961
2500.0	79.7	18.7	60.95	14.50	39.713
3150.0	77.4	16.4	61.02	14.40	39.813
4000.0	76.6	15.8	60.80	15.24	39.350
5000.0	74.7	13.0	61.68	17.58	39.606
6300.0	72.0	11.2	60.85	20.31	38.147
8000.0	69.0	10.7	58.33	24.69	34.781
10000.0	65.9	9.1	56.84	29.25	32.552
12500.0	63.5	9.0	54.45	36.60	29.195

Sound Transmission Loss of U-shaped duct prototype tested (3/5/2001, BBN Labs, Cambridge, MA) with 1/2" acoustical duct lining on all sides for a duct with sharp ends, and again for a duct with curved ends.

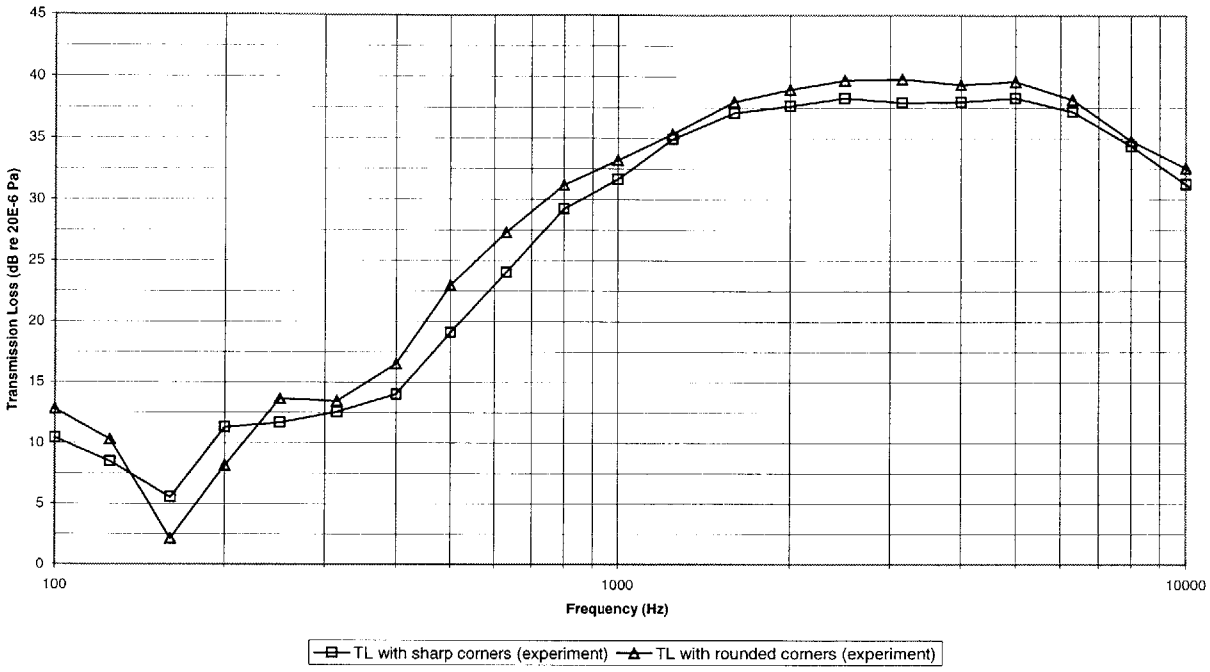

A3 – OUTPUT FROM CFD COMPUTATIONS

Section 3.3 of this thesis presents results of computational fluid dynamics (CFD) software simulations of various transfer ducts and U-shaped ducts. Below are graphical representations of the pressure and velocity results for each test.

Transfer Duct Prototype (as-built)

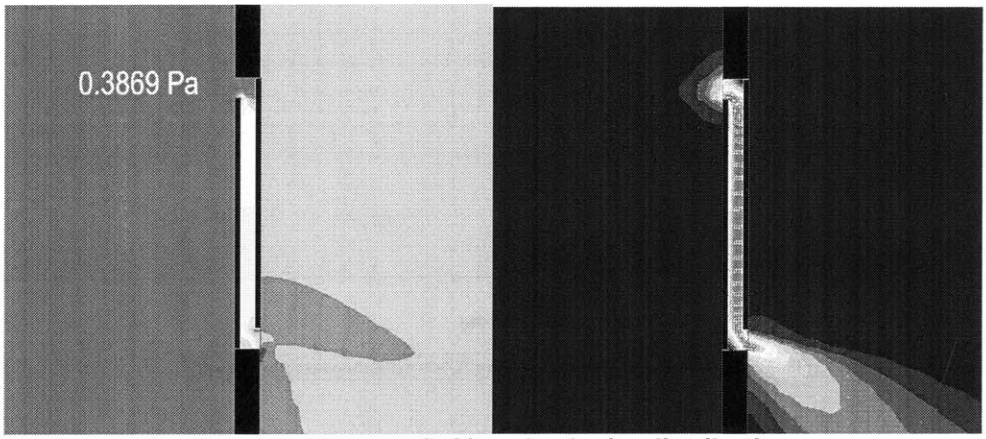

Pressure contour (left) and velocity distribution

U-shaped Duct Prototype (as-built)

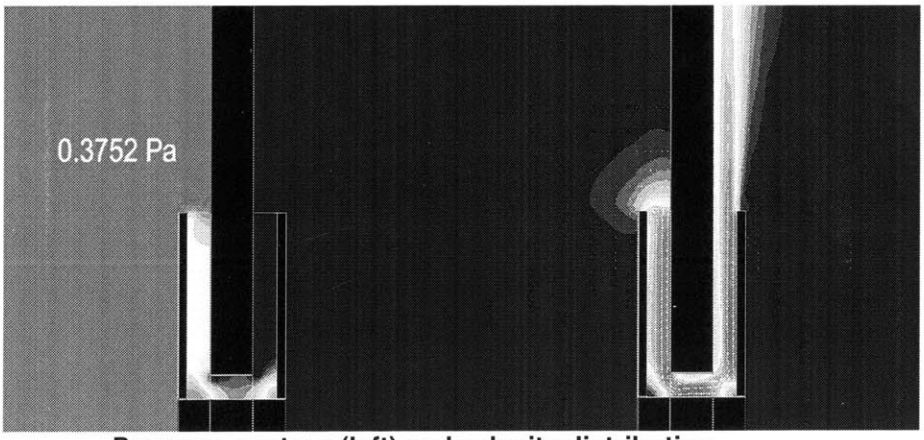

Pressure contour (left) and velocity distribution

Transfer Duct (sharp corners, located at the floor)

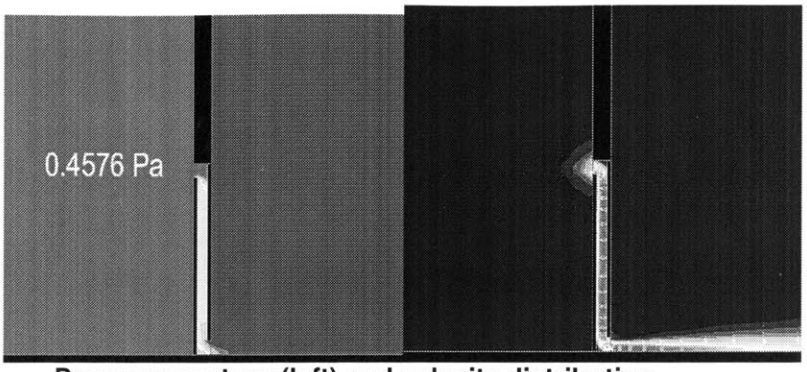

Pressure contour (left) and velocity distribution

Transfer Duct (with rounded corners)

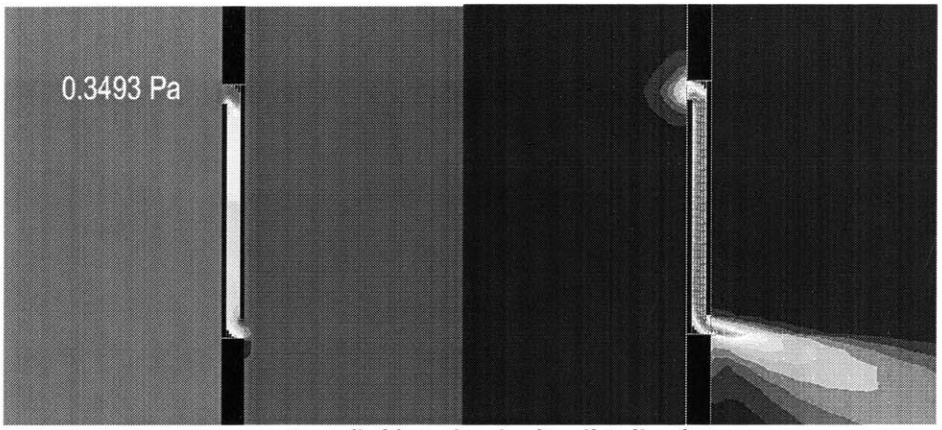

Pressure contour (left) and velocity distribution

Transfer Duct (with increased entrance area and exit area)

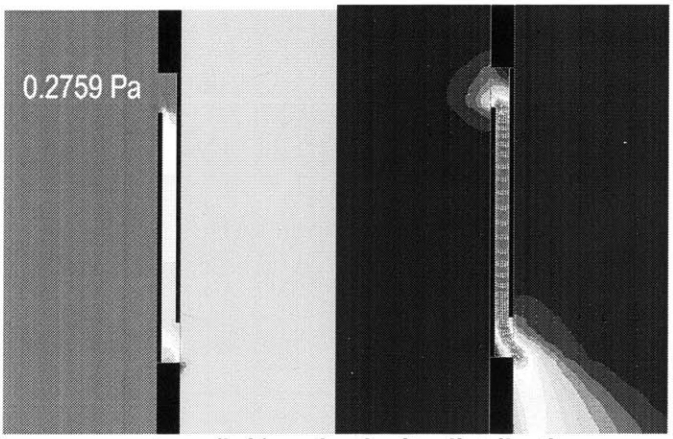

Pressure contour (left) and velocity distribution

Transfer Duct (with rounded corners and increased entrance/exit areas)

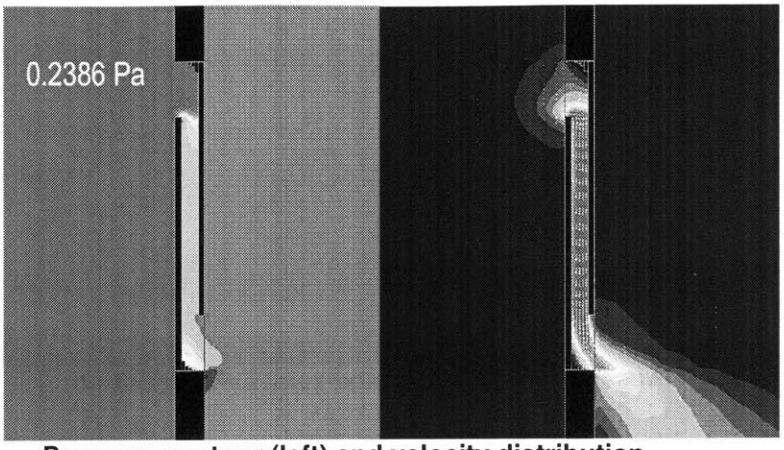

Pressure contour (left) and velocity distribution

U-shaped Duct (with increased area at bend)

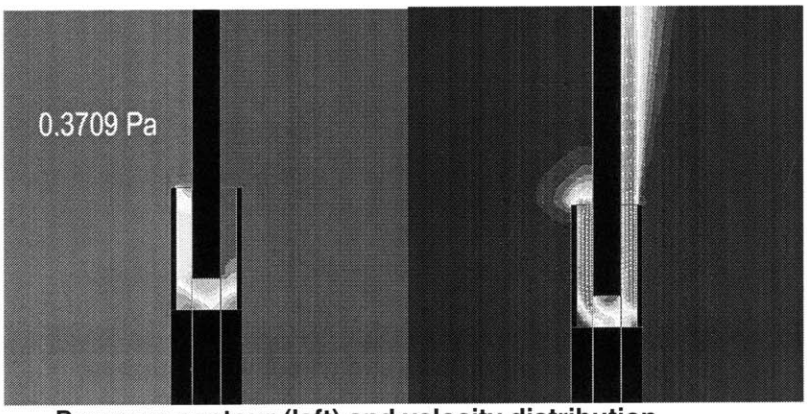

Pressure contour (left) and velocity distribution

Appendix B
Supporting Material

Kammerud, et. al. (1984) performed a study on the energy use of a building. It suggests that annual cooling load reductions up to 80% are possible simply by ventilating the building (at ventilation rates greater than about 10 ACH). The figures below are reproduced from the original study, and provide a quick overview of the study's setup and results.

Figure B1 shows the setup of the building model for the study (including solar and internal load considerations); figure B2 presents baseline energy cooling requirements for various U.S. cities; figure B3 shows the cooling season definitions for three cities (the same three cities that were used in figure 2.4, in chapter 2, to illustrate the energy-saving possibilities of ventilation versus air-conditioning); figure B4 summarizes the results for each city tested.

Prototype Building Description	
Floor Area	109 m^2 (1176 ft^2)
Total Glazing Area	16.4 m^2 (176 ft^2)
Number of Glazing Panes	2
Windows	
Position of Top	1.98 m (6.15 ft) above floor
Position of Bottom	0.76 m (2.5 ft) above floor
South Overhang	
Length	1.07 m (3.5 ft)
Position	2.44 m (8 ft) above floor
Exterior Wall Construction	1.27 cm (0.5") gypboard on frame
Partition Wall Construction	10.2 cm (4") solid concrete
Floor Construction	10.2 cm (4") concrete slab
Ceiling Construction	1.27 cm (0.5") gypboard on frame
Envelope Conductances	
Ceiling	0.166 $W°C^{-1}m^{-2}$ (0.0293 $Btu\text{-}hr^{-1}°F^{-1}ft^{-2}$)
Walls	0.270 $W°C^{-1}m^{-2}$ (0.0476 $Btu\text{-}hr^{-1}°F^{-1}ft^{-2}$)
Floor	0.485 $W°C^{-1}m^{-2}$ (0.0856 $Btu\text{-}hr^{-1}°F^{-1}ft^{-2}$)
Windows	0.31 $W°C^{-1}m^{-2}$ (0.55 $Btu\text{-}hr^{-1}°F^{-1}ft^{-2}$)
Thermostat Settings	
Heating - Daytime	21.1°C (78°F)
Nighttime	15.6°C (60°F)
Cooling	25.6°C (78°F)
Average Infiltration Rate	0.6 air changes per hour
Internal Load	15.6 $kwh\text{-}day^{-1}$ (53,100 $Btu\text{-}day^{-1}$)
Thermal Zones	
Unconditioned	Attic
Conditioned	North, South and East
Percent Solar Radiation	
Absorbed by:	
Furniture	25%
Carpet and Slab	60%
Walls and Ceiling	15%

Figure B1 – Prototype Building Description

Baseline Annual Energy Requirements

Location	Cooling Degree Days (25.6°C) (78.1°F)	Annual Cooling Energy Requirement (KWh)	Heating Degree Days (18.3°C) (64.9°F)	Annual Heating Energy Requirement (KWh)
Phoenix, AZ	952	12240	951	109
Miami, FL	348	11363	147	0
Brownsville, TX	417	10175	443	115
El Paso, TX	398	11691	1571	551
Fresno, CA	377	7966	1762	992
Fort Worth, TX	410	7614	1468	1300
Lake Charles, LA	265	7276	944	602
Albuquerque, NM	179	6232	2641	1793
Charleston, NC	182	5679	1337	995
Cape Hatteras, NC	92	5204	1522	1706
Nashville, TN	174	4809	2079	2857
Dodge City, KS	217	4730	3058	5418
Columbia, MO	141	4205	2924	5868
Washington, DC	122	3752	2780	4707
Medford, OR	127	3495	3064	3477
Ely, NV	49	2678	4491	5135
New York, NY	38	2488	2826	6085
Madison, WI	51	2405	4207	9714
Bismark, ND	68	2355	5101	13046
Boston, MA	57	2186	3304	7599
Great Falls, MT	63	2119	4282	9267
Santa Maria, CA	17	2041	2056	108
Seattle, WA	11	1052	3073	4926
Caribou, ME	9	1009	5321	13273

Figure B2 – Annual Energy Requirements

Cooling Season Definitions

Location	Total Annual Cooling Load (Unventilated) KWh	Cooling Season	Cooling Season Cooling Load (Unventilated) Kwh
Albuquerque	6243	1 May to 30 September	5657
Washington	3752	1 June to 30 September	3400
Madison	2403	1 June to 31 August	2022

Figure B3 – Cooling season definitions.

Location City	State	Cooling Season	Energy Requirements Unvented/Massive Total (KWh)	Unvented/Massive Peak KW	Vented/Massive Total (KWh)	Vented/Massive Peak KW	Vented/Nonmassive Total (KWh)	Vented/Nonmassive Peak KW	Due to Ventilation (%)	Due to Mass (%)	Due to Ventilation (%)	Due to Mass (%)
Phoenix	AZ	1 Apr to 31 Oct	11378	6.15	7844	6.15	8429	6.44	31.1	6.9	0.0	4.5
Miami	FL	1 Feb to 31 Dec	10941	4.07	5156	3.78	5919	4.11	52.9	12.9	7.2	8.1
Brownsville	TX	1 Mar to 30 Nov	9809	4.38	5547	4.34	6242	4.58	43.5	11.1	0.9	5.1
El Paso	TX	1 Apr to 31 Oct	8470	4.79	3534	4.39	4326	4.78	58.1	18.3	8.2	8.5
Fort Worth	TX	1 May to 30 Sep	7215	5.12	4159	5.12	4542	5.43	42.4	11.0	0.1	5.8
Fresno	CA	1 May to 31 Oct	6970	7.55	2243	4.94	3040	5.61	67.8	26.2	34.7	12.0
Lake Charles	LA	1 Apr to 31 Oct	6875	4.35	2991	4.16	3574	4.54	56.5	16.3	4.3	8.3
Charleston	SC	1 May to 31 Oct	5229	8.33	1613	3.81	*	4.22	69.2	*	54.3	9.7
Nashville	TN	1 May to 31 Oct	4712	4.19	1104	3.34	1728	3.92	76.4	36.1	20.3	14.8
Dodge City	KS	1 May to 31 Oct	4617	5.23	1244	4.71	1799	5.17	73.1	30.8	9.9	8.8
Cape Hatters	NC	1 Jun to 30 Sep	4306	3.16	1620	3.76	1923	3.98	82.1	37.6	0.0	5.6
Columbia	MO	1 Jun to 30 Sep	4094	8.51	974	4.50	1393	4.92	76.2	30.1	47.2	8.6
Medford	OR	1 Jun to 30 Sep	3246	4.37	366	2.39	652	3.11	88.7	43.9	45.3	23.1
Ely	NV	1 Jun to 30 Sep	2519	4.44	184	2.21	339	3.04	92.7	45.8	50.3	27.3
New York	NY	1 Jun to 30 Sep	2370	3.69	227	2.69	339	3.47	90.4	43.1	27.2	22.6
Bismark	ND	1 Jun to 31 Aug	2296	4.08	282	2.95	445	3.64	86.9	36.5	27.8	19.1
Boston	MA	1 Jun to 30 Sep	2059	7.69	245	2.82	447	3.75	88.1	45.3	63.4	24.8
Great Falls	MT	1 Jun to 30 Sep	2034	4.07	233	2.18	392	3.11	88.6	40.6	46.4	29.9
Santa Maria	CA	1 Jul to 31 Oct	1260	4.43	33	1.88	59	3.70	97.4	43.2	57.5	29.1
Seattle	WA	1 May to 30 Sep	1047	3.50	37	1.21	72	2.02	96.4	48.1	65.3	40.0
Caribou	ME	1 Jun to 31 Aug	930	7.80	21	0.97	50	2.10	99.0	58.4	88.6	57.7

*Data not available.

243

Figure B4 – Summary of results ("non-massive" tests indicate that thermal storage was not utilized, and "massive" indicates that night-time cooling effects were considered).